R-1798-ARPA

March 1976

APR 9 1976

The Potential of Indigenous Energy Resources for Remote Military Bases

T. T. Connors, P. F. Morrison, C. C. Mow and R. G. Salter

A Report prepared for

DEFENSE ADVANCED RESEARCH PROJECTS AGENCY

Rand

SANTA MONICA, CA. 90406

REPORT DOCUMENTATION PAGE		READ INSTRUCTIONS BEFORE COMPLETING FORM
1. REPORT NUMBER R-1798-ARPA	2. GOVT ACCESSION NO.	3. RECIPIENT'S CATALOG NUMBER
4. TITLE (and Subtitle) The Potential of Indigenous Energy Resources for Remote Military Bases		5. TYPE OF REPORT & PERIOD COVERED Interim rept.
		6. PERFORMING ORG. REPORT NUMBER
7. AUTHOR(s) T. T. Connors, P. F. Morrison, C. C. Mow and R. G. Salter		8. CONTRACT OR GRANT NUMBER(s) DAHC15-73-C-0181, ARPA Order-189
9. PERFORMING ORGANIZATION NAME AND ADDRESS The Rand Corporation 1700 Main Street Santa Monica, Ca. 90406		10. PROGRAM ELEMENT, PROJECT, TASK AREA & WORK UNIT NUMBERS
11. CONTROLLING OFFICE NAME AND ADDRESS Defense Advanced Research Projects Agency Department of Defense Arlington, Va. 22209		12. REPORT DATE March 1976
		13. NUMBER OF PAGES 128
14. MONITORING AGENCY NAME & ADDRESS(if different from Controlling Office)		15. SECURITY CLASS. (of this report) UNCLASSIFIED
		15a. DECLASSIFICATION/DOWNGRADING SCHEDULE

16. DISTRIBUTION STATEMENT (of this Report)

Approved for Public Release; Distribution Unlimited

17. DISTRIBUTION STATEMENT (of the abstract entered in Block 20, if different from Report)

No restrictions

18. SUPPLEMENTARY NOTES

19. KEY WORDS (Continue on reverse side if necessary and identify by block number)

Power
Energy
Military Bases
Solar Power Generation

Wind Power Generation
Tidal Power Generation
Energy Storage
Electric Power Generation

20. ABSTRACT (Continue on reverse side if necessary and identify by block number)

see reverse side

DD FORM 1 JAN 73 1473 EDITION OF 1 NOV 65 IS OBSOLETE

An examination of the potential of solar radiation, wind, and ocean waves to provide thermal and electrical power to standard remote military bases. Sufficient energy is shown to be available in the North Atlantic, Indian, and Pacific Oceans, and the Caribbean to satisfy average remote base power requirements. A survey of indigenous energy technologies indicates that considerable research is needed to bring wave power recovery up to the level of solar and wind systems. An analytic computer model is used to show that indigenous energy systems are extremely costly, in part because of storage requirements, and that a mix of indigenous and conventional (petroleum) systems would be far less so. Since even a combined system is shown to exceed the cost of a pure conventional power supply, use of indigenous energy is justifiable only as a means of reducing the dependence of remote bases on petroleum fuels. (Author)

R-1798-ARPA

March 1976

The Potential of Indigenous Energy Resources for Remote Military Bases

T. T. Connors, P. F. Morrison, C. C. Mow and R. G. Salter

A Report prepared for

DEFENSE ADVANCED RESEARCH PROJECTS AGENCY

PREFACE

For the foreseeable future, the United States is apparently committed to maintaining a certain number of overseas bases, varying from small, single-function electronic facilities to large, multifunction complexes. These bases currently are dependent primarily upon petroleum for their energy requirements. Events of the past two years, however, have demonstrated the need for considering other energy sources in order to conserve a limited petroleum resource and to lessen dependence on oil imports.

This report examines some of the energy resource and technology alternatives for remote U.S. bases. Three indigenous energy resources--solar radiation, wind, and ocean waves--are analyzed as potential substitutes for petroleum fuel. The results of the study should assist the Department of Defense in assessing the energy requirements of remote bases and the costs of providing them with indigenous energy systems.

This research was undertaken as part of a Rand study program on energy availability and national security, sponsored by the Defense Advanced Research Projects Agency, which focused on the implications of the energy shortage for Department of Defense operations, force posture, and long-range planning decisions.

SUMMARY

This report examines the potential for use of indigenous energy resources at remote military bases as a means of both conserving conventional petroleum fuels and reducing the vulnerability of such bases to fuel blockades and embargoes. Although an individual remote base may have a fairly low energy demand (an average of about 10 MW), together they pose a considerable problem in terms of maintenance of supply and of cost.

Three indigenous energy sources were analyzed as potentially suitable for remote base utilization: solar radiation, winds, and ocean waves. Their relative availability was studied, and a brief survey was made of the technological state of the art for their conversion into power.

An analytic computer model developed by this study was used to examine the size requirements and costs of the various remote base energy systems.

The report is divided into an Introduction and four major sections. Section II presents an evaluation of the energy resource potential of the North Atlantic Ocean, the Caribbean, the Indian Ocean, and the Pacific Ocean. The regions, including some eight subregions, were analyzed for the potential power density available from each of the three indigenous energy resources. Power densities were calculated and compared for the midpoint of each of the four seasons of the year.

Section III provides a brief outline of some of the basic state-of-the-art technologies for both resource conversion and storage, including a first cut at some system cost estimates. On the basis of the survey it is apparent that the technologies for the conversion and storage of solar and wind energy resources are well advanced as a result of a national effort. However, with the single exception of work at the University of Edinburgh, there appears to be little effort on the potential of wave power systems. Considerable research and development will be required to bring this technology to the current level of solar and wind systems. Three storage systems--chemical, thermal, and mechanical--were surveyed for their utility at remote bases.

Section IV uses a power system model to evaluate the relative effectiveness of the three indigenous energy sources in satisfying remote base power requirements. The model solves for energy collector size, storage requirements, and conventional power inputs. A standard remote base is positioned in five geographic locations, and the results of the simulation are compared and summarized. Initial cost comparisons are made of the several combinations of systems.

A conclusion of the study is that there are sufficient indigenous energy sources at many remote bases to be of practical value. The state of the art of solar and wind systems is quite mature. The wave energy system, however, is not well understood, nor is it currently receiving much attention. The drawback of total indigenous energy systems is the high initial cost, due in part to the large storage system required. The mixed use of a conventional (petroleum-based) fuel system (generator-furnace) with an indigenous energy system would markedly reduce initial cost because the energy storage requirement would be reduced. For example, a combined solar system and conventional system appears to represent a good mix for Diego Garcia, whereas a combined wind and conventional system is better for Adak.

For all the ranges of parameters examined, the initial cost of the combined conventional and indigenous energy system exceeds the cost of a conventional system by at least a factor of three. Thus the indigenous energy system cannot, at present, be justified on the basis of cost for remote bases. But it does provide an energy alternative to the present situation of complete dependence on petroleum, and it may lessen the vulnerability of these bases in times of crisis.

ACKNOWLEDGMENTS

CONTENTS

FIGURES

TABLES

I. INTRODUCTION

BACKGROUND

For the foreseeable future, the United States is apparently committed to maintaining a certain number of overseas bases, varying from small, single-function electronics facilities operated by one service component to large, multifunction complexes operated by several service occupants. This diverse collection of bases is maintained for a variety of reasons including:

- Fleet support
- Communications
- Surveillance
- Satellite control
- Aircraft support

One common bond unites all bases, regardless of function and size, and that is the need for energy. In peacetime this energy need can generally be satisfied by direct shipment from the CONUS, transshipment from an overseas military support depot, or importation from foreign refineries (including local purchases from the host country if the base were located on foreign territory; an example might be the Naval Station at Keflavik, Iceland).

During periods of international emergency or tension, many bases located either on islands or at coastal locations in foreign countries might find themselves cut off from their usual source of supply. If they had to obtain fuel direct from the CONUS, the delays and consequent effects on the mission of the base could be considerable. Delays might occur because of the increased transit time and the time required to obtain additional tankers to fill the longer "pipeline," and in some cases, if the civilian economy had also been affected, additional time might be required to find an uncommitted or lower priority source of fuel.

Ideally, to circumvent the effect of a cutoff of normal fuel supplies to remote bases, each such base should be capable of providing its own power from a controlled source within its immediate confines. Realistically, however, it is unlikely that such a stringent restriction would be imposed by any conceivable emergency short of an absolute air, ground, and sea blockade of the individual base. In fact, even if access by sea became too difficult or costly (e.g., blockade running) it is conceivable that some quantities of petroleum products could be provided to the base by air tanker. It is likely that some petroleum products would always be required for the base to fulfill its mission.

We are assuming, then, that a certain amount of energy independence is desirable for remote bases but that they will still have access to some reduced volume of the more conventional fuel sources by some means. It next becomes necessary to identify, locate, and describe the various available energy options and how they might be used.

THE STUDY

This study examines the availability of indigenous energy resources and the nature of the technology required for their use on remote bases. Its overall purpose is a determination of whether the use of indigenous resources can substantially reduce DoD's dependence on petroleum for housekeeping functions at remote bases, while lessening the vulnerability of those bases to an energy blockade.

Other studies of the problem of supplying overseas bases with energy during periods of contingency, although useful, have generally been concerned with satisfying the current demands of existing bases from a single indigenous energy source and have disregarded the use of petroleum as a backup source. Gillette and Schubert (1974) have indicated that indigenous energy supplies cost more than conventional energy sources. In this study we have examined a mix of both indigenous and conventional energy sources and have estimated how much this mix lowers costs.

The term "remote base" means any U.S. military installation that could be cut off from its normal source of petroleum products. We do not consider bases in friendly countries with well-established petroleum

storage and distribution systems as being "remote"--for example, those in most of Western Europe.

Although bases involved in handling fuel for major elements of ground, sea, or air combat forces are often excluded from lists of bases "remote" from energy sources, we feel that such an exclusion does not take into account the value of maintaining certain energy-consuming functions on a base--e.g., communications and surveillance--even if its major combat support function were disrupted or entirely negated. We do not address the value of remote bases but concentrate on global indigenous resources and on the cost of and technology for their exploitation.

The term "indigenous resource" means an energy source available on, or in very close proximity to, the base on which it is to be used. Three types seem to have the most utility across the full spectrum of base size and function: solar radiation, wind velocity, and ocean wave motion. The first two sources are found throughout the world and the last only at coastal locations, which are common for remote bases.

A number of other possible indigenous energy resources were con-sidered briefly but rejected for inclusion in this study: tidal action, ocean thermal gradients, geothermal activity, organic waste conversion, and stored water (hydroelectricity). These rejected resources deserve further study, and some undoubtedly have utility for certain classes of military bases. We rejected them for consideration in this study for various reasons. Tidal action and thermal gradients are both extremely limited in their geographical occurrence and not well suited to single base utilization. Geothermal activity is also site-limited, at least in terms of its more accessible forms (hot springs, geysers, etc.). Trapping deep-seated sources of hot rock for the production of steam is likely to be too expensive and complex for the vast majority of remote bases. Organic waste conversion is probably unsuitable for re-mote bases as a major energy source because of the complexity of the operation and the size of the base. The use of falling water to pro-duce electricity is dependent on site topography (for the construction of dams and reservoirs).

The remainder of this report is divided into four sections. In Section II we present the potential worldwide power density of the three selected indigenous energy sources. We also define and characterize four world regions of current and possible future remote base locations in terms of their power density potential. Section III describes the present and future technologies for the conversion and storage of solar, wind, and wave energy. In Section IV an analytic computer model is used to explore various remote base energy systems in terms of their collector characteristics, size, cost, etc. and to determine the penalties consequent to any achieved reduction in fossil fuel consumption. Section V presents conclusions resulting from the study.

II. WORLDWIDE POTENTIAL FOR INDIGENOUS
ENERGY RESOURCES EXPLOITATION

In this section we examine the worldwide distribution of solar radiation, wind velocity, and wave motion. Distribution of these data are displayed on a standard base map for the globe (Appendix A), which shows isopleths of equal power density values that are potentially available from each source.[1] Energy from solar radiation is in the form of heat and can be used directly or converted into electricity. Wind velocity and wave motion are kinetic sources of energy, which must first be converted to electricity before being used.

The potential availability of these indigenous energy sources has been determined for each season of the year. Although not as explicit as a monthly evaluation, it was considered adequate for a general "screening" of their availability. These values should be used for screening purposes only since it is quite likely that they do *not* represent energy potentials at a given island or remote coastal site. For example, islands have more daytime cloudiness and therefore less solar radiation than the surrounding ocean. Also, all the basic wind data used are derived from observations at sea. Coasts and islands often have separate wind regimes controlled by terrain effects, including heating and cooling. Records from a given site, therefore, must be used in the final analysis of power systems.

This section is divided into two parts, supplemented by Appendix A. We briefly discuss the data and their limitations and explain how they were interpreted to derive the qualitative or quantitative values. We then give a regional assessment of the availability of the indigenous resources in terms of their power density potential. Appendix A includes global maps of energy and power density values and a brief explanation of the seasonal worldwide patterns of these values.

---

[1]In all cases the term "potential" refers to the amount of power available before it is degraded by the efficiency of the system being used to translate the pure source to usable heat or electricity.

DATA SOURCES AND LIMITATIONS

Solar Radiation

Solar radiation data used for this evaluation consists of both direct solar radiation (insolation) and indirect or diffuse sky radiation, which reaches the earth's surface after being scattered by the atmosphere. Seasonal sets of these data were obtained from climatic summaries originally prepared for ARPA as part of the current Rand/ARPA Climate Program.[1] These global tabulations were based on six years (1955-1960) of data compiled by Budyko[2] and interpolated into the 4° latitude × 5° longitude grid used by the Rand General Circulation Model. The original Russian data were presented in kilocalories per square centimeter per month; however, the Rand data are in "Langlies" per day (one Langley is equivalent to one gram calorie per square centimeter). For the solar power maps in Appendix A this was further changed to kilowatt hours per square meter per day ($kWh/m^2/day$) where 1 Langley per day (LY/D) = 0.011612 $kWh/m^2/day$. In this form, the isopleth values (Appendix A) directly indicate the potential energy of solar radiation at the surface of the earth. Isopleths over major land masses have not been shown because of the lack of adequate surface radiation data. However, these data may not be necessary since it is reasonable to assume that remote bases will be located either on islands or in coastal environments, as in the past.

Wind Velocity

Wind velocity data necessary to determine the potential power density that would be available for conversion to electrical energy by windmills was obtained from the climatology of the world's oceans.[3] By keying on the percentage of time that wind velocities exceed an

---

[1] Schutz and Gates, 1971-1974.

[2] M. A. Budyko, *Atlas of the Heat Balance of the Earth*, Gidrometeorizdat, Moscow, 1963.

[3] U.S. Naval Weather Service Command, 1969; Office of Climatology, 1959 and 1961; U.S. Naval Oceanographic Office, 1955 and 1966.

average value of 19 knots (Beaufort 5, a fresh breeze),[1] it was pos-
sible to develop a power density distribution.[2] In Appendix A, two
isopleths have been plotted on the global maps, each season represent-
ing kilowatts of power per square meter (kW/m^2). These two values, 0.5
and 1.3, represent the average potential power of a wind passing through
a one square meter "window" and indicate the power equivalent of winds
that exceed the median value of a fresh breeze 30 to 60 percent of the
time.

Wave Motion

Data on wave motion over the oceans of the world were taken from
the climatologies[3] as "swell" or "sea" percentages.[4] Where available
the 10, 20, or 30 percent isopleths for swells ≥ 12 feet were used;
otherwise, the 90 percent isopleths for seas ≤ 4 feet in height were
used.

As with wind velocity, sea and swell data, as related to wave
motion, were converted directly to potential power density as discussed
in Appendix B. The resulting isopleths are expressed in kilowatts per
meter of linear wave front (kW/m/WF) on the maps in Appendix A for
February, May, August, and November.

Wave data were not available for the same months as for solar and
wind data, but since wave activity is generally consequent on the others,

---

[1] The Beaufort Wind Scale is used by mariners and displayed on
Atlases and pilot charts to indicate the force of a wind at sea. A
Beaufort 3 is identified as a gentle breeze ranging from 7 to 10 knots,
while a Beaufort 9 is classed as a strong gale with a velocity range of
41 to 47 knots. The range of Beaufort 3-9 was chosen somewhat arbi-
trarily; however, it was felt that large windmills would not operate
efficiently at much less than 7 knots, nor could they be effectively
designed to continue normal operation during whole gales, storms, and
hurricanes where wind velocities exceed 48 knots.

[2] The method of converting both wind velocity and wave motion data
to power density is described in Appendix B.

[3] Office of Climatology, 1959 and 1961.

[4] Ocean "swell" refers to that portion of the wave spectrum that
is far removed from its source region. "Sea" refers to waves that are
generated by local winds and is defined as the average height of the
highest one-third of the waves observed in a series of waves moving
in one direction (a wave "train").

the months chosen can be considered as midseason for wave power. Also, wave front in meters is used as a measure, rather than surface area, since wave motion conversion devices are essentially linear.

VALIDITY OF THE DATA

It is recognized that global indigenous energy source data collected from a limited number of widely distributed ocean stations are inherently unreliable as a measure of the precise amount of potential power available at a specific remote base. Even the measurements of wave and wind data are less than exact inasmuch as they are derived from observations taken by ships' personnel of varying degrees of skill and training.

This study has not attempted to determine the potential indigenous power available at actual remote bases but rather has developed a "standard" base (see Section IV), which is analyzed as if it were located in each of the general base regions. As a consequence, the coarseness of the global data has little direct effect on either the analysis of the study or its conclusions.

REGIONAL EVALUATION OF INDIGENOUS RESOURCE POTENTIAL

An examination of the distribution of current overseas bases indicates that there are some four major world regions where bases that can be categorized as "remote" (as defined by this study) are concentrated. Since these four regions have obviously been of importance in the past to U.S. interests, and in some cases seem to be experiencing an increasing interest (for example the Indian Ocean), their separate evaluation in terms of indigenous power density potential appeared to be worthwhile.

Because of the size and heterogeneity of the major regions, these have been further subdivided into eight subregions. The four major regions and their subdivisions are as follows:

Major Region	Subregion	Map Symbol
North Atlantic Ocean	Far N.A.O.	A
	Mid N.A.O.	B
Caribbean	(none)	C
Indian Ocean	West I.O.	D
	East I.O.	E
Pacific Ocean	East P.O.	F
	Mid P.O.	G
	North P.O.	H

Both the major regions and their subdivisions have been outlined on
the base map in Fig. 1, along with the approximate locations of some
20 remote U.S. bases. These bases have been listed in Table 1.

Each subregion will be examined in terms of the potential power
density derivable from the three indigenous energy resources of solar
radiation, wind velocity, and wave motion; Table 2 presents this in-
formation in tabulated form. For solar radiation, average solar energy
in $kWh/m^2/D$ will be given for each of the four midseason months April,
July, October, and January,[1] and an average power density (an average
of the four midseason months) will be given in megawatts per square
kilometer (MW/km^2). Wind power densities will be provided for each
of the same four months in kW/m^2 and average power density in MW/km^2.
Wave power densities, in kW/m^2, will be given for May, August, November,
and February, and the average of the four months in MW/km/WF. The
average power density for the same months is in MW/km/WF.

In all cases it must be remembered that the average power density
over the year is not the only factor involved in a choice of which re-
source in a subregion is best suited to exploitation. Also to be con-
sidered are such factors as the design of the energy receptor, its
area and storage requirements, and its cost.

The North Atlantic Ocean

This region, which encompases essentially all of the North Atlantic
north of 30°N latitude, has been divided into two subregions split
roughly along the 60th parallel. In Table 2 the average potential power
density values of the three indigenous energy sources are displayed for
each of the two subregions. It is clear that for both subregions of
the North Atlantic the period of maximum solar energy (July) stands in
inverse relationship to the period of maximum wind power (January).
It is also evident that the average solar energy level in the southern
half (B) of the region, 128.4 MW/km^2, is higher than that in the north,
98.9 MW/km^2. Wind power levels, however, though seasonally varied, aver-
age out to be identical for both subregions, 600 MW/km^2.

---

[1] Solar radiation is expressed in *energy* terms in keeping with the
map data in Appendix A. *Power* density can be obtained by dividing the
energy values by 24.
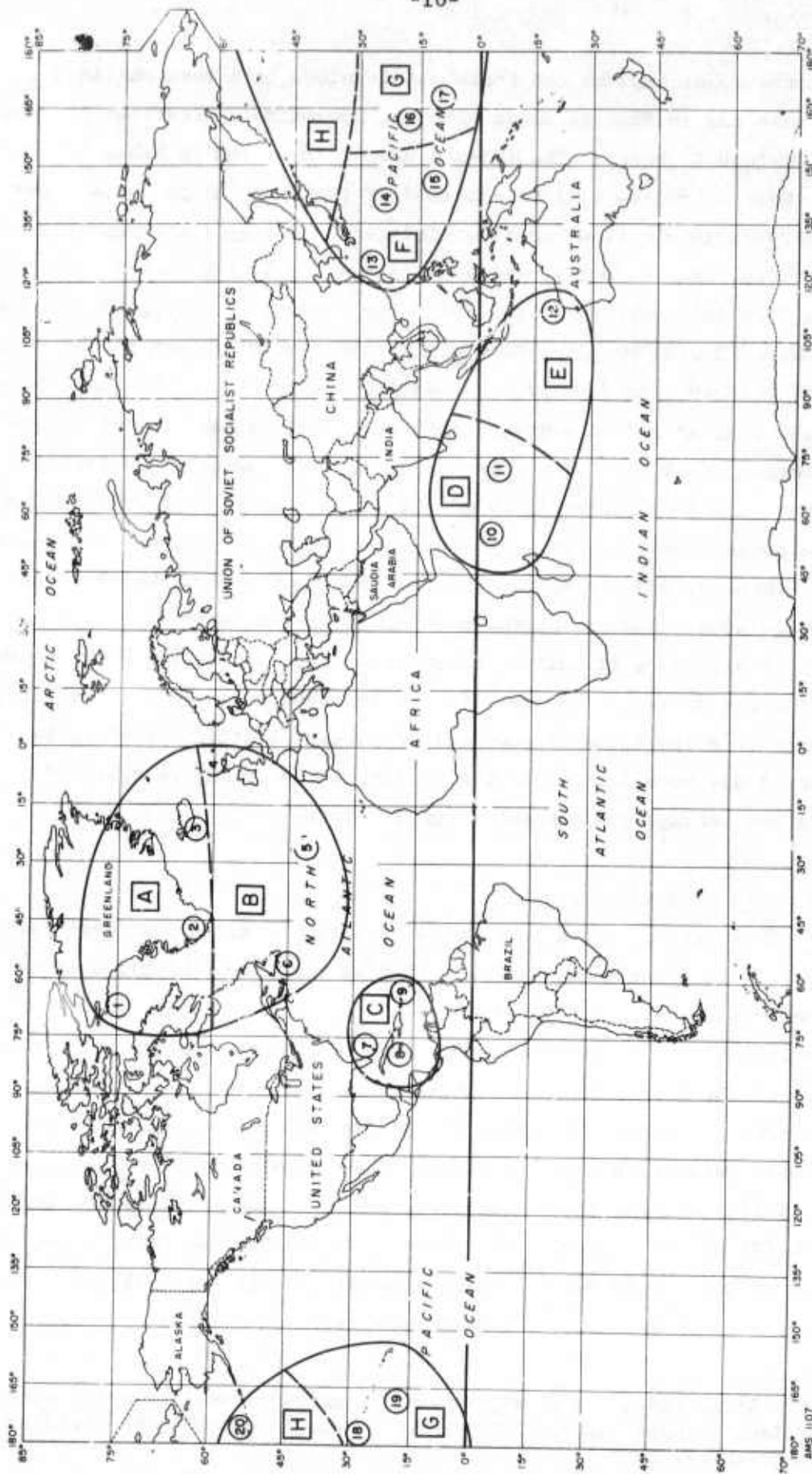
Fig. 1—Selected remote bases by ocean subregions

Table 1

BASE DATA INPUT POINTS

Major Region	Subregion	Data Point Location[a]	Identification Symbol
North Atlantic Ocean	Far N.A.O.	Thule, Greenland	1
		Sondestrom, Greenland	2
		Keflavik, Iceland[b]	3
	Mid N.A.O.	Thurso, Scotland	4
		Azores	5
		Argentia, Newfoundland	6
Caribbean		Bahamas	7
		Guantanamo Bay, Cuba	8
		Puerto Rico	9
Indian Ocean	West I.O.	Mahe, Seychelles	10
		Diego Garcia, Chagos Archipelago	11
	East I.O.	North Cape, Australia	12
Pacific Ocean	East P.O.	Okinawa, Ryukyu Islands	13
		Iwo Jima, Volcano Islands	14
		Guam, Marianas	15
	Mid P.O.	Wake Island	16
		Kwajalein, Marshall Islands	17
		Midway Islands	18
		Johnson Island	19
	North P.O.	Adak, Aleutian Islands	20

[a]The data points are only approximate geographic locations and are not intended to represent specific military bases.

[b]Keflavik was chosen as a data input point strictly on the basis of its regional location. Its geothermal power potential has not been considered in this study.

Table 2

POTENTIAL INDIGENOUS POWER DENSITY LEVELS BY OCEAN SUBREGION

Subregion	Solar Power Density					Wind Power Density					Wave Power Density				
	Average Energy Per Midseason Month[a] (kWh/m²/D)				Power Average of Four Mid-season Months (MW/km²)	Average Energy Per Midseason Month (kW/m²)				Power Average of Four Mid-season Months (MW/km²)	Average Power Per Midseason Month (kW/m/WF)				Power Average of Four Mid-season Months (MW/km/WF)
	April	July	Oct.	Jan.		April	July	Oct.	Jan.		May	Aug.	Nov.	Feb.	
(A) Far N.A.O.	3.29	5.06	0.80	0.34	98.9	0.68	0.25	0.59	0.77	600	30	40	30	30	32.5
(B) Mid N.A.O.	3.78	4.75	2.59	1.21	128.4	0.63	0.30	0.51	0.96	600	30	22	50	40	35.5
(C) Caribbean	6.39	6.70	5.15	4.38	235.8	0.53	0.83	0.41	0.93	680	3	3	21	30	14.3
(D) West I.O.	5.23	4.19	5.57	5.69	215.5	0.17	0.25	0.31	0.19	230	3	30	3	3	9.8
(E) East I.O.	5.23	4.07	6.97	7.09	243.4	0.44	0.20	0.12	0.24	250	3	30	3	3	9.8
(F) East P.O.	5.42	5.40	4.26	3.56	194.3	0.42	0.23	0.38	0.93	490	3	3	12	12	7.5
(G) Mid P.O.	5.51	5.61	4.94	4.15	222.7	0.55	0.32	0.41	0.74	510	13	3	22	13	12.8
(H) North P.O.	2.61	2.32	1.74	0.58	76.7	1.19	0.50	1.17	1.23	1023	30	3	60	30	30.8

[a] Solar radiation for individual mid-season months is expressed in energy terms in keeping with the map data presented in Appendix A. Power density can be obtained by dividing the mid-season value by 24.

Potential power derivable from wave motion also shows seasonal variations, with a slightly lower average value found in subregion (A), 32.5 MW/km/WF, than in (B), 35.5 MW/km/WF. The periods of maximum and minimum wave power levels for the two subregions are strongly at variance when compared seasonally; e.g., in subregion (A) maximum power levels occur in July, which coincides with the minimum for subregion (B). There also appears to be little or no correlation between wind velocity and wave motion for subregion (A) and only partial correlation for subregion (B) where a low average power level for winds in July does coincide with minimum wave motion power for the same period.

Close correlation between average wind and wave power levels at any one location should not be expected inasmuch as the swell component of waves is generated outside of the area, or "fetch," of its occurrence. Wide disparities are unusual and may result from the inherent inaccuracies of wind and wave observations.

In terms of pure power potential (MW/km^2), wind would appear to be the obvious indigenous power choice for remote bases in the North Atlantic, exceeding the average solar power by over five times and wave power by 17 times. This advantage is more apparent than real, as will be seen in Section IV, when other factors are brought into consideration.

The Caribbean

This small region comprises an area somewhat larger than its name implies, inasmuch as we have included within its scope the Bahamas (which lie outside of what is normally considered the Caribbean). Although not as "remote" geographically as the others, this rather homogeneous region does contain bases and areas of past and probable future importance.

In this region solar radiation maintains a fairly high power level throughout the year for an average over the four seasons of 235.8 MW/km^2, or more than twice that of the northern subregion (B) of the North Atlantic (Mid N.A.O.). Potential wind power has also increased but to a much lesser degree, averaging 680 MW/km^2 over the year (600 MW/km^2 for the Mid N.A.O.).

In contrast to the North Atlantic, Caribbean wind power potential is more constant throughout the year, with a maximum occurring during both the summer and winter seasons in response to the northeast Trade Winds blowing across the area. There are also two minimum periods, though not as marked as those in the North Atlantic.

Wave power potential is again not well correlated with wind power, although the winter months appear dominant for both sources.

Wind appears to be the dominant indigenous resource, but to a lesser degree (less than three times more potential power than solar). Again, the apparent advantage will later be negated when other factors enter the analysis.

The Indian Ocean

This region extends through some 75 degrees of longitude and has been divided into a Western (D) and an Eastern (E) subregion. The average potential power values for each of the subregions, based on two bases in the western half and one in the eastern half, are contained in Table 2.

The two subregions are differentiated primarily by a 13 percent increase in solar power potential in the eastern portion and by seasonal differences in potential wind power. The Indian Ocean, insofar as its three base points indicate, apparently has the highest average solar power potential and the lowest average wind power potential of the four major regions.

Although the average potential wind power for the two subregions over the year is roughly the same, the maximum period for the West I.O. (D) occurs during the fall, and the maximum for the East I.O. (E) occurs during the spring. There seems to be little or no correlation of wind and wave power data for the region.

As might be expected, and in spite of the lack of wind and wave correlation, wave power potential in the Indian Ocean is quite low, close to the lowest of any region or subregion examined.

Although the apparent potential power of solar radiation and wind are about equal, later analysis will show solar radiation to be the clear choice for an indigenous power supply.

The Pacific Ocean

Because of both its latitudinal and longitudinal extent, this region has been divided into three subregions, an East P.O. (F), represented by three base input points, a Mid P.O. (G), represented by four data points, and a North P.O. (H) represented by a single base data point.

It is clear from Table 2 that the East and Mid Pacific Ocean subregions differ sharply from that in the north, but from each other hardly at all, a slight edge in power potential for all three indigenous sources going to the Mid P.O. And although there are minor differences in absolute values between subregions (F) and (G), they are fairly comparable in their periods of minimum and maximum power levels.

The North P.O. is distinctive in at least two particulars: first, averaging the four seasonal power levels indicates that this subregion has the lowest potential power from solar radiation--76.7 MW/km^2--of any examined; and second, it has the highest potential wind power of all the subregions examined--1023 MW/km^2. In spite of a fairly close correlation between wind velocity and wave activity, at least in terms of period, the potential power available from wave activity is quite moderate. Although higher than that found in most of the other subregions, it falls somewhat below the power levels found in the North Atlantic.

In the Northern Pacific Ocean (H), wind clearly dominates both solar and wave power as an indigenous energy source for remote bases. In the Mid P.O. and Eastern P.O. subregions, wind power potential is slightly more than twice that of solar power and may not be competitive, all factors considered.

Table 3 compares the yearly average power densities of the three indigenous energy types for the eight subregions; keep in mind the basic noncomparability of such "pure" and potential data.

Table 3

AVERAGE YEARLY POWER DENSITY LEVELS

Region and Subregion		Solar Power Density (MW/km^2)	Wind Power Density (MW/km^2)	Wave Power Density (MW/km)
North Atlantic Ocean				
Far N.A.O.	(A)	98.9	600	32.5
Mid N.A.O.	(B)	128.4	600	35.5
Caribbean	(C)	235.8	680	14.3
Indian Ocean				
West I.O.	(D)	215.5	230	9.8
East I.O.	(E)	243.4	250	9.8
Pacific Ocean				
East P.O.	(F)	194.3	490	7.5
Mid P.O.	(G)	227.7	510	12.8
North P.O.	(H)	76.7	1023	30.8

III. TECHNOLOGIES FOR INDIGENOUS ENERGY RESOURCES

In this section we briefly outline some of the basic state-of-
the-art technologies for both resource conversion and storage, with
each of the three selected indigenous energy resources being discussed
in turn.   Included will be some first-cut system cost estimations.

The enormity of the total energy reaching the earth from the sun
has attracted many people to consider the replacement of some of our
present energy use by solar energy.   The only application of solar
conversion that has been widely used is for domestic water heating.
In Japan, for example, several millions of inexpensive plastic solar
water heaters are currently in use.   Sun-rich Israel and Australia
use a slightly more complex solar water heater system consisting of
a combination glass and metal collector and a storage tank.   Between
1945 and 1960, some 50,000 simple solar water heaters were installed
in Southern Florida where electricity cost was high and other fuel
alternatives were unavailable.

In 1958, two experimental solar houses were constructed in the
United States, one as part of the Hottel Project at M.T.T. and the
other as part of the Löf Project at Denver.   These projects had the
purpose of evaluating the technical and economic feasibility of dif-
ferent solar collector configurations.   The ability of cheap oil to
compete with solar energy sources during the 1960s forced the findings
of these studies into the background.   Recently, however, under the
increased threat of   ifficient petroleum availability, NSF and ERDA
have been exploring various ways of simulating the utilization of
solar energy.

SOLAR POWER

Solar collectors fall into two principal classifications, thermal
energy collectors and photoelectric cells.   Thermal energy collectors
are themselves of two types, flat collectors and focusing collectors.
At present, the maximum efficiency of solar radiation to electrical
power that can be obtained from any of these systems is 12 percent
(Hottel and Howard, 1971).

All thermal collectors must have the ability to absorb incoming radiation while reflecting or reemitting as little energy as possible. Since the early 1950s, a search has been continuing for collector coating materials that optimize the absorption of visible radiation while minimizing the emission of long wavelength radiation. A copper oxide coating on an aluminum surface (Hottel and Howard, 1971) and tungsten deposited on a variety of substrates (Cuomo, Ziegler, and Woodall, 1975) are two coatings that have the required radiation properties. Such coatings do add significantly to collector costs, however.

Currently, the National Science Foundation is funding investigations on the development of interference films, which internally reflect the spectrum of visible radiation into destructive interference patterns, and of bulk absorption by silicon films (Interagency Task Force, 1974). As research continues, coating technology can reasonably be expected to improve and lead to lower costs.

Flat plate collectors are flat, low emissivity surfaces in thermal contact with a piping system carrying a heat transfer medium. Because these devices collect their energy directly from a low density power source, they are usually low temperature units. They are economic at the present time for space and water heating (e.g., recent data indicate that solar pool heating units have a cost of about $1.75 per sq ft plus frame and installation). However, they are considerably poorer candidates for large power generation because the low temperature difference on which the turbines must operate forces the system to have a very low thermodynamic efficiency. Hottel and Howard (1971) have presented an analysis showing that the maximum attainable efficiency in a flat plate power system is no more than 11 percent; devices constructed to date have efficiencies about half that value.

Focusing collectors primarily collect direct radiation from the sun, focusing it on a point or line surface in contact with a working fluid having a high boiling point. These collectors substantially raise the turbine temperature differential and thus the thermodynamic efficiency over flat plate devices. Unfortunately, they are more expensive to construct and maintain, particularly those systems requiring accurate tracking devices, such as parabolic reflectors. One of the

least expensive focusing devices is a cylindrical parabola on an east-west axis. Oriented in this way, the reflector has only to be rotated slightly with season to allow the sun to lie on or near the focal line, thus minimizing tracking costs. Like flat plate collectors, they require a good low-emissivity coating on the focal surface to be highly efficient. An inherent disadvantage of focusing collectors is their inability to collect much diffuse radiation.

One suggestion for a fairly low cost focusing system (Goen et al., 1973) is shown in Fig. 2. This collector is composed of a coated aluminum tube surrounded by a silvered glass pipe, a type of construction that minimizes machining requirements of nonstandard shaped surfaces, such as parabolic reflectors, and thereby reduces cost. This lowered cost is achieved at the expense of some efficiency since the circular cylindrical reflector is optically poorer than parabolic surfaces; and if the entire tube is silvered with a "one-way" mirror, reflectance of incoming radiation will be appreciable. SRI's estimate (1971 dollars) of the cost of this system is $6.19 per sq ft with the collector accounting for 71 percent of this cost.

Special, low
emissivity coating

Clear

Glass pipe

Aluminum pipe

Silvered

Vacuum

Heat transfer medium (Santowax)
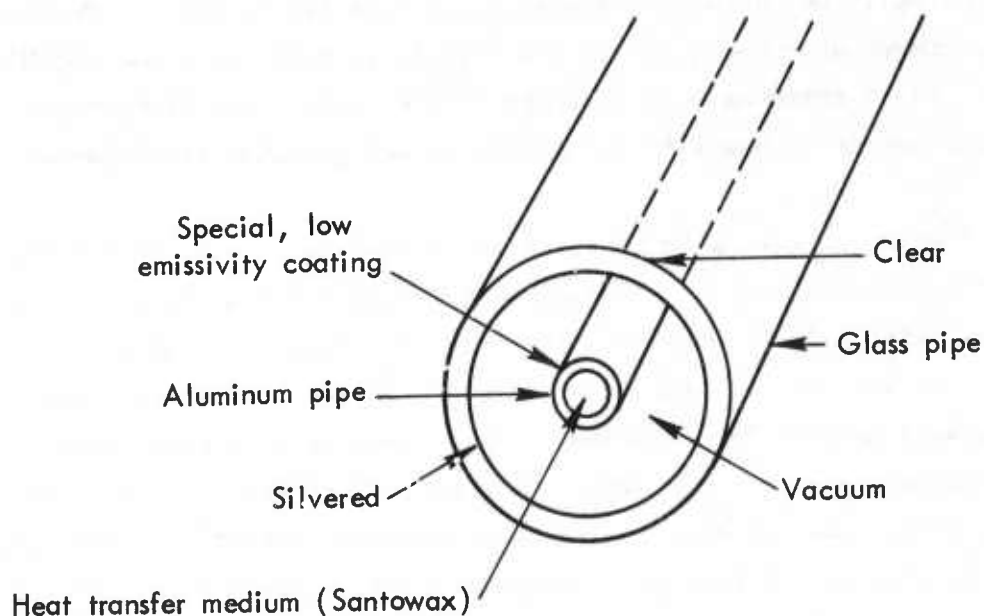
Fig. 2—Moderate temperature collector schematic
for steam production, ~350°F

Another approach to solar focusing is the use of a more widely distributed mirror system that reflects and focuses solar radiation on a central receiver. The mirrors (heliostats) required are quite expensive, one cost estimate being $30/m^2$. A 10 MWe proof-of-concept experiment will be carried out under NSF funding during FY 1975-1980 (Interagency Task Force, 1974).

The third collector type is the photovoltaic cell, which attains direct radiation to electrical efficiencies of 12 percent (silicon cell) or 5 percent (cadmium sulfide) (Hottel and Howard, 1971). Silicon cell costs per installed watt are very high at the present time; aerospace costs have run at $200/watt, while 1974 terrestrial applications may have costs as low as $20/watt. However, a projection that is claimed to be highly accurate states that this cost will drop to $5 per peak watt by 1978 (Interagency Task Force, 1974). If reasonable engineering extensions of conventional silicon crystal growing and slicing techniques were introduced immediately, 1977 costs could be reduced to $2.15/watt ($256/m^2$ of collector area). If allowance is made for expected technological breakthroughs and solar radiation is focused on the collector surface, a lower cost limit of $.76/watt may eventually be approached (Interagency Task Force, 1974). Research on the growth of ribbons of silicon crystal (supported by NSF and NASA), production of inexpensive polycrystalline silicon cells from silane, and development of new slicing technology are possible breakthrough areas.

If solar energy is to be efficiently applied to the power demands of a remote base, the different technical requirements needed to satisfy the two principal end uses of electricity and space heating must be taken into account. In the case of solar thermal conversion, electrical demands have to be satisfied by the output of a turbine connected to a moderately high temperature collector. However, space heating demand should not be met by using the electrical output but rather by directly drawing off heat from the solar working fluid or by using the waste heat (hot water) from the turbine (a so-called "cascaded" system).

The output of photovoltaic systems may also be split into electrical and space heating uses. Because photovoltaic conversion is quite

inefficient, much of the radiation that falls on the collector remains there as heat energy, as in the case of the flat plate collector. Hence if the photovoltaic cell is thermally interfaced with a heat conducting medium, thermal energy that might otherwise be wasted can be utilized for space heating.

Solar collection devices have several inherent difficulties associated with them. The foremost is that collector surfaces must be kept free of dirt and other particulates that reduce transmittability. Another is that wind-driven particles of dirt may etch collector plates or their cover plates, thereby increasing scatter and reducing input fluxes. Finally, even for fairly small power systems on the order of 10 MW, collector areas may be on the order of one-fifth of a square mile, and such a large area means that significant power will have to be diverted from its primary use to run the pumps that handle the thermal working fluid (Hottel and Howard, 1971).

WIND POWER

Because of its general availability, the harnessing of wind energy for various applications has dated from the earliest periods of human history. Using wind as a primary energy source for generating electricity, in the face of a scarcity of other forms, received considerable worldwide attention and was proved practical in Denmark during both World War I and World War II. Most Danish wind power stations currently have a nominal capacity of 50-60 kW, and a windwheel diameter of 17.5 m. In 1941, some 64 stations generated a total of 231,682 kWh (Stein, 1974).

In Russia, where power is needed for large numbers of widely scattered agricultural communities, the Central Wind Power Institute of Moscow was established at the end of World War I. The work of this institute resulted in the building of a 100-kW dc pilot plant in Yalta, on the Black Sea, in 1931. It was reported that as of 1954, there were 29,500 wind power plants in Russia with an aggregate capacity of 125,000 kW (an average of $\simeq$ 4 kW/station).

Wind power also contributed significantly to the development of the Western United States. However, over the last 40 years, because

of the rural electrification program and the availability of gasoline and diesel fuel at low cost, windmills have fallen out of favor as a means of providing electricity.

A notable exception to this trend was an effort just before World War II by Palmer S. Putnam who built a 175-ft, 1250-kW experimental unit on Grandpa's Knob near Rutland, Vermont (Putnam, 1948). The unit generated as much as 1.5 MW in 70 mi/hr wind and withstood winds as high as 115 mi/hr. Although the project was a technical success, it operated only intermittently from 1941 to 1945 because of parts short-ages. Fatigue and stress corrosion caused one of the blades to fail in March 1945. The whole concept was abandoned later that year because it was estimated that it would cost about $190/kW, while the fossil fuel-powered plants were costing about $125/kW, installed.

From 1945 to 1973, there was very little done in the area of wind energy conversion. Then, with the recognition of the impending energy problem, researchers started to reexamine different inexpensive ways of converting wind energy into electricity. At present (1975) there are some seven studies going on with a total funding of about $3 mil-lion, supported by NSF and NASA, on both hardware design prototyping and system analysis (Interagency Task Force, 1974).

Although little effort has been expended in the United States dur-ing the past several decades on the development of wind energy conver-sion systems, major advances have been made in the areas of lightweight, high strength composite materials; structural design concepts; energy storage devices (such as batteries and fuel cells); airfoil concepts; and electronic servo control systems. These new technologies are being exploited by the current NSF/NASA effort.

Since the majority of the remote bases examined by this study have energy demands of 10 MW or less, the fact that the NSF/NASA research has centered around power requirements of from 100 KW to 1 MW would indicate that most would be of significance to the remote base energy problem.

Most of the existing concepts and the prototypes under current development are of the familiar horizontal-axis type. However, Sandia Laboratories under AEC funding is investigating a vertical-axis wind

turbine concept first designed by G.J.M. Darrieus of France in 1925, illustrated in Fig. 3 (Reed, Mayden, and Blackwell, 1974). Regardless of the axis orientation, the maximum amount of energy that can be extracted from the wind is 59.2 percent of the amount available. Past experiments also indicate that a high-speed windmill of good aerodynamic design has efficiencies of about 75 percent (i.e., of the theoretical maximum). Therefore, with an efficient design one may expect that approximately 45 percent of the available energy can be converted to electricity. The overall efficiency of a wind generation system, including storage, falls in the range of 20 to 30 percent.

Taking the potential wind power density for each of the eight subregions developed in Section II and adjusting for the overall efficiency
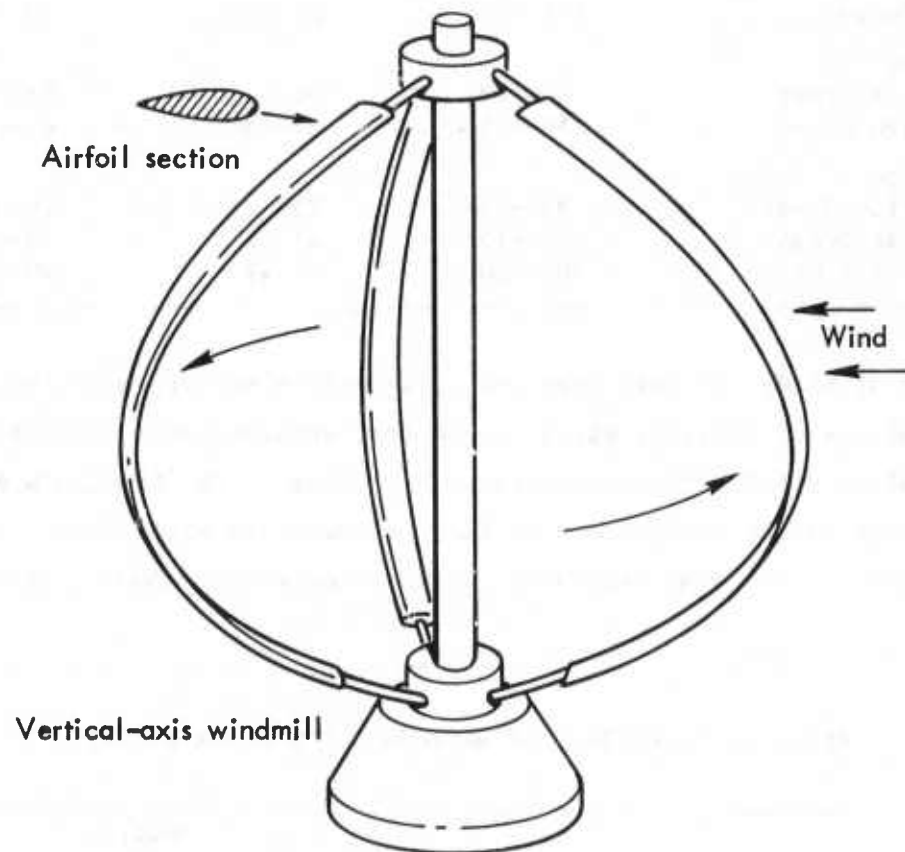
Fig. 3—Vertical-axis wind turbine

of a wind energy system, we can determine the windmill rotor radius requirements (horizontal axis) for any power output. Table 4 presents two possible radius requirements for two selected outputs.

Table 4

NET USABLE POWER DENSITY AND WINDMILL RADII

(For 20 and 30 percent efficiencies)

Region and Subregion	Usable Wind Power Density, MW/km^2	Radius of Windmill, 200 KW System, m	Radius of Windmill, 1 MW System, m
North Atlantic Ocean			
Far North Atlantic Ocean	120--180	23--19	51--42
Mid North Atlantic Ocean	120--180	23--19	51--42
Caribbean Ocean	136--204	22--18	49--40
Indian Ocean			
West Indian Ocean	46--69	38--31	85--70
East Indian Ocean	50--75	37--30	83--67
Pacific Ocean			
East Pacific Ocean	98--107	25--21	56--47
Mid Pacific Ocean	102--153	25--21	56--47
North Pacific Ocean	204--307	18--15	40--34

Rotor blades of this size are quite within the state of the art. The problems of fatigue, stress corrosion, environmental corrosion, and fabrication difficulties encountered by Putnam in the Grandpa's Knob experiment may be ameliorated by the new composite materials. Table 5 shows some of the most promising candidate materials (Adams, 1974).

Table 5

RELATIVE COMPARISON OF MATERIALS FOR ROTOR BLADES

Material	Impact Strength	Fatigue Resistance	Surface Hardness	Environmental Resistance	Repairability
Al. 2024-T6	Moderate	Low	Moderate	High	Moderate
E glass/polyester	High	High	Low	High	High
Graphite/epoxy	Very low	High	Low	High	Moderate
Boron/epoxy	Moderate	Very high	Moderate	High	High

At present, aluminum still has a cost advantage over the composites, but composite technology is rapidly progressing. Adams (1974) indicates that the inherent low cost in composite fabrication, machine forming, joining, etc. should ultimately result in a drastic lowering of the cost over the next few years. In certain applications, such as high-performance rotor blades, composites may become competitive with aluminum.

Wind generators can be sited either onshore or offshore. An example of one possible onshore windmill type (NSF/NASA Wind Generator System Program, 1974) is presented in Fig. 4 and a possible offshore configuration is given in Fig. 5 (Heronemus, 1972). The amount of surface land or water area to be covered by windmills can be reduced by some form of stacking (as shown in the example), and on-site construction can be minimized by preassembly of components.

The total cost per kW for any wind generating system will depend upon the particular combination of subsystems. The estimated cost (1974) for the 100-kW NASA Plum Brook facility is about $1000/kW for
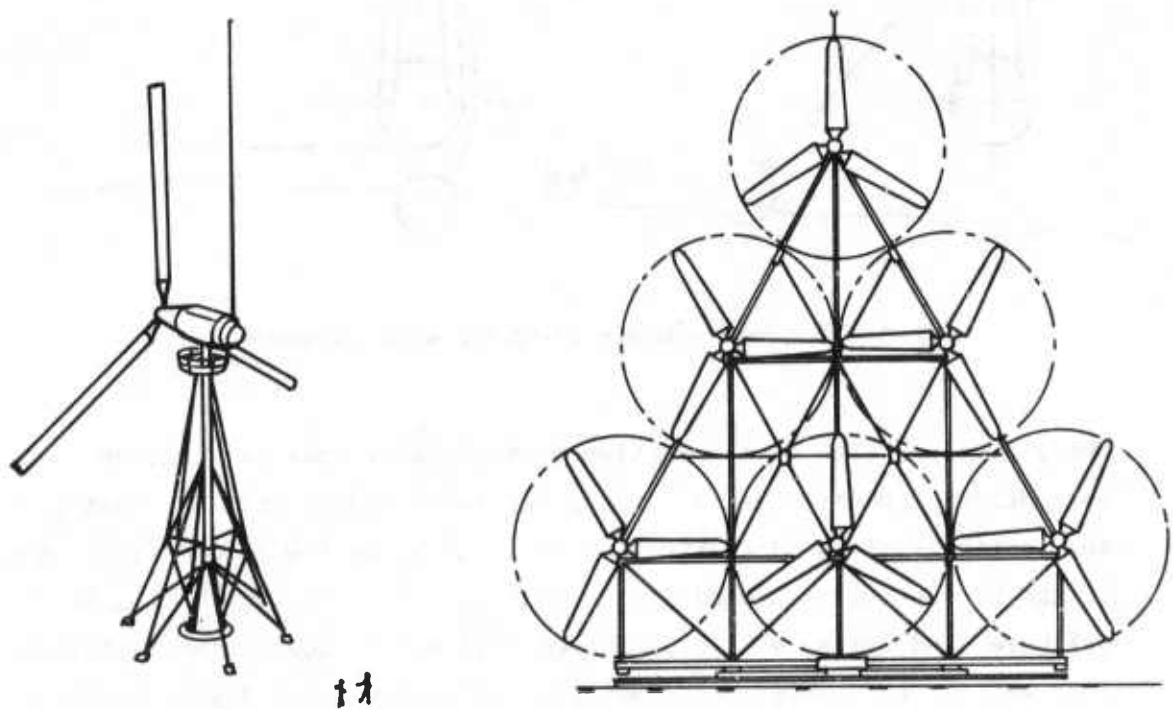
Fig. 4— Proposed onshore siting for wind generator
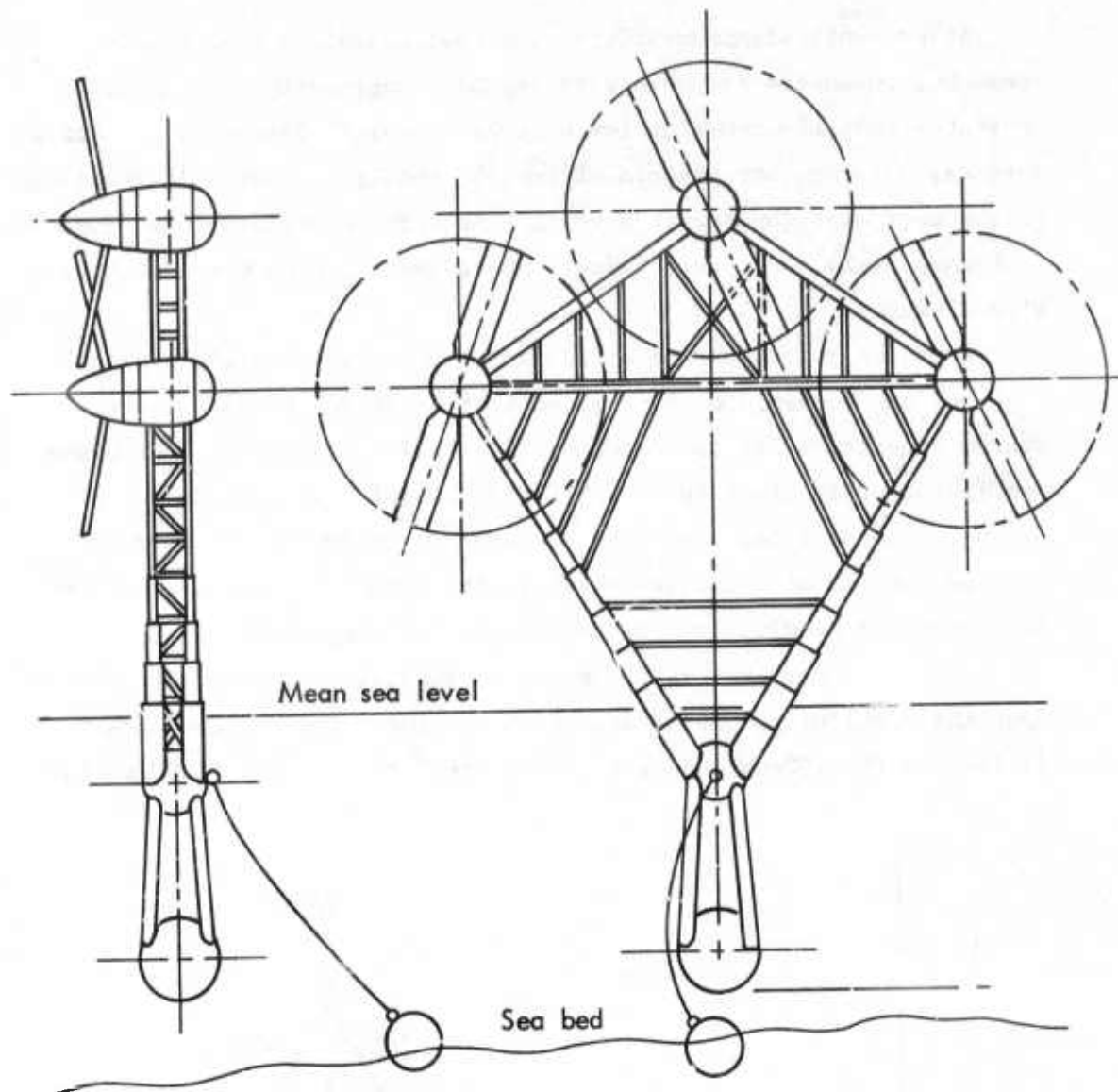
Fig. 5— Proposed offshore siting for wind generator

the prototype, with cost reduction to $500/kW or less as a design goal
for larger production units. South and Rangi (1974) indicate that for
the vertical-axis wind turbine the cost can be as low as one-sixth that
of the horizontal-axis windmill. Their cost figures, which include
offshore wind units, a 24,000-MW fuel cell substation, offshore collec-
tion system, etc., are about $800/kW. We believe this figure could be
lower for DoD application since a remote base system would be much
smaller in terms of its distribution network. A more realistic cost
might be in the neighborhood of $ 00-$800/kW.

OCEAN WAVE POWER

Ocean waves are among the most visible forms of energy. Ocean *swell* is developed over long distances where the interaction of wind gradually exchanges energy with the ocean surface causing long period waves; and *sea* is the disturbance of the surface due to local wind phenomena. The extraction of energy from ocean waves is a very old idea. A fairly complete understanding of the theory of wave motion, relating this motion to the trochoidal wave form, was well in hard in the mid-nineteenth century. This theory is very well explained in Stahl (1892).

The energy contained in a wave is divided equally between potential energy and kinetic energy. The potential energy relates to the vertical position of the rotating particles within the wave, and the kinetic energy relates to the forward progression of this rotating system. Devices that can extract energy from waves generally take one of two forms, one being the "bobber," which rises and falls with the surface and thus operates primarily on the potential energy in the wave, and the other being devices that are moved horizontally by the kinetic energy component of the wave.

The implementation of wave energy extraction devices must contend with the classic problems involved in any offshore installation. These include survival of stormy seas, shifting sands, salt water corrosion, and barnacles. In addition, very little practical power can be extracted from small waves, say, of less than one meter in height; conversely, practical energy may not be extracted from very large waves over five meters. The reason for this restriction is because the energy extraction system must be designed to extract energy and to survive a spectrum of situations ranging from dead calm to the giant wave occurring only occasionally. It is difficult to design a system such that it will be sensitive to small waves and yet be able to sustain the stresses of large waves. Waves above the five meter size occur with low probability, and it is probably not cost effective to design the extraction system for operation above the five meter height. It is enough of a problem just to design the system to survive waves above five meters, let alone extract energy at those heights.

A great deal of impetus for the design of wave energy extraction systems occurred at the turn of the century. The motivation was generally the cost of delivering coal, then the primary fuel, long distances from the mine to the place of use. A good deal of interest, for example, was generated in the region of San Francisco (Stahl, 1892), which was at that time a developing city located a long way from coal reserves. Many of the devices proposed and used in these early times were of the "bobber" variety, which converted the rise and fall motion of the water into mechanical energy for use in pumping water or generating electricity.

The most recent wave energy system proposed takes advantage of the kinetic energy that moves through a vertical window and causes a to and fro motion of a vertical vane. This proposal is the only known active development in wave energy systems at the moment. Salter (1974) performed many laboratory evaluations of the vertical vane system. A continuation of the work is currently being funded by the British Department of Trade with the prospect that a considerable alternative energy source can be developed for the British Isles from the flow of wave energy in the environs of the Hebrides. Efficiencies of 40 percent have been obtained in the laboratory in the converting of wave energy to electrical energy, and Salter predicts that even better efficiencies are possible with improvements in the design of the vane shape. However, we have chosen to use 40 percent in our calculations of system requirements presented in Section IV. Although the 40 percent effi- ciency may be somewhat conservative from an ideal point of view, it is probably appropriate considering the difficulties of mechanizing these systems in the offshore environment.

Comparatively speaking, very little research and development activity is under way regarding wave energy devices. As we have noted, Salter's effort is the only known funded development under way at this moment. If such devices can be shown to be potentially useful in satisfying remote base energy needs, it may be appropriate to consider encouraging further analyses and developments in this area.

DoD Applications

We will determine here the general characteristics of a wave energy system applied to a typical remote base. Assume that the remote base requires an average of 10 megawatts of electrical power over the year. Further, assume that the wave energy system is designed to extract energy from waves of one meter height (4 kW per meter) to 5 meters height (245 kW per meter). Further, assume that the base is located for a rather fortunate incidence of wave energy as might be expected in the Northern Atlantic or Northern Pacific. In such a location we might expect an average year round ideal wave power level of 30 kW per meter of wave front. If the wave energy system extracts this power at a 40 percent efficiency, then we can expect an average 12 kW per meter output from the wave energy machine. In order to service a 10 megawatt average requirement, the required size of the wave machine is then 10/12 = 0.83 kilometers of wave front interception. For purposes of estimating the cost of our system, this 0.83 kilometers represents 203 megawatts of installed capability to transduce wave energy to mechanical energy and 81 megawatts of installed capability to transduce mechanical energy into electrical energy. Applying the aggregate cost factor of 3.5 to the diesel generator costs gives us an expected cost factor on installed capacity (that is, generator capacity, not wave transducing capacity) of $700 per kW. Since the average output of the wave energy system is dependent upon the average wave energy input, this installed capacity cost can be interpreted in terms of useful capacity on the average. Under the wave input conditions assumed in our hypothetical base of 30 kW per meter wave front average input of 12 kW per meter average electrical output, our overall cost for expected output becomes 700 times 81 divided by 12 = $4725 per kW.

On this basis the total cost of wave generation system to service the 10 megawatt average base load with a 30 megawatt per kilometer average wave input results in a total cost of $57 million, not including the energy storage system.

Since the incidence of wave energy will vary markedly across the annual cycles, it would be necessary to supplement the wave energy machine with a capability to store the electrical energy generated

during periods of excess flux, for use in the lean periods. Another prospect would be to supplement the wave energy system with a conventional diesel powered generator. In Section IV we will discuss the tradeoff among storage and conventional generation systems due to the variability of the indigenous input. We have calculated our maximum system sizes and energy output based on maximum wave height, or based on a stress limit. If our nominal input of energy includes levels above this stress limit, these will not be transduced into electrical energy.

System Cost Estimation

The status of development of wave energy devices is such that no useful information is available regarding the cost of such machines. It is thus necessary to develop a cost estimate based on analogy with existing generators. Assume that a diesel generator of the size unit that will be used in the wave system costs $200 per kW. Wave generators will differ in cost because of the following characteristics:

	Characteristic	Cost Multipliers
1.	Low speed	1-1/2
2.	Large stress tolerance	1-1/4
3.	Sea water environment	1-1/2
4.	Low production	1-1/4
	Aggregate cost factor	π = 3-1/2

The above cost factors are our subjective determinations but may give some feel for the incremental costs of wave energy transducers compared with diesel generators.

ENERGY STORAGE

The variable nature of indigenous energy supplies and the fluctuations of demand require a combination of conversion and storage systems to meet the remote base requirements. Wind and wave devices will inherently produce energy in the form of electricity and will benefit most by energy storage systems taking electricity as input. The solar devices considered produce thermal energy, which is used directly to

handle thermal loads or is converted to electricity through a Rankine
cycle system. Solar energy can thus be stored at either the thermal
or electrical stages, the former being more efficient in the short term.

Some current concepts for energy storage that seem applicable to
DoD needs are: chemical storage, in the form of either fuel cell pro-
duced hydrogen or electrochemical energy in the battery; thermal stor-
age; and the mechanical storage of energy by means of the flywheel.
Each of these techniques is discussed briefly with respect to its
applicability.

Chemical Storage

Fuel Cells. The purpose of the fuel cell is the direct conversion
of the chemical energy of fuel to electrical energy. The inherent ad-
vantage of the fuel cell is that it is not subject to the second law
of thermodynamics as is the more conventional heat engine. In the fuel
cell, electrochemical reactions supply power by driving current through
a loaded circuit. The electrochemical reactions take place as a result
of a continuous supply of fuel to the anode and oxidizing agent to the
cathode.

Two types of fuel cells that have been studied for central-station
power generation are the molten carbonate fuel cell and the solid elec-
trolyte fuel cell. Molten carbonate fuel cells use an electrolyte that
consists of a , .ary or tertiary eutectic of lithium, sodium, and po-
tassium carbonates.

A study of a large-scale fuel cell power plant of this type was
performed by the Central Electricity Generating Board in Great Britain
in 1962. The results made it apparent that the fuel cell generating
station does not achieve economic parity with the more conventional
steam turbine plant. A study by the Institute of Gas Technology in
1970 indicated that more research is needed in such problem areas as
cell performance and material technology of cell components.

A second type of fuel cell that might show applicability is the
solid-electrolyte variety. This fuel cell was examined by the West-
inghouse Electric Corporation in 1970 under Project Fuel Cell. The
electrolyte is a thin film of zirconia, the anode is a metal, and the

cathode is an electronically conductive oxide. The problems associated with the implementation of this fuel cell lie in the fabrication process for making the complete cell. There is no guarantee that solutions to the problems involved in the wide use of fuel cells will be forthcoming in the near future. Before large-scale development is practical, more research is needed at the small-scale stage.

Battery Storage. Electrical power is delivered by the storage battery as a result of electrochemical reactions occurring at two electrodes immersed in an electrolytic solution. Electrical energy is accepted and stored by reversing the chemical reactions. The important characteristics of the storage battery include its energy density expressed in watt hours per pound of total weight, its power density or rate of energy delivery, its life as determined by the number of cycles or recharges possible, and its cost.

Three types of batteries can be considered for bulk storage--conventional, metal-gas, and high-energy density alkali metal types. Table 6 shows some of the promising systems and their associated problems. As can be seen from Table 6, power density falls in the range of 30-100 W/lb and energy density falls in the range of 10-100 Wh/lb. The average life of the batteries is about five years. The cost of lead-acid batteries is about $80/kWh.

Table 6

STORAGE AND CONVERSION SYSTEMS

| System | Type | Performance | | | Problems |
		Energy Density (Wh/lb)	Power Density (W/lb)	Cycle Life	
Lead acid	Conventional	10	20-30	1500	--
Zinc-chlorine	Metal-gas	50-70	40-60	Unknown	Life
Sodium-sulfur	Alkali	80-100	80-100	200-2000	Life and cost
Lithium-sulfur	Alkali	100	> 10	2000	Corrosion and cost

Advances in battery technology are expected to come from metal-gas and alkali-metal high-temperature batteries. There are many problems remaining with regard to the battery system. Among them are the materials availability question (such as zinc and lead), the problem of scaling up from the present-day kW size to the MW size, and heat transfer and dissipation.

Thermal Storage

Energy storage is possible through the vaporization, melting, or simply the heating of a material. The energy becomes useful heat when the process is reversed. There are two methods currently available for thermal storage.

The Sensible-heat Method. The sensible-heat method accomplishes storage by causing a material to rise in temperature. For the most effective results, the object chosen should have a high specific heat. Materials frequently used in this way include water, rock, and liquid sodium. Limitations to the sensible method include the requirement for large amounts of space and extensive insulation.

In a feasibility study of a solar energy plant for the southwest, it was found that to accommodate 10 hours of storage, 1 million cubic meters of sodium acting as both the storage medium and the transfer fluid would be necessary.[1] It was concluded that solar power plants utilizing the sensible method could be most useful as a supplement to the primary load source.

The Latent-heat Method. A phase change is, of course, necessary for a method that utilizes latent heat. Thus, either fusion or vaporization may be considered. For example, storing of heat might be accomplished by the melting of a solid storage medium. When the heat is required, the liquid is simply resolidified, giving up its latent heat of fusion. The advantage of this method over the sensible method is that a greater amount of heat may be stored in the equivalent volume of material. Additionally, a much smaller temperature range (a few degrees on either side of the transformation point) is required by the latent heat method.

---

[1] Mason Watson, Aerospace Corporation, El Segundo, California.

The latent heat method also has limitations, many resulting from the heat-of-fusion material itself. These materials are expensive, usually corrosive, and prone to supercooling. Storage effectiveness is limited, as well, by the problem of the transfer of heat to the storage medium from the working fluid.

The materials considered for heat-of-fusion storage probably number in the thousands. Currently several laboratories are examining eutectic salts, such as sodium nitrate-sodium chloride, as possibilities for solar energy generating plants. When thermal storage is the only heat source in a system, its high cost may be bearable. However, if circumstances require the addition of an auxiliary or backup heat source then the total cost of the system could be economically prohibitive.

Flywheels

The energy stored in a rapidly rotating flywheel is given by

$$E = \tfrac{1}{2}\, I\omega^2$$

where E is the stored energy, I is the moment of inertia, and ω is the angular frequency in radians per second.

Theoretically, by increasing the mass of the flywheel material, unlimited capacity could be achieved. However, the high stress placed on materials of limited strength often causes the flywheel to fail. Currently, research is being done on materials shaped into long thin fibres that exhibit unidirectional mechanical properties. Materials of this type include boron filaments, fiberglass, steel wires, bulk glass, and Kevlar, an organic material from the DuPont Company. Although the cost of these unusual materials is quite high, it might be lowered by the use of ballast materials. The unidirectional materials would be configured as either a fanned circular brush or as consecutive loops of fibres. Such a flywheel system has an estimated storage efficiency of 80 to 90 percent.

Materials and design testing is well underway at a number of facilities (for example, the Johns Hopkins Laboratory), but widespread use of the flywheel in power station energy storage applications is not predicted for the near future.

IV. PARAMETRIC ANALYSIS OF COMBINATION BASE ENERGY SYSTEMS

In this section we evaluate the relative usefulness of solar,
wind, and wave indigenous energy sources in satisfying remote base
power requirements by minimizing equipment sizes and capitalization
costs of various combined indigenous and conventional engine generat-
ing systems for a standard base and then comparing the results. The
methodology developed to do this involves constructing a power-system
flow scheme common to all three indigenous sources. Next, we describe
how solar, wind, and wave power fluxes have been chosen to represent
the power inputs to a standard-remote base (defined below) at various
geographic locations. Standard-base electrical and space heating de-
mands are similarly selected and tabulated. The power inputs and
demands are then used in conjunction with the power-system flow scheme
to obtain optimal equipment size parameters for various combined in-
digenous and conventional engine generating systems. Finally, using
unit cost estimates presented below, capitalization costs of these
various combined systems are calculated and discussed.

METHODOLOGY

The Standard Base

To compare indigenous fuel sources, it was necessary to define a
standard base and ask how its particular energy demand could be met by
each of the indigenous sources as the base was conceptual moved from
one world region to another. A survey of remote bases indicated that
the total energy demand of these facilities was generally on the order
of 10 MW (thermal) or less. These power demands are low because these
bases are specialized and consequently require only a small area and
group of personnel to carry out their assigned tasks. An exception to
this is the base at Adak, Alaska, which carries out NAVFAC, NAVCOM,
SECGRU, and NAVSTA activities and has a base energy demand of nearly
40 MW (thermal) (excluding motor vehicle and aircraft fuel demands).
Because the NAVCOM base at Diego Garcia has an energy demand representa-
tive of the more populous smaller remote bases, it was chosen as our
standard base (SB).

It is clear that the energy demands of a standard base will include both space heating and air-conditioning demands. These demands are primarily dependent on the location of the base and not on the actual operations of the base. Electrical energy demand that does not include the power requirements of air-conditioning may therefore be identified as the energy demand that is characteristic only of SB function. The annual average electrical demand at Diego Garcia is 2.74 MW (electrical) (Gillette and Schubert, 1974), and the average (SB) demand exclusive of air-conditioning requirements has been estimated to be 2.35 MWe.

The Power System

A power scheme capable of describing the use of any of our three indigenous energy sources by a simple change of parameters was developed in order to facilitate comparison of alternative power systems. Because there was an expectation that there were particular combinations of indigenous and conventional hydrocarbon systems that would reduce fuel oil requirements, system cost, or dependency on developing technology below certain desired levels, the power scheme was structured to provide for varying degrees of utilization of conventional and indigenous energy sources.

The power system uses SB space heating and electrical demands by location as input in conjunction with indigenous input power levels for any one of the solar, wind, or wave sources. The fraction of total demand satisfied by the indigenous source in the combined systems is determined by taking an arbitrary percentage of the size of the energy collection device needed for totally indigenous operation. The power scheme calculates equipment size parameters as output, and these are used in making the equipment cost estimated below.

Because indigenous energy sources are not usually in an immediately useful form--i.e., either thermal or electrical energy--power systems using such sources must include appropriate energy conversion devices. Furthermore, because indigenous energy fluxes seldom equal corresponding demand, optimized systems generally require that energy be stored during periods of excessive input for later use. The power system

developed here and shown in Fig. 6 incorporates both of these general features. In this power model, the storage of energy has been assumed to be accomplished by the use of either fuel cells (to produce hydrogen) or batteries, since their technologies are fairly far advanced.

We now briefly discuss the operational characteristics of the power system in Fig. 6. For a more detailed discussion, including the derivation of appropriate energy balances and operations equations, see Appendix D.

Indigenous energy is collected and input at a power rate $J \cdot A$ at the top of the figure. Solar radiative energy is assumed to be absorbed by a solar thermal collector, and wind and wave energies are assumed to be converted to electrical power by windmill and wave machine devices. Because the heat from solar energy is immediately useful for space heating, it is used for this purpose before being used for electricity generation. This solar heat flows along the path denoted by $Q5$ and $q5$. The remainder of the solar energy and all wind and wave energy passes along the path $Q4$, $q4$ where it is converted to electrical power. The direct use of solar power for heating avoids the severe efficiency losses incurred by the options of using solar energy to produce electricity and then heating electrically, or producing hydrogen electrically and then combusting it for heat.

In order to minimize the energy losses that occur when any form of energy is stored, the electrical power produced by the generators has first been used to satisfy instantaneous electrical demand with only the excess going to storage. The power used immediately for electrical demand is $Q3$, and the input to storage is $Q1$.

When indigenous energy is not available in sufficient quantities to fully satisfy space heating and electrical demands, the excess of demand over the amount available is met by withdrawing power from storage at the rate $Q2$ to satisfy electrical requirements and at the rate $Q6$ to satisfy space heating requirements.

When storage capacity has been completely exhausted in the case of combined indigenous and engine generator systems, the excess electrical demand is met by operating an engine generator at the rate b_1 (see right-hand side of Fig. 6), and excess space heating demand is
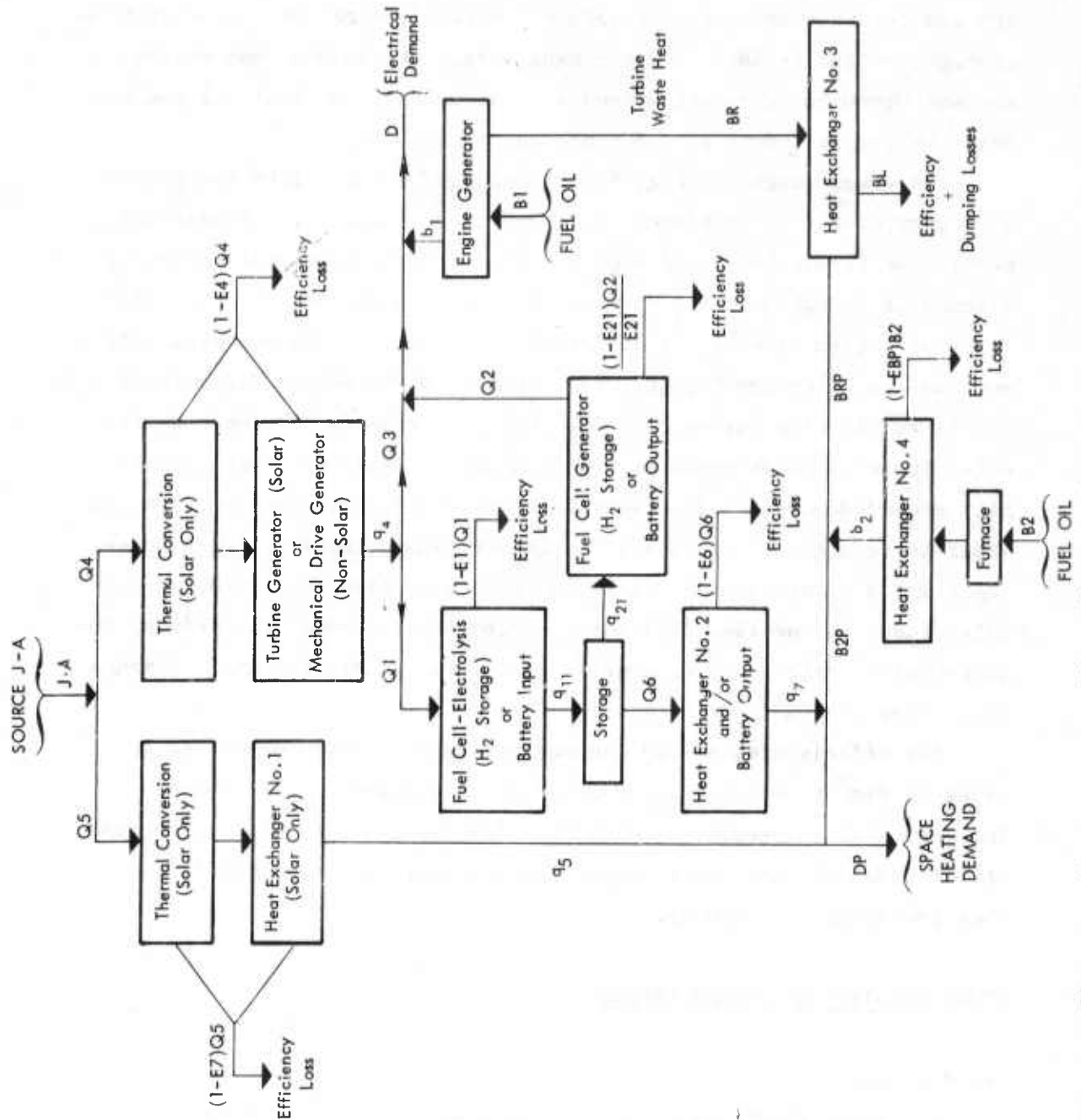
Fig. 6— The general power system flow scheme applicable to solar, wind, or wave indigenous energy sources used in combination with conventional diesel/turbines

met by operating a furnace (see bottom of Fig. 6) at the rate b_2. The demands on the furnace are reduced when the engine generator is operating since it is assumed that some of the turbine waste heat may be recovered at rate BR and used for space heating. Because energy from the indigenous source, either obtained directly from the source or from storage, satisfies base energy demand before the furnace and engine systems are used, the system uses a minimum amount of fuel oil and thus helps to reduce remote base dependence on fuel oil.

The power scheme of Fig. 6 has been used to calculate the amount of energy contained in storage as a function of the time of year for a particular remote base (see Appendix D). This is important because it allowed us to optimize the storage capacity and collector device size of remote bases with widely different time dependencies of total demand and indigenous energy inputs. For example, when average daily input fluxes remain high for an extended period of time (as is the case for solar input in polar regions), it is apparent that input will generally exceed demand and considerable storage will have to take place in order to have energy available for leaner times. However, if average daily input fluxes remain nearly constant over time (as in the case of solar input in constant cloudiness equatorial regions), the primary requirement of storage is to provide energy to satisfy the small demands that occur over a 24-hr period.

The efficiencies of the various energy conversion processes indicated in Fig. 6 have been collected in Table 7 for each of the three indigenous energy sources. Note that for the case of solar energy use, efficiencies E4, E6, and E7 represent combined conversion efficiencies (see footnotes of Table 7).

POWER DENSITY AND DEMAND INPUTS

Input Fluxes

The power densities of solar radiation and wind and wave motion have been shown in Section II to be highly dependent upon latitude and longitude as well as the time of year. The specific locations chosen to provide input data for our power system model are representative of

Table 7

OPERATING EFFICIENCIES EMPLOYED IN THE SOLAR, WIND,
AND WAVE POWER SYSTEMS

(Percent)

Variable	Definition	Value		
		Solar	Wind	Wave
E1	Electrolysis	83	83	83
	Battery storage	75	75	75
E4	Radiative-thermal and thermal-electric	11[a]	--	--
	Mechanical-electric	--	40	40
E21	Chemical-electric	60	60	60
	Battery storage	75	75	75
E6	Heat exchanger	80	80	80
	Heat exchanger and battery storage	60	60	60
EB	Thermal-electric	30	30	30
EBP	Heat exchanger	80	80	80
ER	Heat exchanger (low ΔT)	47	47	47
E7	Radiative-thermal and heat exchanger	52[b]		--

[a]This is a combined efficiency. The radiative-thermal conversion efficiency is 60 percent and the thermal-electric efficiency is taken as 18 percent.

[b]This is a combined efficiency. The radiative-thermal conversion efficiency is 65 percent and the heat exchanger efficiency is 80 percent.

the Far North Atlantic Ocean, Mid North Atlantic Ocean, Caribbean, West Indian Ocean, and North Pacific Ocean regions described earlier, each region corresponding to remote bases at Keflavik (Iceland), the Azores, Sebana Seca (Puerto Rico), Diego Garcia, and Adak (Aleutian Islands). It is important to note, however, that the results obtained below correspond not to the actual bases at these locations but rather to *our*

standard base if it were located there. This distinction is of particular consequence in the case of Keflavik (Iceland), because although geothermal sources are known to be capable of providing significant power for this particular location, these sources are not generally available throughout the Far North Atlantic region.

The input data for these locations are summarized in Table 8 where the solar and wind fluxes for months other than January, April, July, and October, and wave fluxes for months other than February, March, August, and November, have been obtained by linear interpolation. Although more detailed data are available for solar radiation, the wind and wave data are generally limited to these few months.

As may be seen from a comparison with Table 2, the wind and wave fluxes generally agree with the regional average monthly values. However, the solar fluxes compiled in the earlier table refer to radiation that falls on a unit surface tangent to the earth's surface. Since the best solar collectors do not lie flat on the ground, these data were converted to the appropriate incident surface.

The solar collector assumed to be used in our model power system is a flat plate collector with a very low emissivity coating mounted inside an evacuated tube. This selective coating must be present if the temperature of the working fluid has any possibility of reaching the moderately high temperatures (400°F) required to give an 18 percent turbine-generator efficiency (the efficiency used in Table 7) (Hottel and Howard, 1971). The surface has been assumed to convert 60 percent of the collected radiation into thermal energy.

The collector has also been assumed to be oriented so that the rays of the sun are normal to the collector at noon (requires season adjustment). Although this orientation of the collector gives up some energy (approximately 33 percent) by not tracking the sun throughout the day, it does avoid using fairly sophisticated tracking equipment and thus the accompanying capital and maintenance costs. If land area at a remote base were extremely valuable, then the expense of the land

Table 8

INPUT FLUXES: J_{solar}, J_{wind}, J_{wave} [a]

Total radiation (MW/km^2)
(Monthly avg. solar radiation on a fixed surface normal to sun's ray at zenith)

Location	J	F	M	A	M	J	J	A	S	O	N	D
Diego Garcia	287	264	242	219	219	218	218	220	222	224	245	266
Sebana Seca	281	281	280	280	282	285	287	267	246	226	244	263
Adak	124	141	158	175	148	120	93	101	109	117	119	122
Azores	191	204	218	231	224	216	209	211	214	216	208	199
Iceland	95	155	216	276	255	233	212	169	127	84	88	91

Wind (MW/km^2)
(Monthly avg. wind power density on a windmill cross-sectional area)

Location	J	F	M	A	M	J	J	A	S	O	N	D
Diego Garcia	230	200	170	150	180	210	240	330	410	500	410	320
Sebana Seca	460	370	280	190	210	240	260	250	240	230	310	380
Adak	1230	1220	1200	1190	960	730	500	720	950	1170	1190	1210
Azores	850	730	620	500	460	420	380	360	340	320	500	670
Iceland	1360	1380	1410	1430	1090	740	400	670	940	1210	1260	1310

Wave (MW/km)
(Monthly avg. wave power density per unit length of wave machine frontage)

Location	J	F	M	A	M	J	J	A	S	O	N	D
Diego Garcia	3	3	3	3	3	12	21	30	21	12	3	8
Sebana Seca	27	30	21	12	3	3	3	3	9	15	21	28
Adak	40	30	30	30	30	21	12	3	22	41	60	50
Azores	60	60	50	40	30	21	12	3	22	41	60	60
Iceland	30	30	30	30	30	40	50	60	50	40	30	30

[a]It should be remembered that the input locations are only approximate geographic locations and do not represent specific military bases. Local power densities at specific military bases could differ markedly, depending on local conditions, from those shown.

committed to collectors to make up for this tracking loss might be better spent on a tracking system.[1]

This collector geometry has been used to recalculate the horizontal incidence data presented in Section II to give the average daily total radiation on a fixed surface (representing the cross-sectional area of collector) perpendicular to the incoming radiation when the sun is at its zenith. These calculations are performed in Appendix C and the results are presented in Table 8 for each of our five regional locations. The radiation values include corrections for local cloudiness conditions.

The cylindrical parabolic collector system (or possibly a cylindrical tube collector) is more easily capable of reaching 400°F. However, when this system is used, it is necessary to reduce the total radiation values in Table 8 by an average of about 40 percent to remove the non-focusable diffuse radiation; this implies, of course, that collector areas (and costs) have to be increased proportionately in any final system configuration.

The radiation and efficiency data of Tables 7 and 8 also apply to the case of photoelectric solar cells. Silicon solar cells have a radiation to electricity efficiency of 12 percent (Hottel and Howard, 1974) rather than the 11 percent efficiency used here for the thermal solar system. If these cells are assumed to be only seasonally adjustable, then the same collector geometry as described above would still be applicable.

The wind and wave power densities have been obtained by the technique described in Appendix B for converting worldwide isoprobability data into power potential information. The wind velocity probability distribution (as shown in Fig. B-1) corresponding to each remote base location was selected for various times of the year, and then the

---

[1]Calculations on flat plate collectors were performed to determine daily fixed and steerable system energy losses, taking full account of the interference between steerable collectors at low angles of solar incidence. The steerable case leads to a greater collection efficiency than the fixed collector for all spacings between collectors except when they are immediately adjacent to each other, in which case the efficiencies are equal.

average power for each base area was determined from the wind power potential plot of Fig. B-2. An analogous procedure was followed for the wave data.

The actual input data used in solving our model power systems also had to reflect the fluctuations that occurred in the energy fluxes over periods of 24 hr or less. When an indigenous power source falls to a very low value for even a short period of time, the energy that fills demand during this period has to have been stored earlier in the day. In the process of storing this energy, considerable loss is incurred owing to the fuel cell or battery inefficiencies. If only monthly average values had been used for the input fluxes, much of the implied constant daily generator output would have gone to satisfy electrical demand directly and would therefore have (incorrectly) bypassed the storage losses.

Solar fluxes were accordingly assumed to be equal to twice their monthly average value for 12 hr and zero over the following 12 hr. More detailed treatment of the length of day by latitude and season was not generally necessary since it was shown to make only insignificant changes in our computed power system parameters. Wind fluxes generally show less extreme fluctuations than solar insolation, the average daily high fluxes being only about four times the low (Golding, 1955). Trial runs of our model were made using this factor of four, but only 9 percent maximum variations in power system parameters (particularly windmill areas) were found to result. Thus average monthly values were used for most wind calculations. Finally, because wave power densities show the least daily fluctuation, average monthly flux values were used throughout this work.

Demand Data

Energy demand for each remote base location is composed of an electrical and a space heating demand. Space heating demand is currently met by the output of steam plants, and it is assumed here that steam will continue to serve this function into the foreseeable future. Electrical demand has been assumed to be composed of a fraction representing location-independent base-function demand and another fraction representing location-dependent air-conditioning demand.

Monthly cooling estimates were obtained for the Azores, Sebana
Seca, and Diego Garcia from the basic heating, ventilating, and air-
conditioning (HVAC) energy requirements determined by Salter et al.
(1975). This work gave data for several geographic locations in the
United States. Using the annual temperature profiles of each of the
remote base areas, we have approximated electrical cooling demand in
the Azores by the demand in Los Angeles and demands in Diego Garcia
and Sebana Seca by that in Miami. Lighting levels were taken to be
2.7 W/sq ft, and the average building was represented as a half glass
and half opaque structure. HVAC cooling demands were given as Btu/
sq ft per month, and these were converted to standard base demand by
multiplying by the total square footage at the base (602,000 ft^2 was
used for our standard base). The average cooling demand was thus cal-
culated to be 0.39 MW at Diego Garcia and Sebana Seca, and 0.23 MW at
the Azores. This amounts to an air-conditioning demand in the former
two bases that is about 14 percent of total electrical demand. Heat-
ing requirements for the Azores were also obtained from the HVAC data,
but heating estimates for Diego Garcia and Sebana Seca were taken to
be zero since the mean winter temperature in these regions is much
greater than in Miami.

Because no city treated in the HVAC work was representative of
Adak or Iceland, their heating and cooling estimates had to be obtained
elsewhere. They could be treated together since their mean January
and July temperatures are quite similar: 33°F and 50°F for Adak, 31°F
and 52°F for Iceland (Times Atlas, 1967). With a mean high of only
50+°, cooling demand was assumed to be zero. Space heating demand
variation as a function of the time of year was estimated from the
DEIS (1974) monthly fuel oil (FSX) consumption figures since space
heating requirements dominate the demand for fuel oil at this northern
latitude. This variation was scaled to give an annual heating demand
that equaled the average Adak steam plant output per sq ft multiplied
by the square footage of our standard base.

The annual average electrical power at Diego Garcia is 2.74 MW
(Gillette and Schubert, 1974). This was spread over the year according
to the DEIS (1974) fuel oil consumption data (fuel oil in Diego Garcia

is used for electricity generation since space heating demand is gen-erally absent). Then the HVAC monthly cooling power demands were sub-tracted from the total monthly demand, giving an estimate of our standard base *location-independent* electrical demand. The cooling power demands at other locations were then added to this, giving us the *location-dependent* electrical demands summarized in Table 9.

Table 9

ELECTRICAL AND SPACE HEATING DEMAND BY REGION (MW)

Location	Month											
	J	F	M	A	M	J	J	A	S	O	N	D
Electrical Demand												
Diego Garcia	2.87	2.54	2.80	3.07	2.91	2.75	2.59	2.43	2.27	2.58	2.89	3.20
Sebana Seca	2.87	2.54	2.80	3.07	2.91	2.75	2.59	2.43	2.27	2.58	2.89	3.20
Adak	2.62	2.32	2.50	2.69	2.47	2.27	2.06	1.86	1.79	2.10	2.59	2.90
Azores	2.80	2.48	2.70	2.88	2.71	2.53	2.37	2.19	2.03	2.36	2.79	3.10
Iceland	2.62	2.32	2.50	2.69	2.47	2.27	2.06	1.86	1.79	2.10	2.59	2.90
Space Heat Demand												
Diego Garcia	0		0	0	0	0	0	0	0	0	0	0
Sebana Seca	0		0	0	0	0	0	0	0	0	0	0
Adak	3.90	4.11	2.93	1.75	2.01	2.26	2.52	2.78	3.03	3.26	3.48	3.70
Azores	.42	.24	.26	.24	.15	0	0	0	0	.10	.26	.27
Iceland	6.23	6.55	4.67	2.79	3.20	3.61	4.02	4.43	4.84	5.19	5.55	5.90

Standard-base space heating demands in our five regions also appear in Table 9. It is apparent that space heating variations are the dominant demand variable, particularly when they are compared by location. In Adak and Iceland, where space heating demands are high, fluctuations in total demand by season are also dominated by space heating variations.

POWER SYSTEM SIMULATIONS

The power system model represented by Eqs. (D.1) through (D.17) was solved for ten system configurations for each indigenous energy type. The first configuration was for a remote base run entirely on indigenous energy supply. The next nine configurations progressively reduced the size of the energy collection device--i.e., the area of solar collectors and windmills and the frontage length of wave machines--by equal increments so that the tenth configuration represented a totally diesel-turbine powered system. The model equations were solved for indigenous energy collector size, energy storage, and engine and furnace power inputs as a function of time of year. Additionally, storage capacity (determined by the difference between maximum and minimum storage values) and annual fuel oil consumption (representing the time integral of both engine generator and furnace inputs) were calculated.

The results of these simulations for each of five locations are summarized in Tables 10-14. Collector sizes, storage capacities, and annual fuel consumption data are listed.[1] Also included are the maximum and minimum average monthly electrical (D) and space heating (DP) power demands since they are used later in our costing estimates.

Examination of the data in Tables 10-14 reveals several general trends. The most important one is that as use of the engine generator is phased into the power system, the storage capacity requirements rapidly drop off. At some point they become zero when indigenous input power being generated is always less than electrical demand and thus provides no excess energy for storage. This effect holds for all three energy sources, although the storage drops to zero most rapidly in the case of solar energy.

The storage capacity is the smallest for solar input at Diego Garcia and Sebana Seca because of the three input fluxes, solar insolation (on a daily average basis) is the closest to being constant and thus most able to be scaled (by an appropriate choice of collector size) to equal the also nearly constant electrical demand. As total solar

---

[1]Fuel consumption values are given in units of megawatt-hours and may be converted to bbl of fuel oil by multiplying by 0.5855 bbl/MWH.

Table 10

POWER SYSTEM PARAMETERS, DIEGO GARCIA

(H_2 storage)

Power Demand Extrema: D_{min} = 2.269 MW, D_{max} = 3.196 MW, DP_{min} = 0 MW, DP_{max} = 0 MW

Indigenous Energy Type	Collector Area (km^2)	Storage (MWH)	Fuel (MWH)
Solar	.1313	1143.	0
"	.1167	245.	6708.
"	.1021	23.	13252.
"	.0875	15.	19795.
"	.0729	8.	26549.
"	.0583	2.	35257.
"	.0438	0.	46050.
"	.0292	0.	56999.
"	.0146	0.	67950.
"	0.	0.	78888.

Indigenous Energy Type	Windmill Area (km^2)	Storage (MWH)	Fuel (MWH)
Wind	.02772	5163.0	0.
"	.02464	3664.6	7007.8
"	.02156	2428.4	14449.8
"	.01848	1215.0	21937.2
"	.01540	452.3	30292.1
"	.01232	0.	39285.5
"	.00924	0.	49190.5
"	.00616	0.	59095.6
"	.00308	0.	68996.6
"	0.	0.	78887.6

Indigenous Energy Type	Wave Machine Frontage (km)	Storage (MWH)	Fuel (MWH)
Wave	.9631	14554.6	0.
"	.8561	12102.9	7099.4
"	.7491	9648.9	14243.9
"	.6420	7195.1	21282.2
"	.5350	4854.2	28587.6
"	.4280	3012.7	36906.5
"	.3210	1170.6	45207.9
"	.2140	82.7	55033.9
"	.1070	0.	66885.4
"	0.	0.	78887.6

Table 11

POWER SYSTEM PARAMETERS, SEBANA SECA

(H_2 storage)

Power Demand Extrema: D_{min} = 2.269 MW, D_{max} = 3.196 MW, DP_{min} = 0. MW, DP_{max} = 0. MW

Indigenous Energy Type	Collector Area (km^2)	Storage (MWH)	Fuel (MWH)
Solar	.1158	1104.	0.
"	.1029	31.	6538.
"	.0901	17.	13101.
"	.0772	11.	19666.
"	.0643	4.	26449.
"	.0515	0.	35043.
"	.0386	0.	46004.
"	.0257	0.	57012.
"	.0129	0.	67953.
"	.0129	0.	78888.

Indigenous Energy Type	Windmill Area (km^2)	Storage (MWH)	Fuel (MWH)
Wind	.02576	2551.	0.
"	.02290	1501.	6672.
"	.02004	744	14613.
"	.01717	175	22878.
"	.01431	0.	31915.
"	.01145	0.	41313.
"	.00859	0.	50710.
"	.00572	0.	60109.
"	.00286	0.	69500.
"	0.	0.	78888.

Indigenous Energy Type	Wave Machine Frontage (km)	Storage (MWH)	Fuel (MWH)
Wave	.5989	9732.	0.
"	.5323	7495.	6556.
"	.4658	5279.	13097.
"	.3992	3172.	19868.
"	.3327	1334.	26862.
"	.2662	421.	35955.
"	.1996	0.	46092.
"	.1331	0.	57029.
"	.0665	0.	67965.
"	0.	0.	78888.

Table 12

POWER SYSTEM PARAMETERS, ADAK

(H_2 storage)

Power Demand Extrema: D_{min} = 1.792 MW D_{max} = 2.896 MW, DP_{min} = 1.748 MW, DP_{max} = 4.1087 MW

Indigenous Energy Type	Collector Area (km^2)	Storage (MWH)	Fuel (MWH)
Solar	.2650	2059.	0.
"	.2356	819.	7352.
"	.2061	130	14455.
"	.1767	16.	21558.
"	.1472	10.	29351.
"	.1178	4.	37743.
"	.0883	0.	47625.
"	.0589	0.	57573.
"	.0294	0.	66903.
"	0.	0.	73864.

Indigenous Energy Type	Windmill Area (km^2)	Storage (MWH)	Fuel (MWH)
Wind	.01666	2770.	0.
"	.01481	1263.	5509.
"	.01296	506.	10946.
"	.01110	31.	16393.
"	.00925	0.	21989.
"	.00740	0.	27804.
"	.00555	0.	34687.
"	.00370	0.	46269.
"	.00185	0.	59309.
"	0.	0.	73864.

Indigenous Energy Type	Wave Machine Frontage (km)	Storage (MWH)	Fuel (MWH)
Wave	.5614	6499.	0.
"	.4990	4146.	5885.
"	.4367	1865.	11481.
"	.3743	0.	17260.
"	.3119	0.	23089.
"	.2495	0.	29040.
"	.1871	0.	36144.
"	.1248	0.	46150.
"	.0624	0.	59089.
"	0.	0.	73672.

Table 13

POWER SYSTEM PARAMETERS, AZORES

(H_2 storage)

Power Demand Extrema: D_{min} = 2.034 MW, D_{max} = 3.095 MW, DP_{min} = 0. MW, DP_{max} = .4160 MW

Indigenous Energy Type	Collector Area (km^2)	Storage (MWH)	Fuel (MWH)
Solar	.1400	1474.	0.
"	.1244	503.	6417.
"	.1089	32.	12653.
"	.0933	15.	18890.
"	.0788	9.	25555.
"	.0622	3.	33757.
"	.0467	0.	43929.
"	.0311	0.	54358.
"	.0156	0.	64788.
"	0.	0.	74253.

Indigenous Energy Type	Windmill Area (km^2)	Storage (MWH)	Fuel (MWH)
Wind	.01426	2087.	0.
"	.01268	1086.	6297.
"	.01109	449.	12772.
"	.00951	0.	20013.
"	.00792	0.	27785.
"	.00634	0.	36821.
"	.00475	0.	46176.
"	.00317	0.	55529.
"	.00158	0.	64883.
"		0.	74253.

Indigenous Energy Type	Wave Machine Frontage (km)	Storage (MWH)	Fuel (MWH)
Wave	.2088	5523.	0.
"	.1856	3600.	6126.
"	.1624	1779.	12514.
"	.1392	292.	18277.
"	.1160	0.	24484.
"	.0928	0.	33367.
"	.0696	0.	43585.
"	.0464	0.	53802.
"	.0232	0.	64019.
"	0.	0.	74253.

Table 14

POWER SYSTEM PARAMETERS, KEFLAVIK

(H_2 storage)

Power Demand Extrema: D_{min} = 1.792 MW, D_{max} = 2.896 MW, DP_{min} = 2.7785 MW, DP_{max} = 6.5541 MW

Indigenous Energy Type	Collector Area (km^2)	Storage (MWH)	Fuel (MWH)
Solar	.2393	8967.	0.
"	.2127	6117.	7763.
"	.1861	3298.	15042.
"	.1595	1202.	22263.
"	.1329	32.	30980.
"	.1063	19.	41215.
"	.0798	6.	51963.
"	.0532	0.	63154.
"	.0266	0.	75539.
"	0.	0.	91209.

Indigenous Energy Type	Windmill Area (km^2)	Storage (MWH)	Fuel (MWH)
Wind	.02153	6041.	0.
"	.01913	3808.	7673.
"	.01674	1622	15225.
"	.01435	795.	22792.
"	.01196	0.	30465.
"	.00957	0.	38314.
"	.00717	0.	46314.
"	.00478	0.	56012.
"	.00239	0.	73210.
"	0.	0.	91211.

Indigenous Energy Type	Wave Machine Frontage (km)	Storage (MWH)	Fuel (MWH)
Wave	.6315	10869	0.
"	.5614	6854.	7676.
"	.4912	3499	15256.
"	.4210	1120.	22806.
"	.3509	0.	30351.
"	.2807	0.	37897.
"	.2105	0.	46005.
"	.1403	0.	58146.
"	.0702	0.	73198.
"	0.	0.	91185.

radiation and total energy demand become slightly more variable over the year, as in the Azores, they are less able to be scaled into each other. Thus, a slightly increased storage capacity is needed to smooth out input energy to match demand. Solar input and total energy demand are most poorly matched in Iceland and one must go to a collector size that is only 55 percent of the totally indigenous value before the storage requirement is reduced to a nominal value.

Similarly, the often slow rate of decrease in storage capacity requirements for wind and wave systems results from the difficulty of matching of wind and wave power input to demand. From Table 8 the wave energy fluxes for Diego Garcia and Sebana Seca are seen to be the most variable of all inputs and thus most mismatched with base energy demand. The fact that the wave energy storage requirement in Table 10 for Diego Garcia does not drop to zero until the ninth configuration is a reflection of this.

The importance of the rapidly decreasing storage capacity is that another storage system besides the fuel cell and hydrogen system may be substituted for it, particularly if it is technologically feasible or cost effective only at low storage levels. We have therefore also considered a battery storage system. Because the efficiency of charging and discharging storage batteries (75 percent) is about the same as fuel cell electrolysis (83 percent) and electricity generation (60 percent), the power system parameters in Tables 10 through 14 are little changed with this alternative storage scheme. However, as will be seen below, costs are strongly affected.

Another general trend in the data is the consistently smaller windmill area (vertical) than solar collector area (horizontal) required at the same geographic location. If one were to assume that windmill base areas were equal to their blade cross-sectional area, then windmill systems require five to ten times less land area. There would be an even smaller land requirement in the case of stacked arrangements of windmills spread out over a thin strip of land where one row of windmills would not lie in front of another, and great distances between windmills would not be required to prevent the "shadowing" of one by another.

The relative sizes of the solar collectors follow the order expected from the demands in Table 8--i.e., Diego Garcia and Sebana Seca have collector sizes that are less than those for the Azores, and the Azores values are less than those for Adak and Iceland. Adak, however, has a slightly larger collector area requirement than Iceland, even though Keflavik has the higher space heating demand. This reversal is explained by the 31 percent higher average annual solar radiation in Iceland than in Adak, which results from the prevalence of clean conditions during Icelandic summer months while generally cloudy conditions prevail at Adak. This solar radiation increase more than makes up for the increased heating load.

Windmill areas and wave machine frontage for both Diego Garcia and Sebana Seca are large and comparable to the corresponding parameters for Adak where total energy demand is significantly higher, simply reflecting the low indigenous power densities found in Caribbean and Indian Ocean areas. The windmill areas in the Azores are comparable to the areas required in Adak or Iceland because although wind power densities in the Azores are less than in Adak, so is total energy demand. Wave machine frontage in the Azores is less than that required for Adak because the Azores' energy demand is lower while the power densities are comparable.

The annual fuel consumption for the engine generator-furnace system in the five regions (Tables 10-14) is approximately 75,000 MWH (44,000 bbl) except in Iceland, where consumption jumps to 91,000 MWH (53,000 bbl). This results from the greatly increased space heating demand at Iceland relative to the others. A similar jump in fuel consumption, although expected, is not observed when one compares Diego Garcia with Adak because the waste heat that is recovered from the engine generator at Adak is nearly always sufficient to satisfy peak demands for space heat. Because we have used the operating rule that turns on the engine generator and furnace only when the storage is completely exhausted, engine waste heat always becomes available at the moment space heating demand exceeds the ability of storage to provide it.

Finally, the annual fuel consumption figures for the engine generator-furnace system for Diego Garcia, Sebana Seca, the Azores, and Adak, although of the same general order of magnitude, show an ordering that is the reverse of total energy demand. This reversal also comes about because of the ability of waste engine heat to satisfy space heating demand, thus leading to a fuel consumption ordering that parallels the electrical demand for these regions (see Table 8).

COSTING

As stated earlier, our purpose in examining the use of indigenous renewable energy resources at remote bases are to reduce the current dependence of the bases on petroleum fuel and to lessen the vulnerability of energy supply to a long line of transportation. There are many options for achieving either purpose; for example, completely depending on indigenous resources, stockpiling petroleum, or using combinations of petroleum fuel and indigenous resources.

The choice of a solution is at least partially based on how much it will cost to provide a desired capability. Because the technologies for utilizing the resources examined are in different stages of maturity, we focus in this study on the first costs (i.e., unit production costs plus R&D costs) of the devices required for power production. Operating costs will not be included in the cost figures because some of the devices--e.g., wave motion machines--are in the prototype stage and therefore do not provide accurate information about either their long-term manpower operating requirements or their maintenance characteristics. Should the first cost estimates in this study make the use of a particular indigenous power device appear desirable in the future, more data on routine operation need to be collected and analyzed before total system costs can be known.

Cost Factors and Equipment Costs

First costs depend on research and development costs. Because the nondefense sector, primarily the National Science Foundation, is actively exploring solar and wind technologies (Interagency Task Force, 1974), it is expected that this sector, and not the DoD, will bear the primary

weight of R&D costs. Less work is being performed by the nondefense sector on wave energy conversion devices, and hence these R&D costs would have to be supported by the DoD.

The R&D costs of wave machine development are expected to make a small contribution to first costs, primarily because the basic mechanical energy conversion technology is well known. If we conjecture that the R&D cost of wave machines will be *up to* ten times the actual manufacturing cost of the first unit (this R&D factor being far in excess of that found in the mechanical development of generators or moderate stress airframes), it is apparent that a total production of 100 units will lead to a unit cost only 10 percent or less of which is attributable to R&D. A total production run of 100 units does in fact appear reasonable because a single wave machine unit should deliver 1 MW power and thus only ten 10 MW bases would have to use wave power to account for these 100 units.

The cost factors used in this work are listed in Table 15. The solar collector cost is not well established since units of this size meant for electrical generation have never been commercially available. However, it has been estimated by Stanford Research Institute that a

Table 15

COST CONVERSION FACTORS

Item	Cost	
Solar collector (thermal)	$65,000,000/km^2	($6.00/ft^2)
Windmill-generator	1.466×10^9/km^2	($700/installed kW; $1037K/30 meter diameter windmill)
Wave machine	$700/installed kW	
Turbine-generator	$300/kW	
Heat exchangers	$18/kW	
Storage		
Hydrogen	$300/MWH	
Batteries	$80/kWh	
Fuel cells	$200/kW	
Fuel (JP4)	$14.5/bbl	($8.49/MWH)

possible cost range is $4.00 to $8.00 per sq ft, which includes collector and frame materials and labor as well as constructor's overhead and profit (Goen et al., 1973). Accordingly, an average value of $6.00/ft^2 has been used here.

The windmill-generator costs have been taken as $700/installed kilowatt. Units constructed in the early 1950s had a cost on the order of $1100/kw in 1971 dollars (Savino, 1973). Taking into account the improved materials that have been developed since 1951 and the economy of scale effects of a possible larger production volume, a projected cost of $700/kw does not seem unreasonable. If the peak velocity handled by the windmill is 40 kt, the peak input flux is 5237 MW/km^2. Assuming a windmill efficiency of 40 percent, $700/kW is equivalent to (5237 $\times$ 10^3 kW/km^2 $\times$ .40 $\times$ $700/kW) $1.466 billion/km^2 of windmill area, or $1037K per 30-meter diameter windmill.

The wave machine costs are the least certain of the indigenous energy collection devices considered here. A value of $700/kW has been estimated and used in this work. Although the wave machine construction and installation cost per km of wave frontage is high, it is offset by a high output per km so that the estimated cost per killowatt is about the same as for the windmill-generators.

Engine generator systems have costs that depend strongly on the capacity of the plant. Because our standard remote base required less than 10 MW delivered power, the cost of the engine generator systems has been estimated to be $400/kW instead of the $150/kW figure often quoted for much larger plants (Solar Energy Panel, 1972). Fuel cell, heat exchanger, and hydrogen storage costs are the estimated costs for Stanford Research Institute (Gillette and Schubert, 1974). The battery cost of $80/kWh refers to lead-acid batteries.

The equipment cost of the storage or indigenous energy collection device for a particular power system configuration is given by the product of the appropriate size parameter in Tables 10-14 and the cost factor listed in Table 15. Costs of the other power system components are determined by the peak power loads they must satisfy during a year's operation, where these peak loads are in turn determined by the maximum indigenous input fluxes encountered during the year. These have been

taken as 1000 MW/km^2 for solar input (radiation incident on a surface
normal to the incoming flux vector on a cloudless day), 5237 MW/km^2
for wind input (corresponds to a maximum allowable velocity of 40 kn
before feathering the windmill), and 200 MW/km for wave input (corre-
sponds to a maximum wave height of 4.5 meters from which energy may
be extracted). Peak power loads for the turbine-generators, fuel cells,
and heat exchangers of Fig. 6 have been calculated from these peak in-
digenous energy inputs and equations developed in Appendix E. Multi-
plication of peak power demands by the corresponding cost factors in
Table 15 give the individual equipment costs.

Total Equipment Costs

The cost information for five of the ten system configurations
simulated above has been summarized in Tables 16 through 18 and Figs.
7 through 13. Data are presented for Sebana Seca, the Azores, and
Adak. Although not shown in the three tables, the costs for Diego
Garcia are quite similar to those for Sebana Seca; Iceland capacity
requirements are similar to those for Adak except for fuel oil con-
sumption.

The total cost figures in Tables 16 through 18 are equal to the
equipment costs of the individual components *plus* a 5 percent increase
to account for initial investment in repair parts. The heat exchanger
costs for Sebana Seca are zero because these devices are only asso-
ciated with the delivery of space heat, and heating demand at Sebana
Seca is completely absent.

When all three indigenous energy sources are used in combination
with hydrogen storage facilities, the largest single contributor to
total equipment cost is the cost of the energy collection device. The
expense of fuel cells is the next largest contributor in the wind and
wave cases; turbine expense is the next largest in the solar systems.
In the systems using battery storage, the order of collector and stor-
age cost contributions is variable. Hydrogen storage costs, primarily
reflecting tank construction costs, are only small contributions to
total cost and would remain so even if the cost factor of $300/MWh were
to double or triple. Although not as small as the storage contribution,
heat exchanger costs do not add much to the total equipment cost.

Table 16

COST OF SOLAR SYSTEMS

(H. storage)

System No.	Fuel	Collector Size	Fuel Cell	Turbine Generator No. 1	Turbine Generator No. 2	Heat Exchangers	Storage	Total[a]

Location: Caribbean - Sebana Seca

System No.	Capacity							
	(bbls)	(km^2)	(MW)	(MW)	(MW)	(MW)	(MWH)	
1	0	.116	10.9	12.7	0.	0	1104	--
2	7670	.090	8.1	9.9	4.	0	'7	--
3	15486	.064	6.7	7.1	4.	0	4	--
4	26934	.039	6.7	4.2	4.	0	0[b]	--
5	46178	0	0.	0	4.	0	0	--

System No.	Costs (thousands $)							
1	0	9032	2621	4586	0	0	397.	17469
2	111	7028	1943	3568	1438	0	6.	14683
3	225	5015	1598	2546	1438	0	1.4	11130
4	391	3011	1598	1529	1438	0	0.	7955
5	670	0	0	0	1438	0	0	1511

Location: North Atlantic - Azores

System No.	Capacity							
	(bbls)	(km^2)	(MW)	(MW)	(MW)	(MW)	(MWH)	
1	0.	.140	13.8	15.4	0	1.3	1476	--
2	7408	.109	10.4	12.0	3.9	10.3	32	--
3	14962	.078	7.1	8.6	3.9	10.3	9	--
4	25720	.047	7.1	5.1	3.9	10.3	0	--
5	43475	0	0	0	3.9	9.0	0	--

System No.	Costs (thousands $)							
1	0	9555	2892	4851	0	24.6	465.	18677
2	107	7432	2174	3773	1219	195.	10.	15544
3	217	5310	1491	2696	1219	195.	2.8	11458
4	373	3187	1491	1618	1219	195.	0	8095
5	630	0	0	0	1219	171.	0	1459

Location: North Pacific - Adak

System No.	Capacity							
	(bbls)	(km^2)	(MW)	(MW)	(MW)	(MW)	(MWH)	
1	0	.265	27.4	28.9	0	12.8	2059	--
2	8463	.206	20.9	22.4	3.6	27.1	130	--
3	17185	.147	14.5	15.9	3.6	27.1	10	--
4	27884	.088	12.5	9.4	3.6	27.1	0	--
5	43247	0	0	0	3.6	14.3	0	--

System No.	Costs (thousands $)							
1	0	34450	10968	17313	0	462.	1235	67650
2	123	26793	8377	13425	2172	976.	78	54412
3	249	19136	5185	9538	2172	976.	6	39494
4	404	11479	4981	5650	2172	976.	0	26522
5	627	0	0	0	2172	514	0	2820

[a]Total includes a 5 percent increase over the total obtained by adding across rows in order to account for investment in repair parts.

[b]This value is based on average input fluxes and demands; to be fully consistent with the fuel cell power given, storage must also be capable of handling peak conditions for short periods of time, which implies a maximum possible increase of 50 MWH.

Table 17

COST OF WIND-DRIVEN SYSTEMS

(H_2 systems)

System No.	Fuel	Windmill Size	Fuel Cell	Turbine Generator No. 2	Heat Exchanger	Storage	Total[a]

Location: Caribbean - Sebana Seca

System No.	Capacity						
	(bbls)	(km^2)	(MW)	(MW)	(MW)	(MWH)	
1	0	.0258	52.5	0	0	2551	--
2	8556	.02004	40.4	4	0	7440	--
3	18686	.0143	28.3	4	0	0	--
4	29691	.0086	16.3	4	0	0	--
5	46188	.00503	0	4	0	0	--
	Costs (thousands $)						
1	0.	45329	12597	0	0	918	61787
2	124.	35264	9703	1438	0	268	49007
3	271.	25181	6804	1438	0	0	35095
4	430.5	15116	3910	1438	0	0	21488
5	670.	0	0	1438	0	0	1511

Location: North Atlantic Azores

System No.	Capacity						
	(bbls)	(km^2)	(MW)	(MW)	(MW)	(MWH)	
1	0	.014	28.4	0	.65	2087	--
2	7478	.011	21.8	4	9.7	449	--
3	17368	.008	15.1	4	9.7	0	--
4	27036	.005	8.4	4	9.7	0	--
5	43475	0	0	4	9.0	0	--
	Costs (thousands $)						
1	0.0	21956.	5971	0	12.3	657	30027
2	108.4	17075.	4568	1219	183.	141	24345
3	236.	12195.	3164	1219	183.	0	17598
4	392.	7313.7	1761	1219	183.	0	11000
5	630.	0	0	1219	171	0	1459

Location: North Pacific - Adak

System No.	Capacity						
	(bbls)	(km^2)	(MW)	(MW)	(MW)	(MWH)	
1	0	.017	33.7	0	6.4	2770.	--
2	6409	.013	25.9	3.6	20.7	757.8	--
3	12875	.0093	18.1	3.6	20.7	0	--
4	20309	.0056	12.5	3.6	20.7	0	--
5	43247	0	0	3.6	14.3	0	--
	Costs (thousands $)						
1	0.	48860	13474	0	231	1662	67439
2	93.	38009	10354	2172	745	304	54163
3	186.5	27128	7226	2172	745	0	39135
4	294.5	16277	4981	2172	745	0	25384
5	627.	0	0	2172	514	0	2820

[a]Total includes a 5 percent increase over the total obtained by adding across rows in order to account for investment in repair parts.

Table 18

COST OF WAVE-DRIVEN SYSTEMS

(H_2 storage)

System No.	Fuel	Wave Machine Frontage	Fuel Cell	Turbine Generator No. 2	Heat Exchangers	Storage	Total[a]

Location: Caribbean - Sebana Seca

System No.				Capacity			
	(bbls)	(km^2)	(MW)	(MW)	(MW)	(MWH)	
1	0	.6	46.1	0	0	9732	--
2	7668	.47	35.1	4	0	5279	--
3	15728	.3	24.8	4	0	1334	--
4	26987	.2	14.2	4	0	0	--
5	46188	0	0	4	0	0	--
				Costs (thousands $)			
1	0.	40246	11063	0	0	3509	57553
2	111.2	31302	8508	1438	0	1900	45306
3	228.1	22357	5952	1438	0	480	31740
4	391.3	13413	3397	1438	0	0	19161
5	669.8	0	0	1438	0	0	1511

Location: North Atlantic - Azores

System No.				Capacity			
	(bbls)	(km^2)	(MW)	(MW)	(MW)	(MWH)	
1	0	.2	15.1	0	.65	5523	--
2	7327	.2	11.4	3.9	9.7	1779	--
3	14335	.1	7.7	3.9	9.7	0	--
4	25519	.7	7.1	3.9	9.7	0	--
5	43475	0	0	3.9	9.0	0	--
				Costs (thousands $)			
1	0	12277	3166	0	12	1740	18055
2	106	9549	2387	1214	18	560	14593
3	208	6821	1607	1215	18	0	10321
4	370	4092	1491	1219	18	0	7333
5	630	0	0	1219	17	0	1459

Location: North Pacific - Adak

System No.				Capacity			
	(bbls)	(km^2)	(MW)	(MW)	(Mw)	(MWH)	
1	0	.56	43.5	0	6.4	6499	--
2	6722	.44	33.5	3.6	2.1	4146	--
3	13519	.3	23.5	3.6	2.1	0	--
4	21162	.19	13.5	3.6	2.1	0	--
5	43135	0	0	3.6	1.4	0	--
				Costs (thousands $)			
1	0.	62877	17391	0	231	3899	88619
2	97.5	48910	13401	2172	745	1199	69665
3	196.	34933	9407	2172	745	0	49620
4	306.8	20955	5414	2172	745	0	30750
5	625.4	0	0	2172	514	0	2820

[a]Total includes a 5 percent increase over the total obtained by adding across rows in order to account for investment in repair parts.
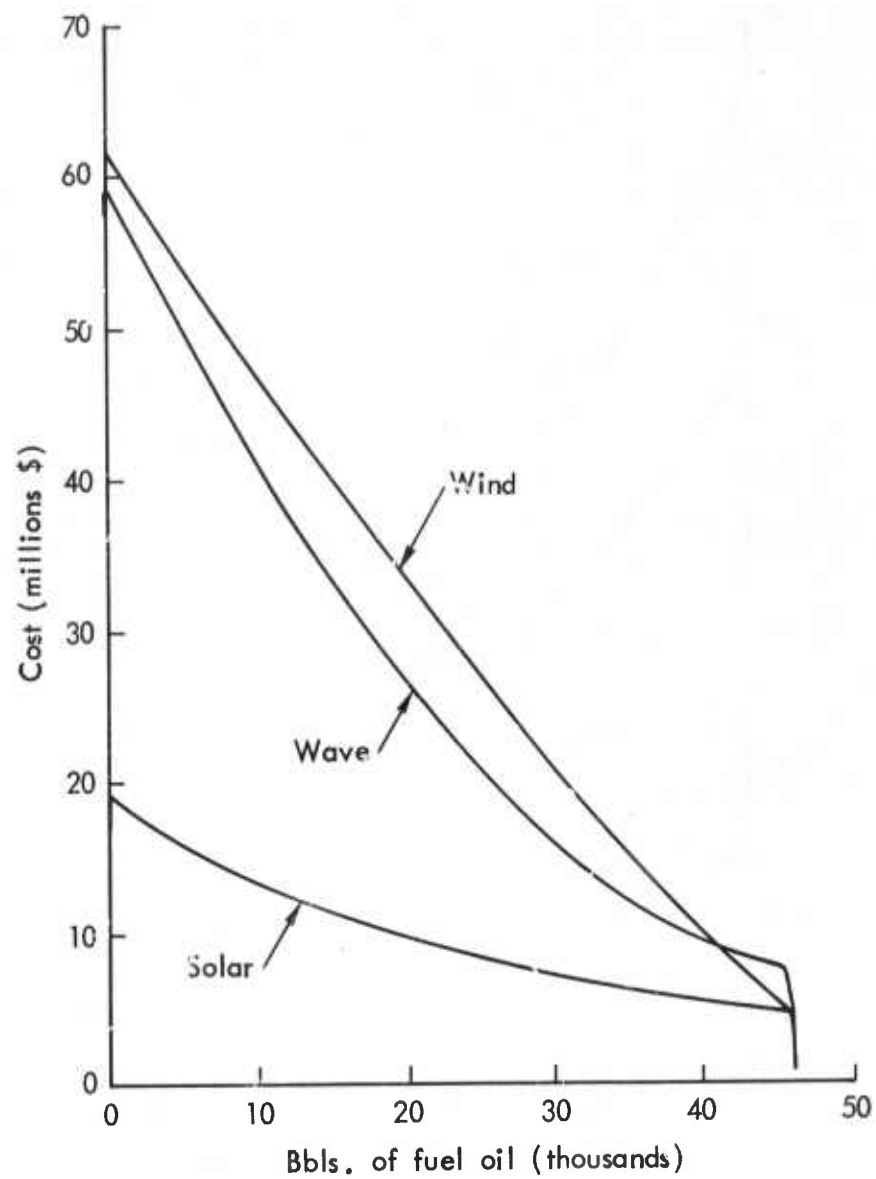
Fig. 7— Total equipment costs for combined power systems
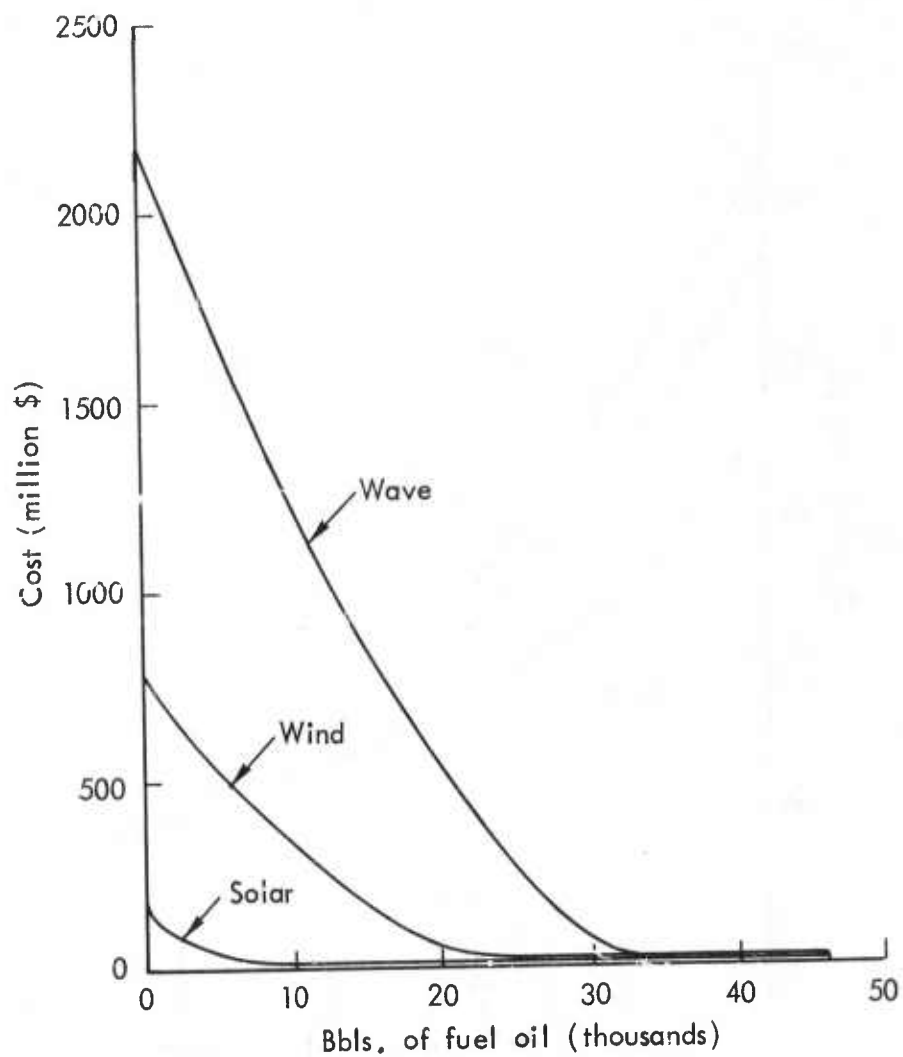using hydrogen storage at Sebana Seca
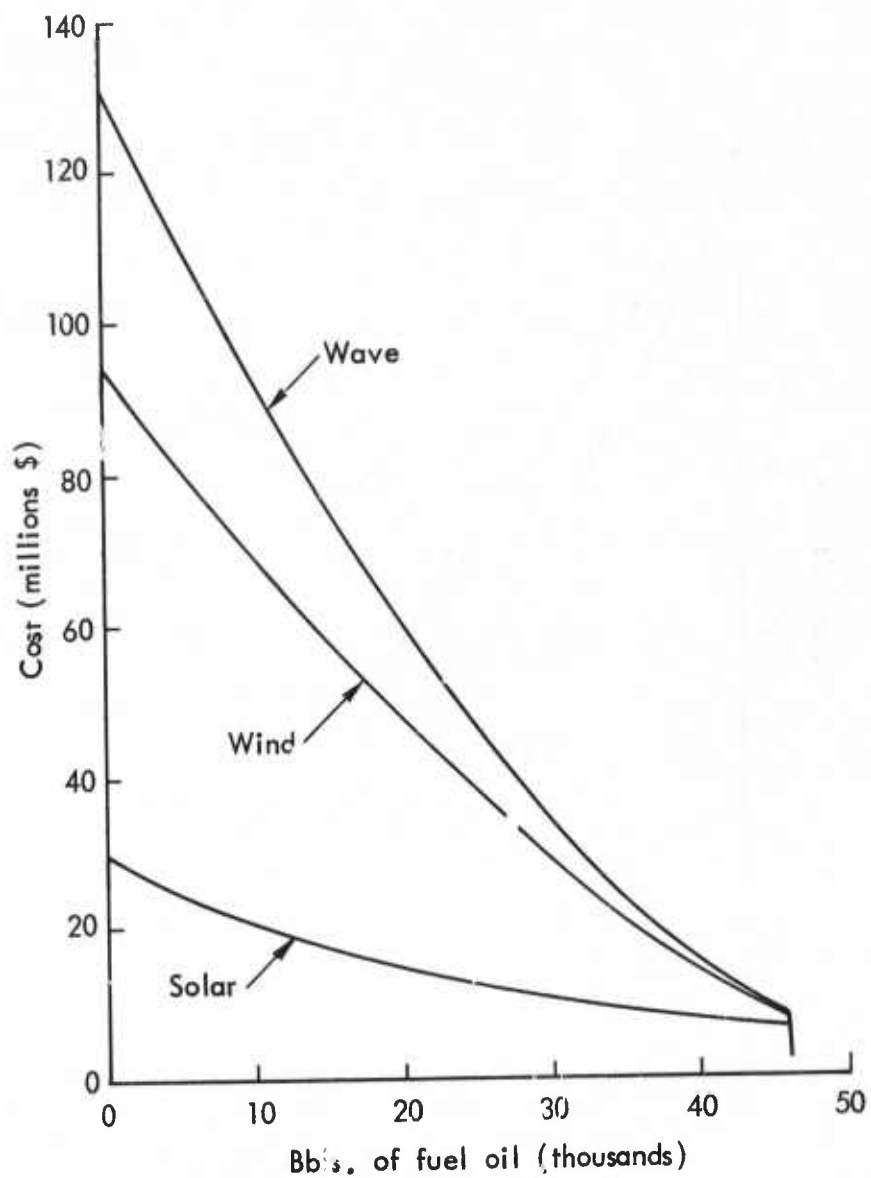
Fig. 8— Total equipment costs for combined power systems
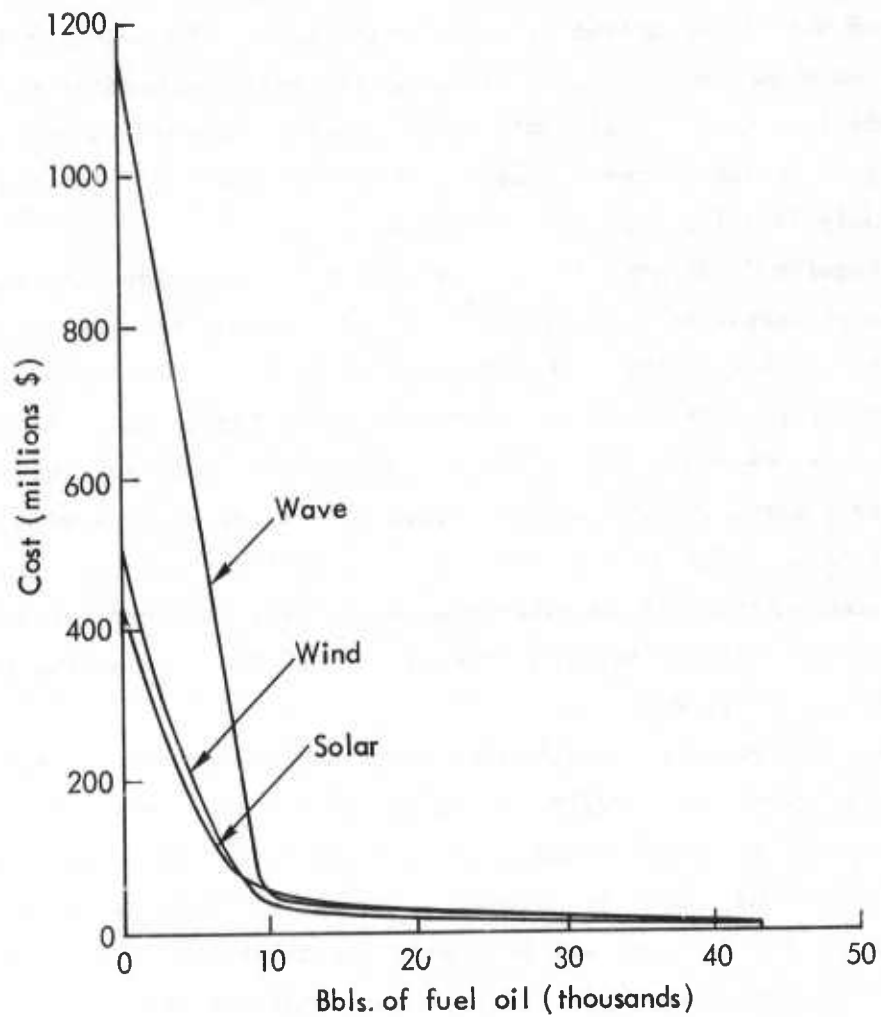using hydrogen storage at Diego Garcia
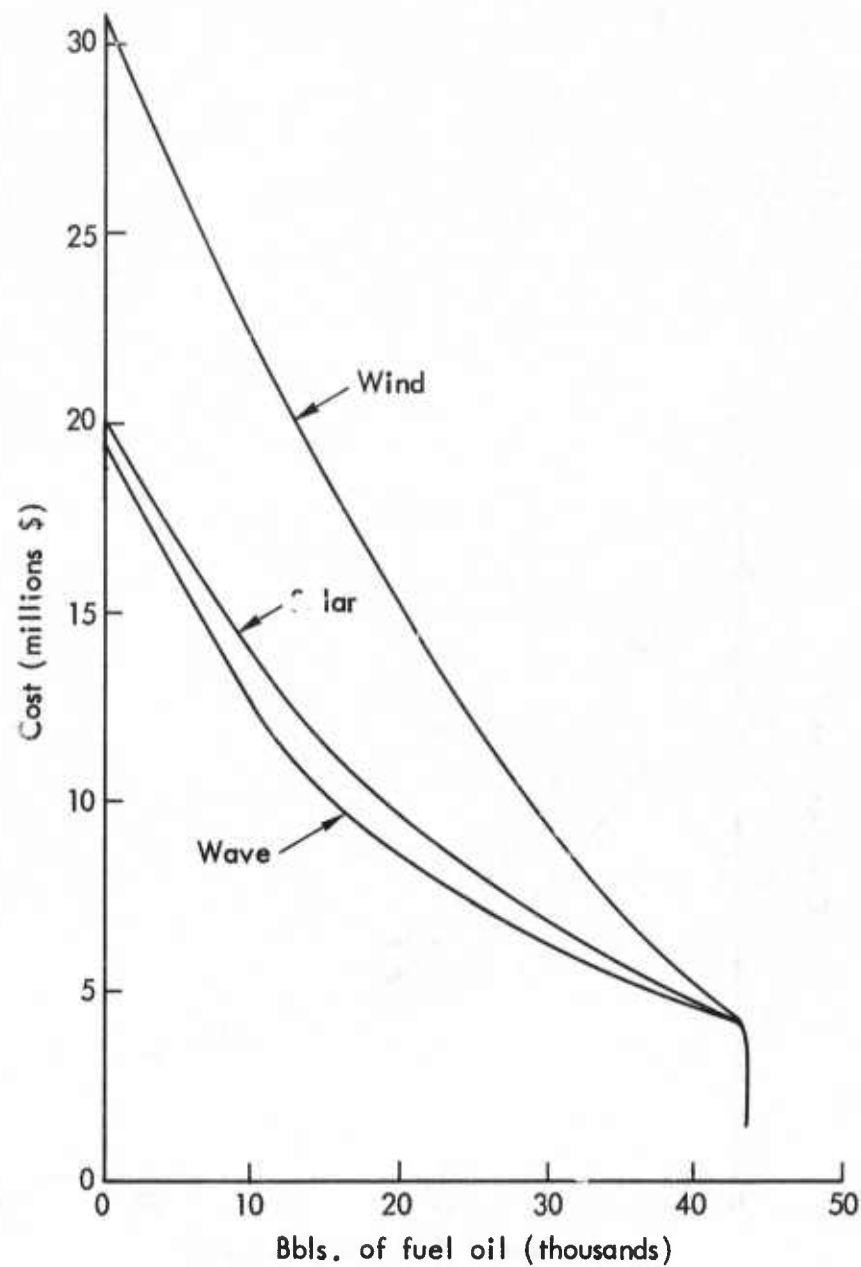
Fig. 9— Total equipment costs for combined power systems using hydrogen storage at the Azores
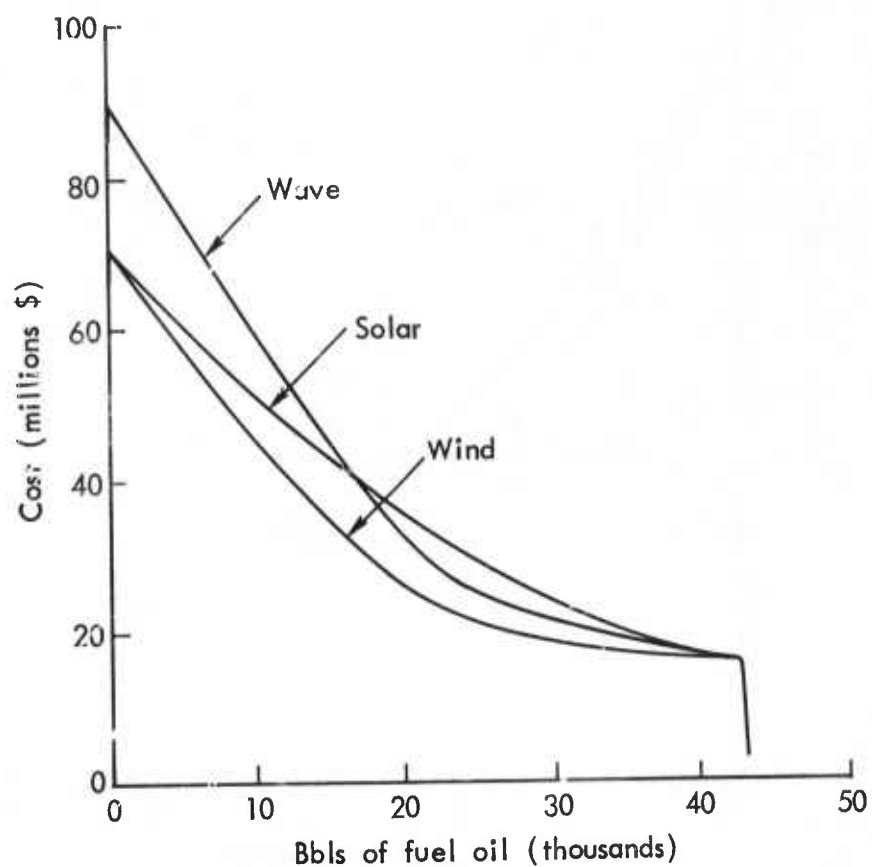
Fig. 10 — Total equipment costs for combined power systems using hydrogen storage at Adak
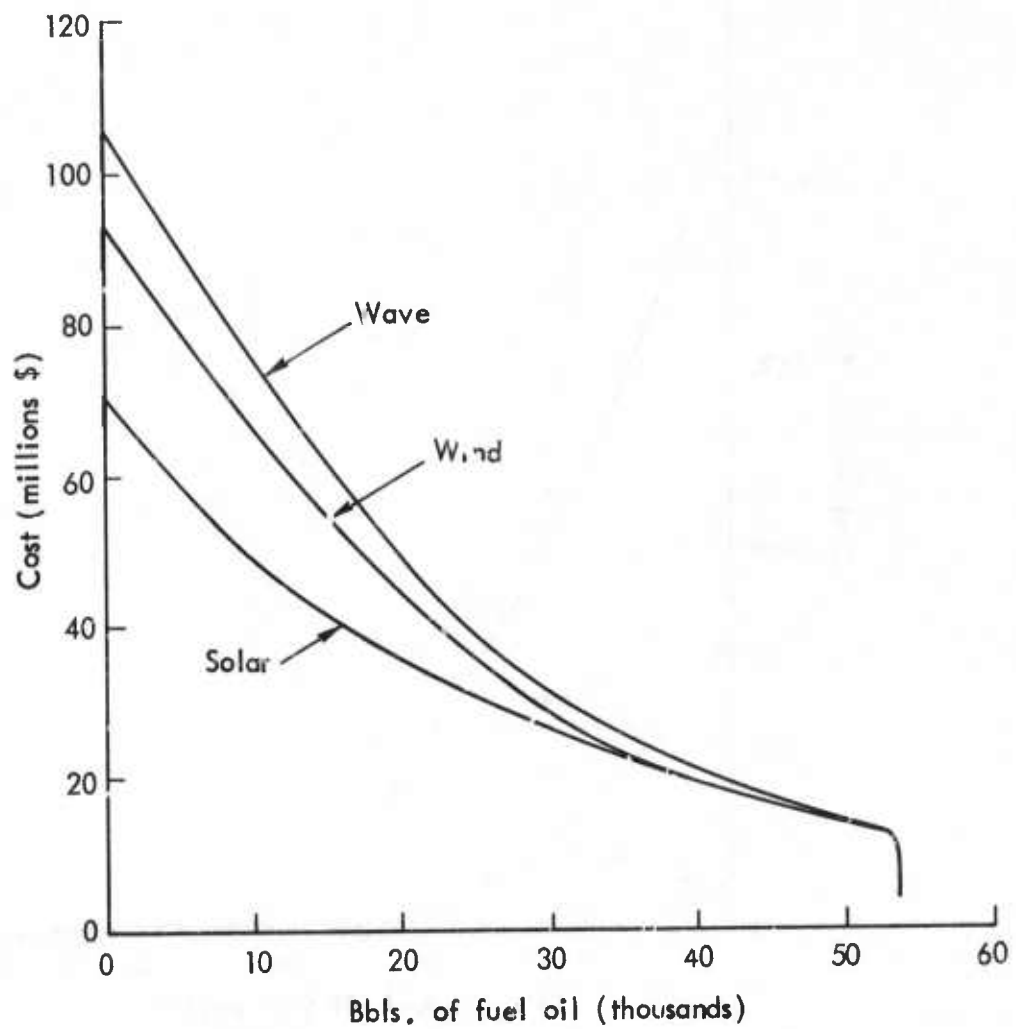
Fig. 11— Total equipment costs for combined power systems
using hydrogen storage at Iceland

Fig. 12 — Total equipment costs for combined power systems using battery storage at Diego Garcia

Fig. 13— Total equipment costs for combined power systems
using battery storage at Adak

Total equipment costs of the combined indigenous and conventional power systems using hydrogen storage are plotted as a function of fuel oil consumption in Figs. 7-11. Data are given for all five regions investigated in this work. Similar plots for systems using battery (lead-acid) storage are presented in Figs. 12 and 13 for the Diego Garcia and Adak locations.[1] As one reads from left to right, the increasing fuel oil consumption may be regarded as a measure of the increased use of the diesel or gas-turbine unit. The point at the far right on each graph gives the cost of the engine-generator-dependent system; this point is discontinuous from the curve immediately preceding it because certain heat exchanger and fuel cell costs discontinuously drop for this configuration.

Figures 7, 8, and 11 indicate that the least expensive indigenous system at Sebana Seca, Diego Garcia, and Iceland (from an equipment cost viewpoint) is the combined solar system. Combined wind and wave systems at the first two locations are about three times more expensive, but such systems are only about 40 percent more expensive at Iceland. The least expensive indigenous system at the Azores is a wave system, and at Adak a wind system. The latter result reflects the well-known high wind activity in the Aleutian chain. All combined systems are competitive at Adak, particularly in view of the substantial uncertainty in cost figures.

At this point we reemphasize that these comparisons pertain to the large geographic regions of which the specific locations are merely representative. This distinction is particularly important for the case of Iceland, where geothermal areas are known to be useful sources of energy; but they are not generally available and able to be counted upon throughout the entire Far North Atlantic region.

The Adak and Icelandic solar inputs are somewhat excessive here because the large Arctic diffuse radiation component of total radiation has been overestimated by about 50 percent on extremely cloudy days. Consequently, this leads to an underestimate of collector areas and

---

[1] The reader should note the variations in scale for capital costs in Figs. 7-13.

costs. It is probable that wind and wave devices are somewhat more reasonable cost alternatives than is indicated in Figs. 10 and 11.

Figures 12 and 13 show that those totally indigenous system configurations using batteries are very expensive relative to the fuel cell and hydrogen storage systems. However, as the use of the engine generator unit is phased in, a point is reached where the battery system becomes equal to or less expensive than the fuel cell system. In all cases, this corresponds to the situation when required storage capacity drops to 50 MWh or less. These equicost points are listed in Table 19 as a function of the annual fuel consumption as well as percent of the annual all engine fuel consumption. Note that these points generally occur at fuel consumption levels that are only about 25 percent of the amount required for full engine operation. This is important since a low fuel consumption combined system may be constructed that depends not on developing storage technology but rather on available storage technology.

As in previous studies, the cost of all engine generator systems has been found to be many times less expensive than the totally indigenous dependent systems. As Figs. 7 through 13 show, this engine generator cost remains low throughout the spectrum of combined systems investigated here.

Table 19

EQUICOST POINTS OF HYDROGEN AND
BATTERY STORAGE SYSTEMS

	System Type	Diego Garcia	Adak
Solar	Consumption, bbl	7,760	12,600
	Percent[a]	17	29
Wind	Consumption, bbl	23,000	9,600
	Percent	50	22
Wave	Consumption, bbl	32,000	10,110
	Percent	69	23

[a]This refers to the percentage of fuel oil consumed at an all engine-generator system that represents the amount of fuel oil consumed by a combined system at the equicost point.

Although this study reports detailed calculations only on power systems combining one indigenous with one conventional power supply, there are other possibilities that combine two indigenous sources in a single system. The primary advantage of this latter configuration would be to reduce the storage requirement of the system by better matching a given indigenous power input to the given power demand at a particular instant. The collector size and cost are reduced by an amount proportional to the energy saved by reducing storage conversion losses. Although the size of the system components may be somewhat reduced by this approach, the conclusion that conventional engine-generator systems will be significantly cheaper than indigenous systems, even in combination, is not believed to be changed.

We have compared the equipment costs for the all solar system at Diego Garcia with those of the system investigated by SRI (Gillette and Schubert, 1974). Our estimate, using SRI cost factors instead of those in Table 19, is $15.9 million rather than the SRI estimate of $61 million. There are several reasons for this difference. First, our collector area is smaller by a factor of nearly three. The SRI study determined this area by a peaking calculation in which the area required at annual average solar radiation to give the base peak power demand was computed. We calculated the area required to give the annual average demand and allowed energy to be withdrawn from storage to satisfy the peak condition. This accounts for about half the difference between the two estimates of collector size. Second, our power model does not route all energy through storage, thus saving significant electrical-to-chemical conversion losses and decreasing collector size. In other solar systems, such as at Adak and Iceland, a collector area relative to the SRI value is reduced further because we allow a large amount of solar thermal power to flow directly to satisfy space heating demands rather than first being inefficiently converted to electricity. Third, fuel cell capacities determined here are much smaller than previous estimates. For the case of Diego Garcia, this is a direct consequence of smaller collector areas (see Eq. (E.2), Appendix E). We note that fuel cell capacities in the wind-driven systems are also lower than the SRI estimates, partly because of the

smaller collector areas, as was the case for solar systems, but also because of our use of a lower maximum velocity before feathering is required (40 kn instead of 47 kn).

V.   CONCLUSIONS

This work has investigated the relative merits of combinations
of indigenous energy systems and conventional systems to satisfy elec-
trical and thermal power demand for a standard military base in various
remote regions around the globe. Some of the first data on such appli-
cations of ocean wave-dependent systems have been developed. The sys-
tem capacity and initial cost figures have been optimized with regard
to the use of storage as well as variable indigenous energy fluxes and
power demand.

The observations and conclusions that have been made may be sum-
marized as follows:

A.   The distribution of indigenous energy source availabilities
throughout the world leaves little doubt that one or more of these
resources will be available in practical quantities at most existing
or potential base locations.

B.   Design and construction of solar and wind systems is quite
mature; and with additional current effort by EkDA and NSF, it is quite
within the state of the art that they could be installed on remote
bases. The wave energy system, however, is not as well understood nor
is it currently receiving the same research funding as the other two.
Because of the limited applicability of wave power--i.e., island base
or coastal region only--the likelihood of its receiving the same level
of support seems remote; thus, if a wave power system is considered as
a candidate, R&D effort will be needed.

C.   The mixed use of a system run by conventional engine-furnace
with an indigenous energy system results in marked improvements over
reliance on a totally indigenous system.

1.   As the proportion of the conventional system increases,
storage requirements drop off rapidly.

2.   A combined power system using battery storage may become
cost-competitive with systems using fuel-cell and hydrogen
storage devices when the engine generator system is used

at an annual fuel consumption that is 25 percent of the amount used by a wholly conventional system. Thus, while still obtaining a significant reduction over current fuel oil use, a combined system may be constructed that uses current-day technology storage devices at no greater cost than more futuristic systems.

3. Preferred combined indigenous energy power systems for each of our five regions are:

- Solar in the Caribbean (Sebana Seca) and Indian Ocean (Diego Garcia)
- Wind in the North Pacific (Adak)
- Wave in the Mid Atlantic (Azores)
- Solar or wind in the North Atlantic (Iceland).[1]

4. Combined indigenous energy and engine generator systems offer lower costs than entirely indigenous power sources. For example, a hydrogen-storage combined solar power and conventional system at Diego Garcia uses 25 percent of the fuel required by a conventional system, with capital costs only about 80 percent as much as the corresponding all-solar system. A similar comparison between the same two systems but with battery storage shows that the combined system costs only about 6 percent as much as the totally indigenous system.

5. Direct use of solar thermal energy for space heating and the storage of only that energy in excess of immediate electrical and space heating demand has allowed us to reduce the cost of indigenous systems to 50 to 20 percent of previous estimates (Gillette and Schubert, 1974). This improvement is still subject, of course, to the considerable uncertainty that remains in various cost factors.

---

[1]While solar energy is attenuated considerably by cloud cover in this region annually, it still compares favorably with wind power in part because of the greater relative efficiency with which solar energy may satisfy space heating demand.

D. Combination conventional and indigenous energy systems exceed the cost of a conventional system with a year's supply of fuel in storage tanks by a wide margin. For the range of conditions considered, conventional system capital costs are in the range of $1.5 to 3 million with a one-year's supply of fuel in storage adding only $1 million more. Comparing this with the costs of indigenous systems used in combination with the conventional system indicates that indigenous systems will cost at least three times as much. Thus indigenous systems should not be viewed as competitive with conventional systems but as an option for achieving an energy alternative to complete dependence on petroleum and lessening vulnerability to supply interruption.

Appendix A

GLOBAL CIRCULATION AND ASSOCIATED WEATHER INFLUENCING
SEASONAL POWER DENSITY ANALYSES

Indigenous energy from solar radiation, wind velocity, and wave
motion is largely dependent on the macroscale or global general cir-
culation and its relationship to the annual migration of the sun.
This is most dramatically illustrated by the flow of the monsoons
through the offshore subregions (Fig. A-1) surrounding East and South-
east Asia (Schatz, 1967). From May through September when the sun is
furthest north, a massive thermal low pressure system (Fig. A-2) de-
velops from Mongolia to Afghanistan with a resulting monsoonal flow
from the south across subregions D, E, and F. This flow brings moist
tropical air into the low, which results in considerable daytime
cloudiness and occasional tropical cyclones with strong winds and high
waves offshore. By contrast, from November through March, when the sun
is furthest south, a strong high pressure develops over Mongolia (Fig.
A-3). Circulation out of the high results in a monsoonal flow of dry
continental air from the north across most of subregions D, E, and F
with much less cloudiness. However, several times per month during
this period, large-scale cyclonic storms associated with migrating low
pressure areas influence areas F and H. Each storm brings a massive
cloud cover and greater than normal winds, which influence a given
point for 3-5 days.

Cyclonic storms are a regular part of the flow through subregions
A, B, and most of H, making them cloudy and windy throughout the year.
Storms and weather are most intense, however, around the winter months,
especially in the North Atlantic near Iceland, and in the North Pacific
along the Aleutian chain.

The Trades make up the wind system of the tropics, except offshore
around Southeast Asia, and extend from the equator to 30°N and 30°S.
They too are a major component of the general circulation, flowing from
the northeast in the northern hemisphere and from the southeast in the
southern hemisphere.
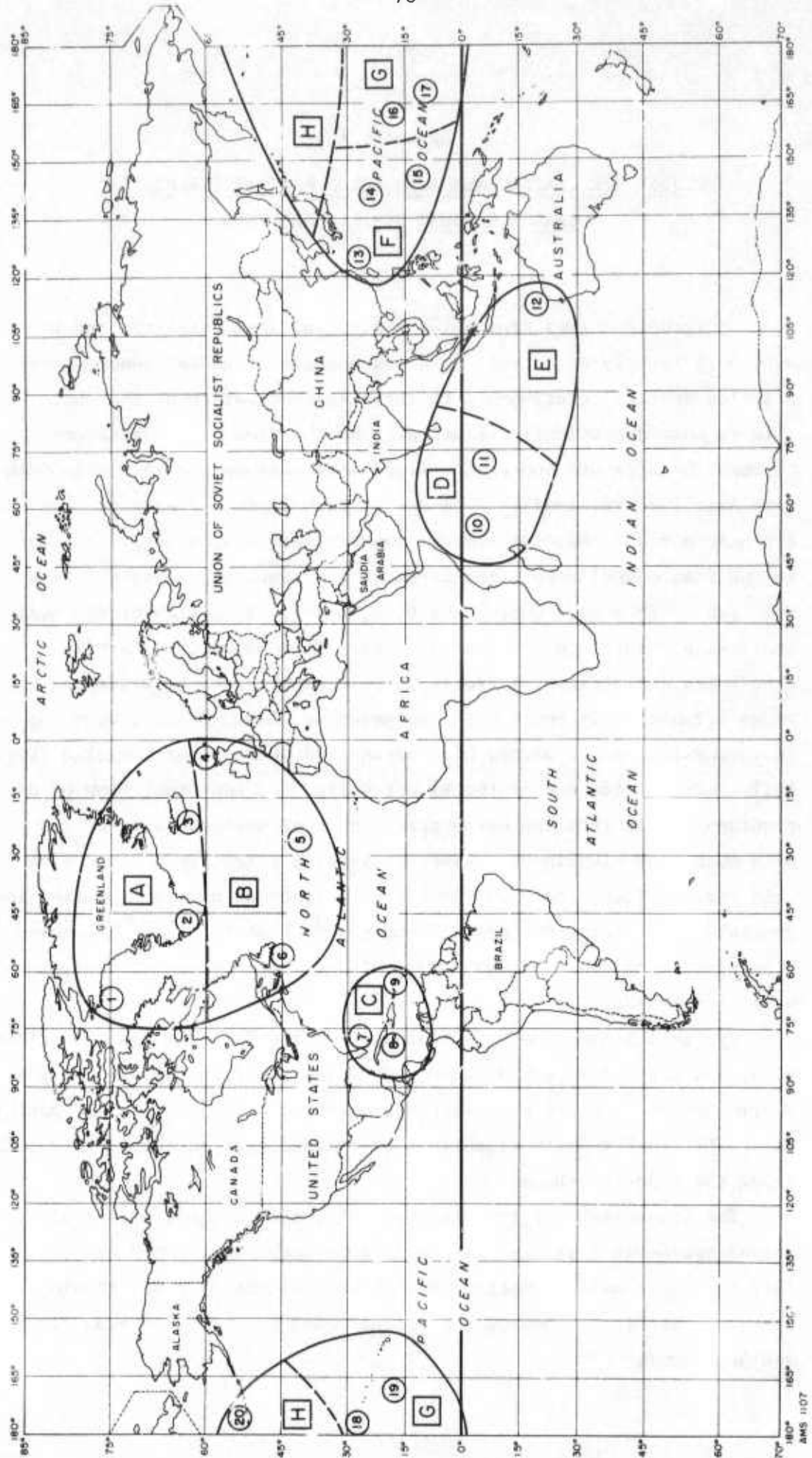
Fig. A-1 — Selected remote bases by ocean subregions
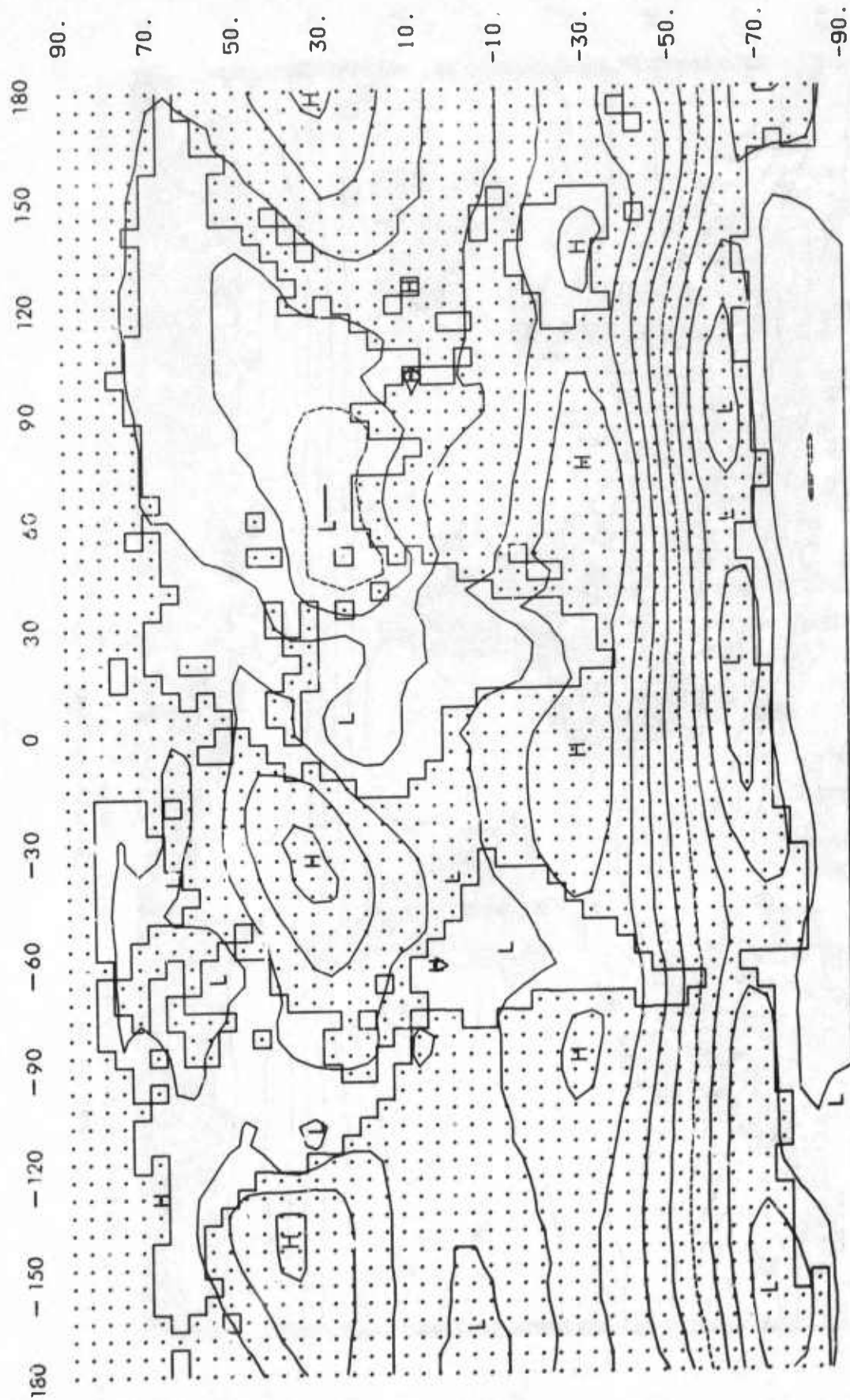
Fig. A-2—Mean July sea-level pressure in mb. The analysis interval is 5 mb and the 1000-mb isobar is dashed. From Schutz and Gates (1972).
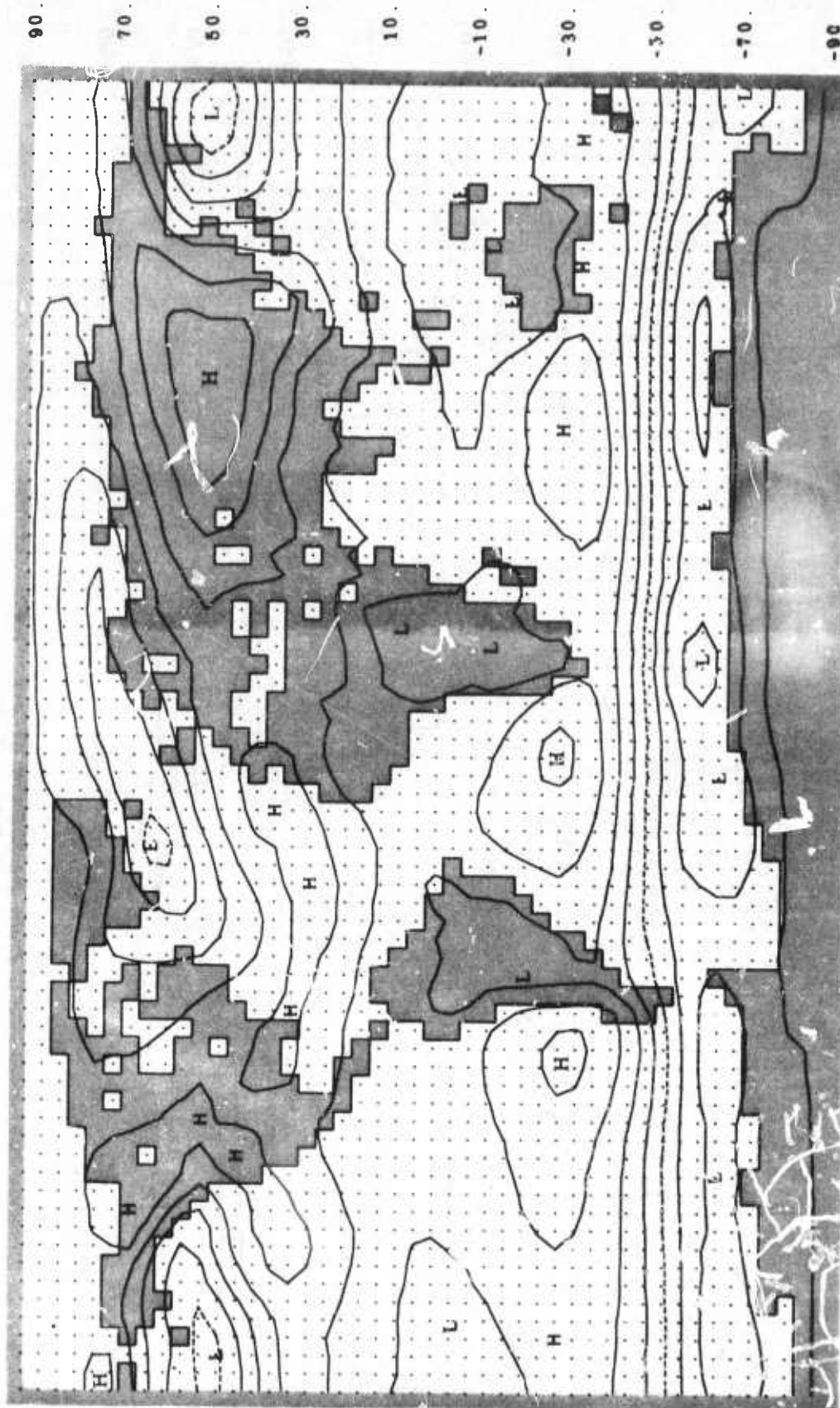
Fig. A-3—Mean January sea-level pressure in mb. The analysis interval is 5 mb and the 1000-mb isobar is dashed. From Schutz and Gates (1971).

The Trade Winds and moist tropical air are the dominating influence throughout subregions C and G annually. In general, these areas are not bothered by cyclonic storms, but they do come under the influence of small-scale weather changes brought about by the terrain. Heavy la ers of upslope clouds form on the windward side of the mountains during the day. The surrounding ocean has very little cloud cover where there is no lifting of the moist tropical air. Also, wind patterns are affected by diurnal heating and cooling of the land.

SOLAR POWER

Figure A-4 shows average solar energy in $(kWh/m^2/D)$ for the month of April, which coincides roughly with the vernal equinox. These seasonal data are based on the mean solar radiation received at the surface (Schutz and Gates, 1971-1974). Since both the southern and northern hemispheres receive the same degree of "potential" radiation, the variations in intensity at identical northern and southern latitudes are related to the attenuating effects of cloud cover. The low readings north of 30°N are associated with clouds from cyclonic storm systems, which are still near maximum intensity in April.

In July (Fig. A-5) marked lowering in solar energy is noted along the moist Asian monsoon flowing from the south over subregions D, E, and the western portion of F. Very little change occurs in the remaining subregions, except north of 60°N where high potential solar power values result from longer hours of daylight. These range from near 24 hr at the Arctic Circle (66-1/2°N) to a full six months at the Pole. This is the cloudiest period of the year at the Pole, because of an increase in low-level moisture resulting from the breakup of the ice. Nevertheless, cloud influence on solar radiation is offset by a long exposure to the sun's rays. Figure A-6 shows the approximate hours of daylight in the northern hemisphere at four mid-season dates.

By October (Fig. A-7) following the autumnal equinox, the solar energy values north of 30°N show marked decreases as the sun moves south and cloudiness increases with the intensification of cyclonic storms. In the southern hemisphere, as a consequence of the drying influence of the northeast monsoon, cloudiness decreases in subregions D and E, and the solar energy increases.
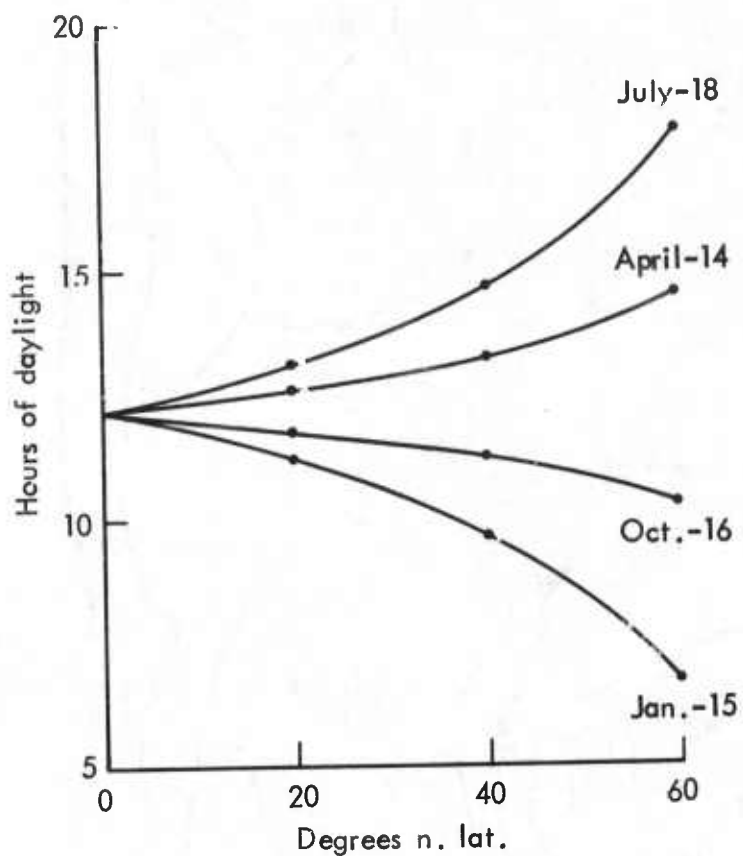
Fig. A-4— Average solar energy: April (kWh/m²/D)
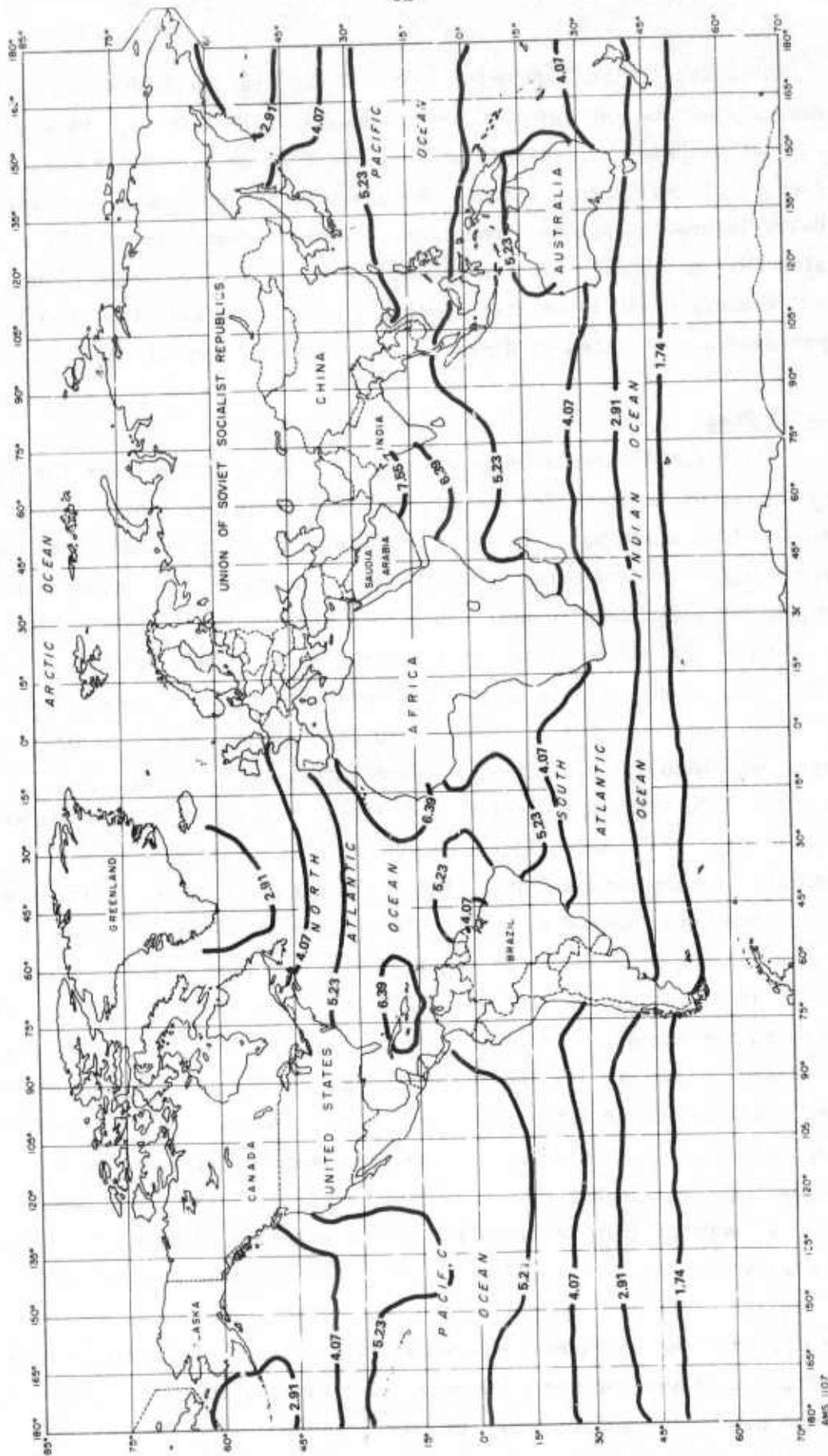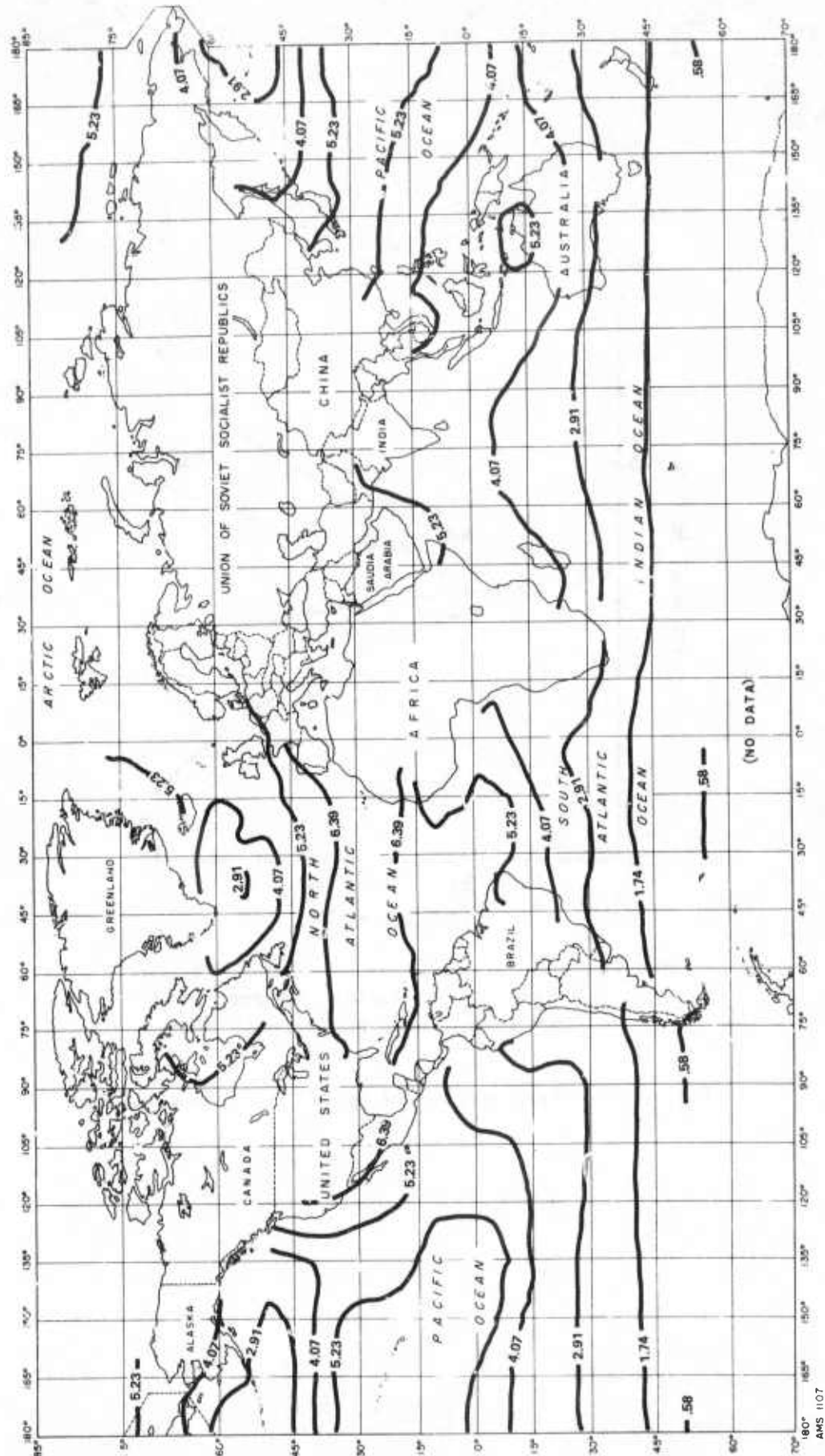
Fig. A-5—Average solar energy: July
(kWh/m²/D)

Source: U.S. Naval Observatory, The American
Ephemeris and Nautical Almanac for the
Year 1975. Nautical Almanac Office, 1974.
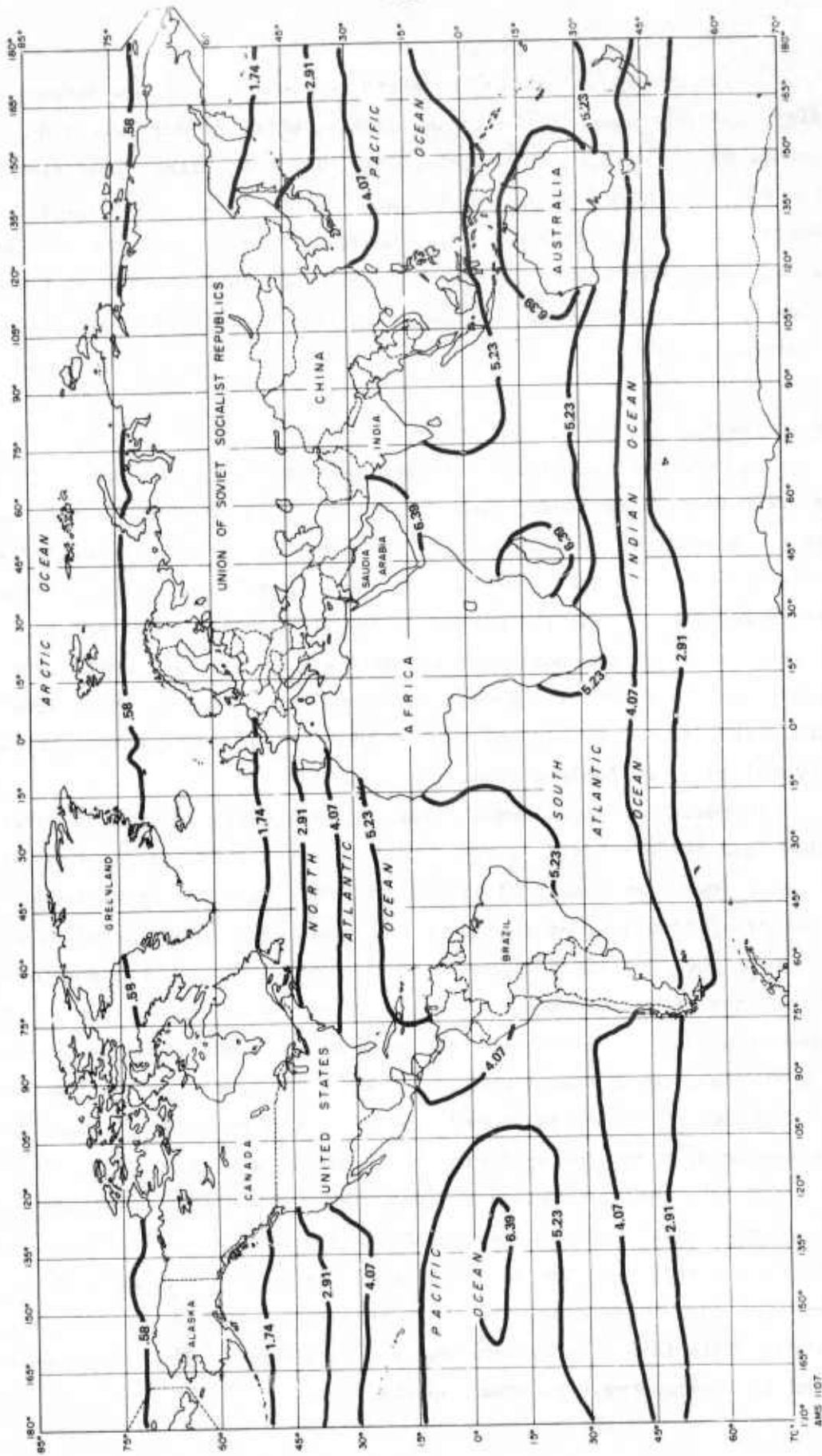
Fig. A-6—Hours of sunlight for the northern hemisphere

Fig. A-7—Average solar energy: October
(kWh/m²/D)

Solar energy values in the north continue to fall in January (Fig. A-8), because of the longer nights, which effectively reduce the amount of recoverable potential energy, the less direct character of the sun's rays, and storms that track further south. Subregion E, however, shows the greatest solar power density of the year because of the more direct rays of the sun, the combined influence of the dry flow of the monsoon from the north, and the undisturbed flow of the Southeast Trades.

Wind Power

Since April is the time of year when the sun's rays are vertical at zero degrees latitude, wind throughout the subregions in the vicinity of the equator is generally light and variable. This zone of relative calm is known nautically as the Doldrums. Also, in the area of the Asian monsoon this is the period of subtle transition between the winter flow from the north and the summer flow from the south through subregions D, E, and F. Except for subregions C and G, which come under the persistent flow of the Trades, the remaining subregions are controlled by cyclonic storms.

In potential power density terms of kilowatts per square meter of flow area (kW/m^2) Fig. A-9 shows that in April there is a rather broad band of low power potential in the tropics. With the exception of the southern portions of subregions D and E where the power level exceeds 1.3 kW/m^2 because of the flow of the Southeast Trades, the potential fluctuates at levels generally below .5 kW/m^2. South of 40°S in the area of almost uninterrupted, strong westerly winds known as the Roaring Forties, power levels exceed 1.3 kW/m^2 every month. In the northern hemisphere, power levels exceed 1.3 kW/m^2 only in a narrow zone within subregion B, where the cyclonic storms are at a maximum.

By July the Asian monsoon gives a strong and persistent flow of southerly winds across subregions D and E. At the same time the Trades reduce the effect of the Doldrums in subregion G. Only in western subregion F does there remain a rather persistent area of low velocity winds. This is in the extreme western extension of the Trades where land influences begin to break up the flow.
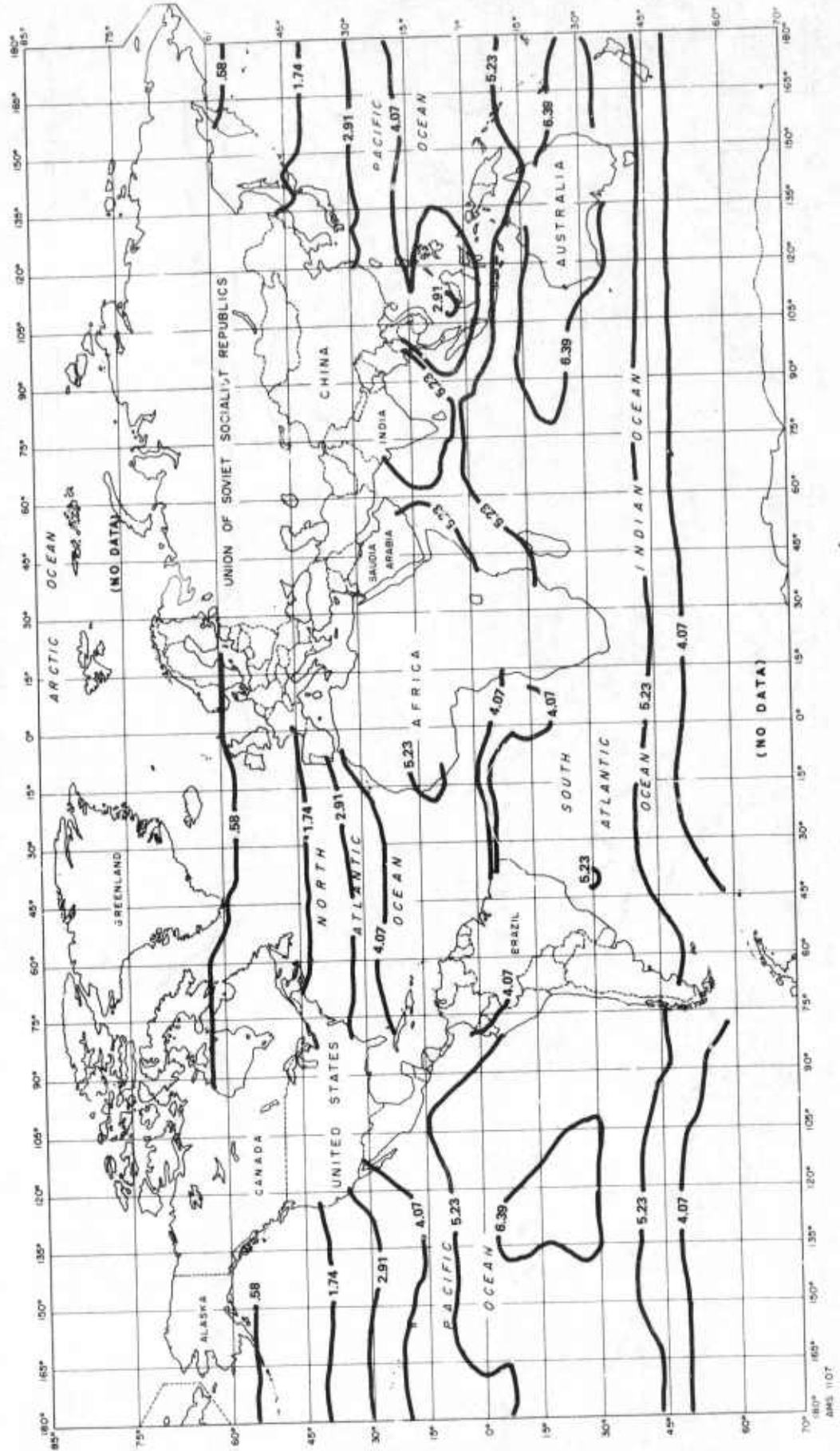
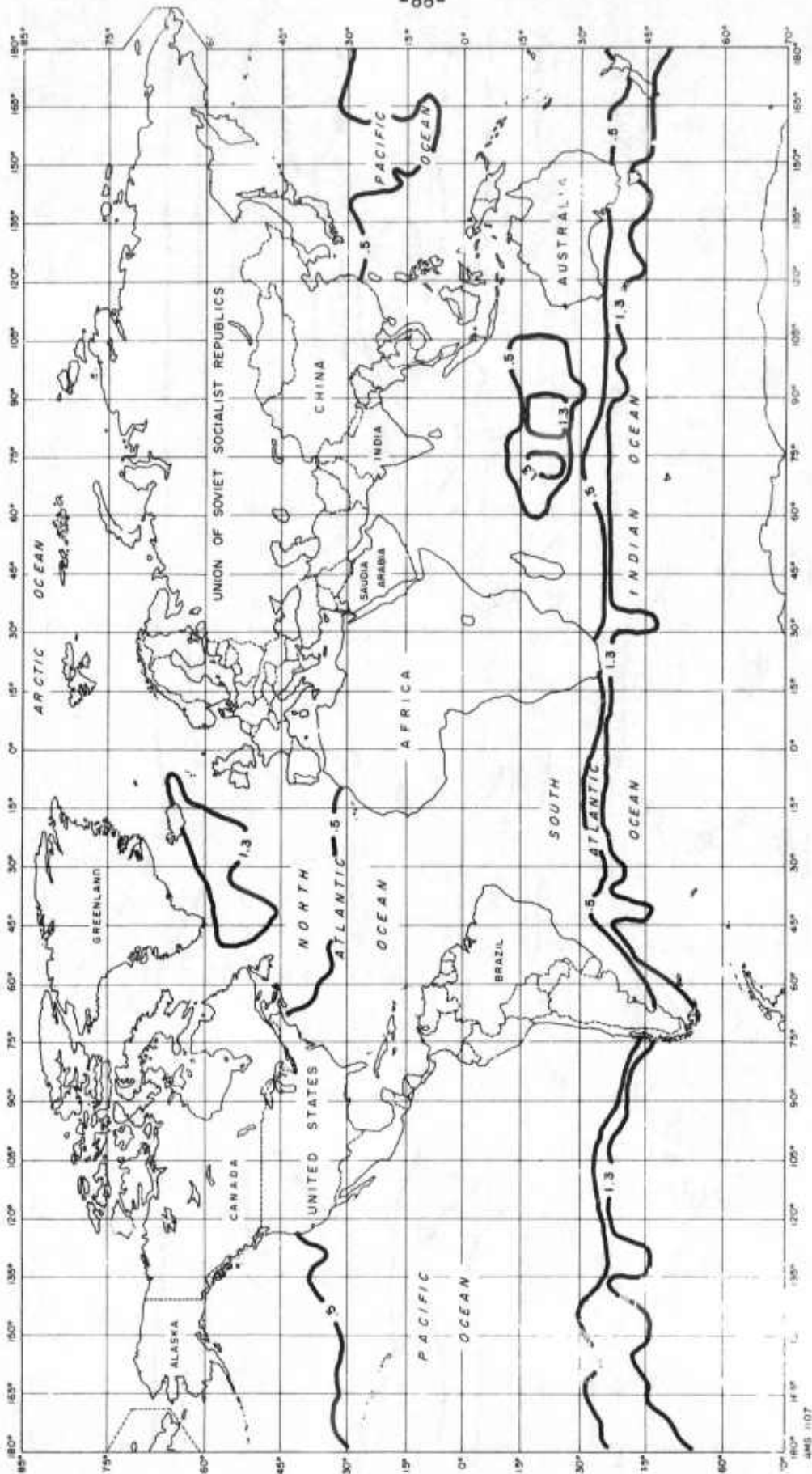Fig. A-8 — Average solar energy: January (kWh/m²/D)

Fig. A-9—Average potential wind power density: April (kW/m2)

Power levels in July (Fig. A-10) strongly reflect the Asian monsoon flow, particularly in subregion D where power levels have increased to exceed 1.3 kW/m^2. Further to the south through subregion E, strong Southeast Trades and winds in the Roaring Forties expand the .5 kW/m^2 power level isopleth northward. In the northern hemisphere, as the cyclonic storms weaken, power levels fluctuate around the .5 kW/m^2 level without ever reaching the previous April level of 1.3 kW/m^2, even in the northern North Atlantic.

In October the situation is somewhat analogous to that in April except that there is a more vigorous Asian transition from the summer monsoon, with a flow from the south, to the winter monsoon, with a flow from the north. The greater strength of the northern hemisphere summer winds in the tropics and the displacement of moist tropical air by cold continental air causes this transition season to be somewhat more windy than that in April.

As the transition to the northern winter progresses, power levels (Fig. A-11) exceed 1.3 kW/m^2 in subregions A, B, and H as the cyclonic storms once again increase in intensity. A comparison of the power level isopleths again makes this period analogous to April.

By January the Icelandic Low of the North Atlantic and the Aleutian Low of the North Pacific have reached maximum development with an associated increase in the winds over subregions A, B, and H. Although the influence of the Siberian High, and the consequent flow of the monsoon from the north, tends to increase the amount of wind found in subregions D and E, its weakness compared with the reverse flow in July is seen in the rather extensive zone of low velocity winds lying directly south of the equator.

In potential power terms (Fig. A-12), cyclonic activity in the northern hemisphere has expanded power levels in excess of 1.3 kW/m^2 over a considerable area. In the southern hemisphere, the weaker flow from the north through subregions D and E has decreased the power density below .5 kW/m^2 and only the effect of the Roaring Forties remains, well to the south.
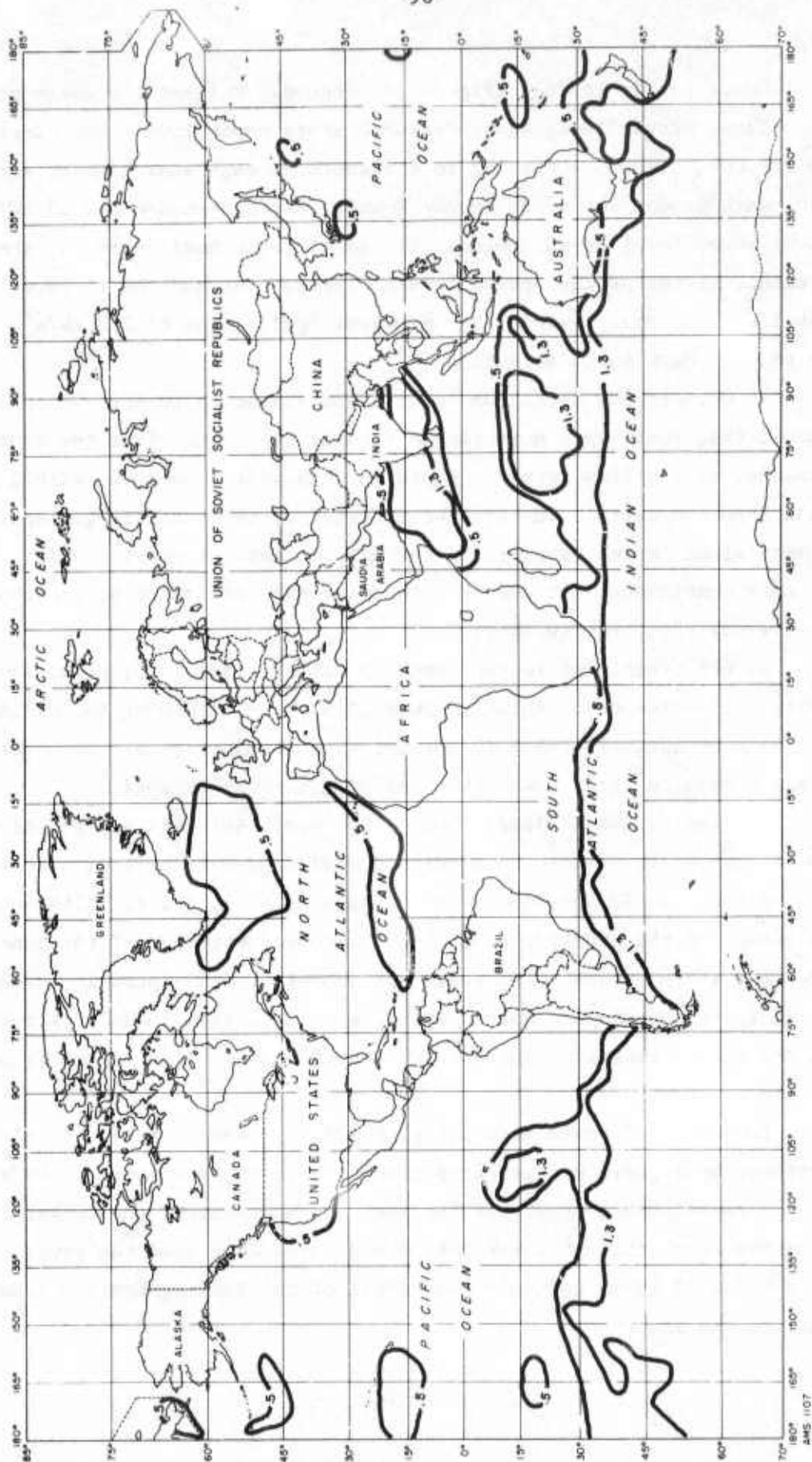
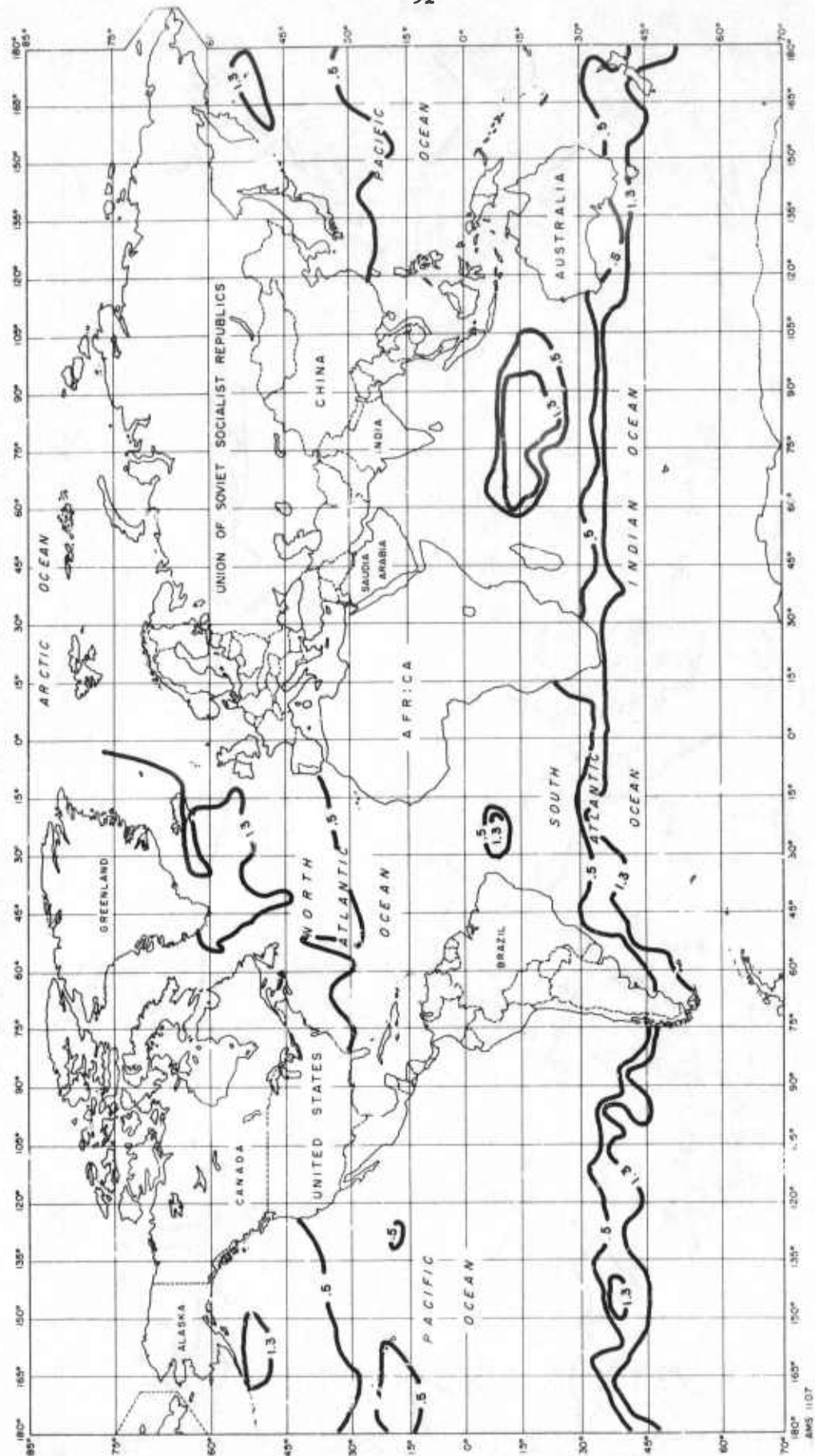Fig. A-10— Average potential wind power density: July (kW/m²)

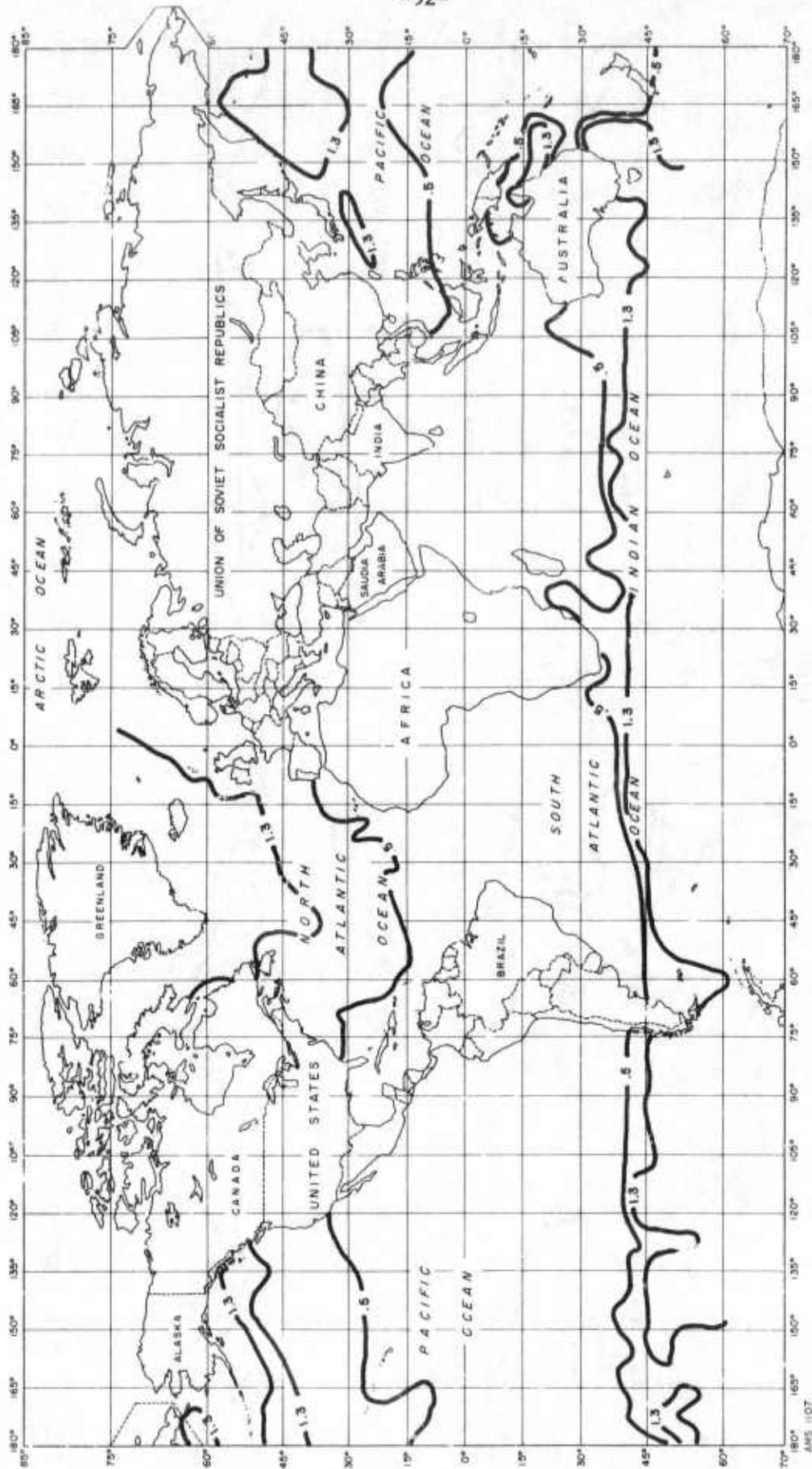Fig. A-11 —Average potential wind power density: October (kW/m²)

Fig. A-12—Average potential wind power density: January (kW/m²)

WAVE POWER   (TION)

The worldwide distribution of potential wave energy, in terms of
its seasonal variations, relates quite well on the macroscale with
comparable wind data. This is not surprising inasmuch as the wave
height of "seas" over the open ocean are generally proportional to the
velocity of the wind blowing over the area at the time. However, it
is difficult, if not impossible, to correlate wind and wave data for
a specific location with any degree of accuracy since wave height and
velocity are not only related to wind velocity but also to the previous
state of the sea, the size or "fetch" of the area affected by the wind,
and the duration of the wind.

In May in the northern hemisphere (Fig. A-13), the northern North
Atlantic covering subregions A and B provides the highest average po-
tential wave energy for the period, reaching levels in excess of 60
kilowatts per meter of wave front (kW/m/WF). In this area wave ac-
tivity appears to correlate fairly well with the wind for April, as
seen in Fig. A-9. There is also a fair match made between the somewhat
lesser wave power levels shown for subregion H in the North Pacific.

For the most part, the broad zone of ocean straddling the equator
is characterized by low to moderate wave energy potential (3-30kW/m/WF);
however, beginning at about 20°S, including the southern portion of
subregion E, the power potential appears rather consistently at 30
kW/m/WF. South of 30°S, wave power potential reaches its maximum
value of 90 kW/m/WF (with 60 kW/m/WF dominating) and correlates very
well with the strong westerly winds of the Roaring Forties.

During the month of August (Fig. A-14), the most significant power
level change in the northern hemisphere is found in the northern portion
of subregion D, where values along the flow of the monsoon exceed 90
kW/m/WF. In the southern hemisphere during the period, a slight north-
ward movement of potential power isopleths takes place in the Indian and
South Pacific Oceans. Both of the above changes correlate very well
with the wind power level changes for July, as seen in Fig. A-10.

By November, the wave activity in the northern hemisphere along
the storm tracks has markedly increased, with considerably higher power
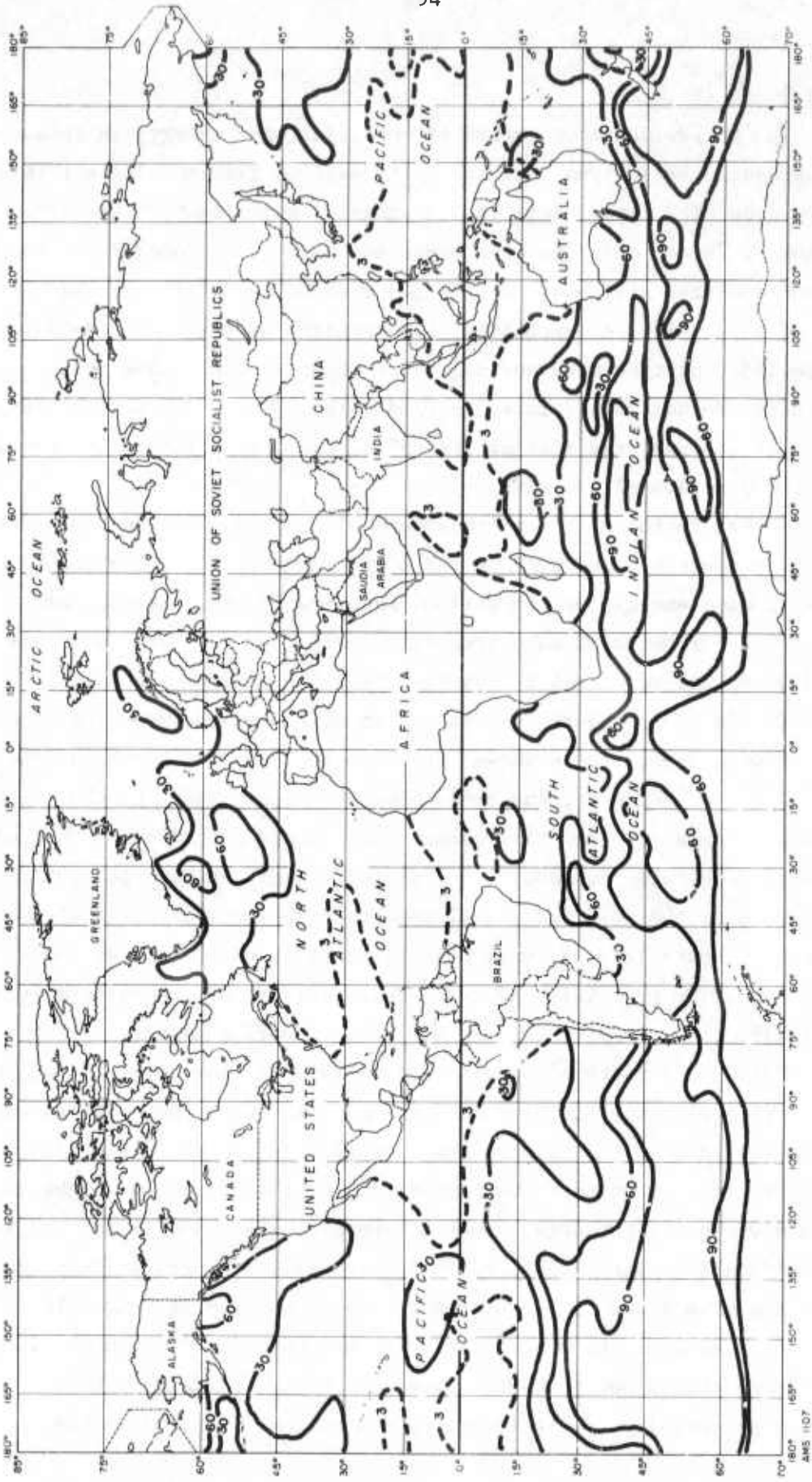levels potentially available in the subregions of the North Pacific

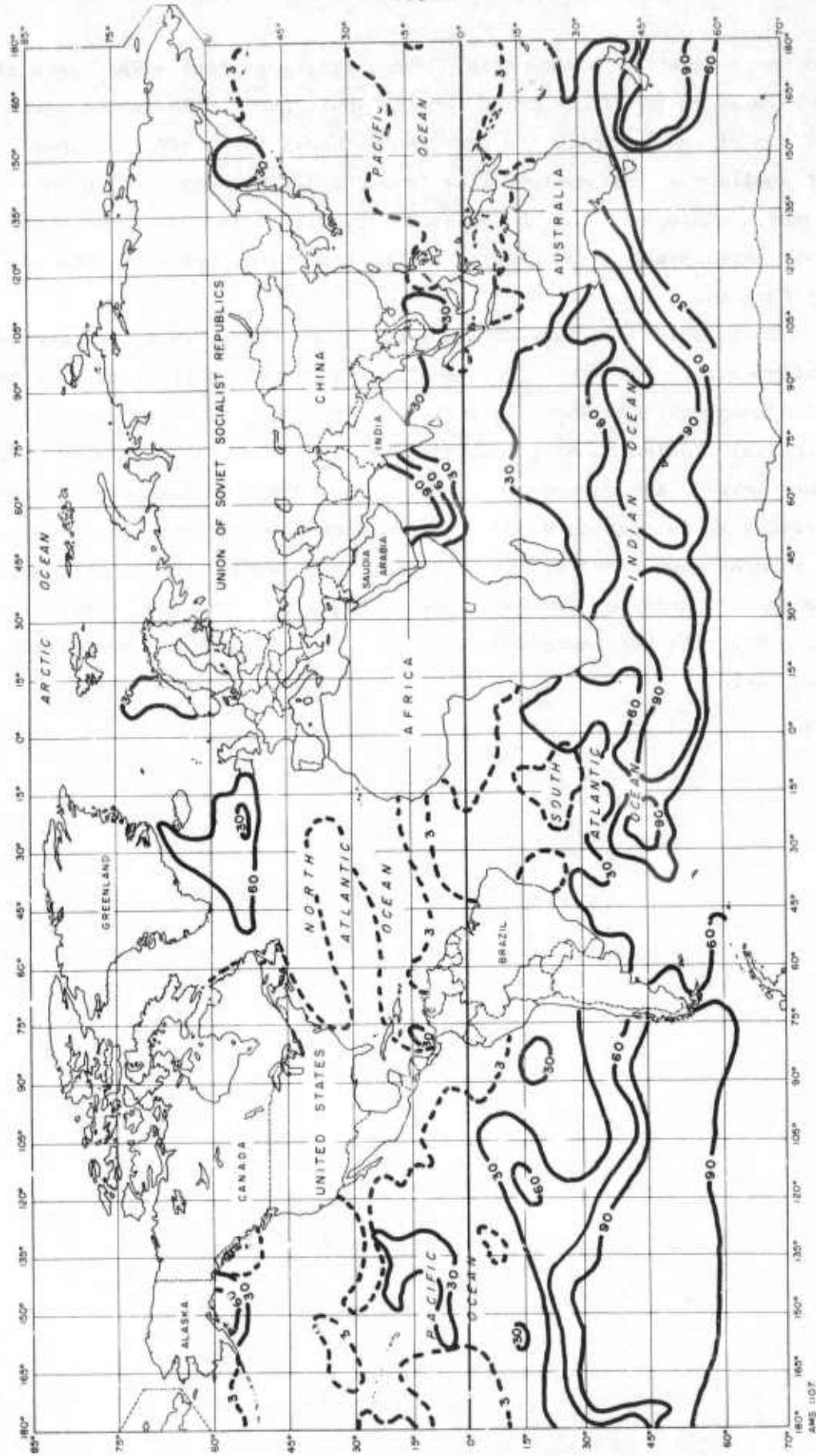Fig. A-13—Average potential wave power density: May (kW/m/WF)

Fig. A-14—Average potential wave power density: August (kW/m/WF)

and North Atlantic Oceans (Fig. A-15), rising to levels in excess of 90 kW/m/WF in the vicinity of the Icelandic Low. Only in the northern portion of the Indian Ocean have the values dropped off in response to a transition to the monsoon flow from the north. Wave action in the southern hemisphere has abated somewhat, with less continuous high power level areas of 90 kW/m/WF south of 30°S, except along the Roaring Forties.

This decreasing wave activity in the southern hemisphere generally continues into February (Fig. A-16). During this northern winter period, subregions over the North Atlantic continue to show high power level potential, including an expansion in area of the higher than 90 kW/m/WF power level. Somewhat more marked is the increased intensity of wave activity in subregions H and G of the North Pacific at both the 60 and 90 kW/m/WF power levels. As with the other seasons the significant changes in potential available power levels for February generally correlate with the increased wind activity for the month preceding (Fig. A-12).
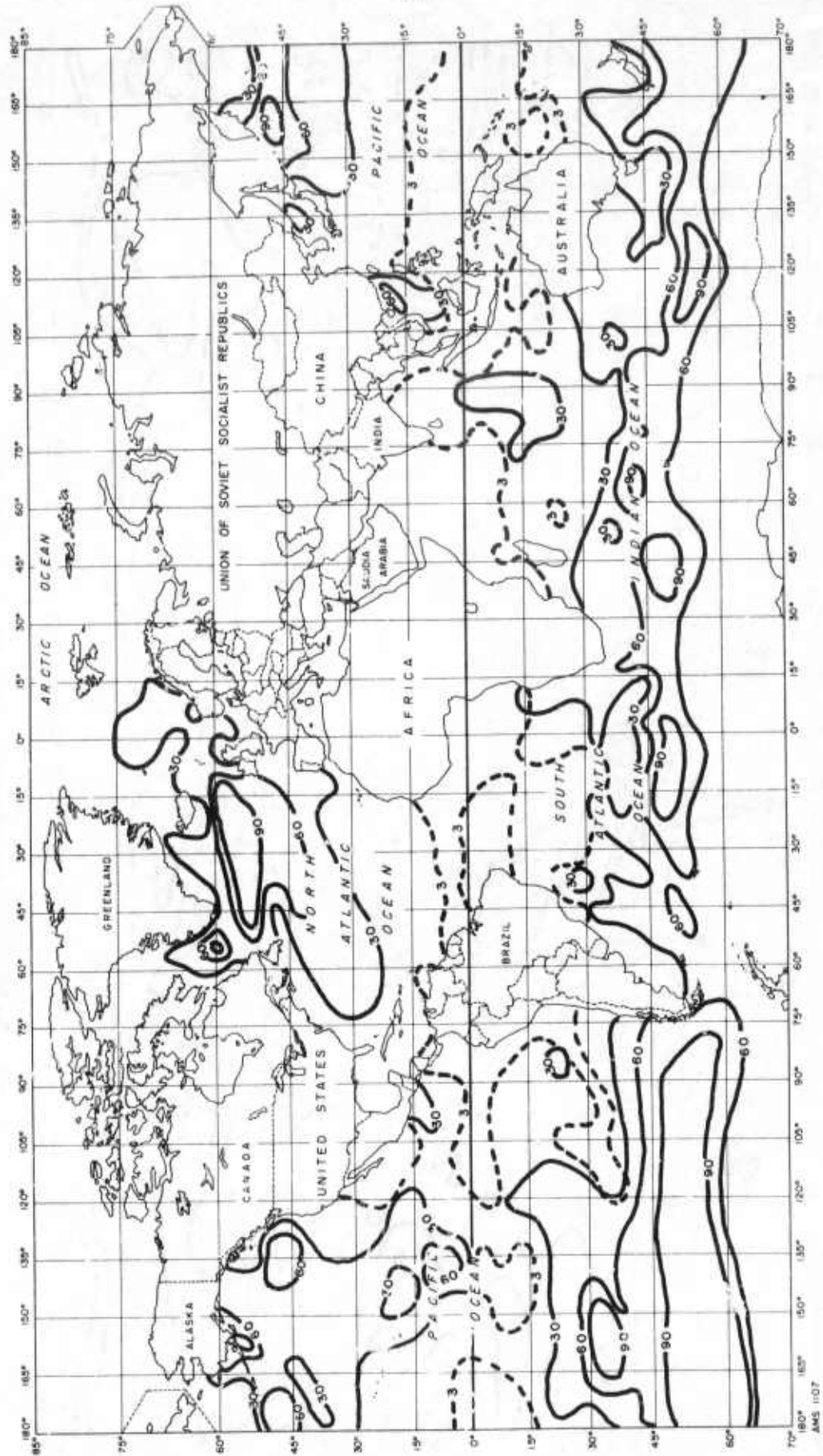
Fig. A-15—Average potential wave power density: November (kW/m/WF)

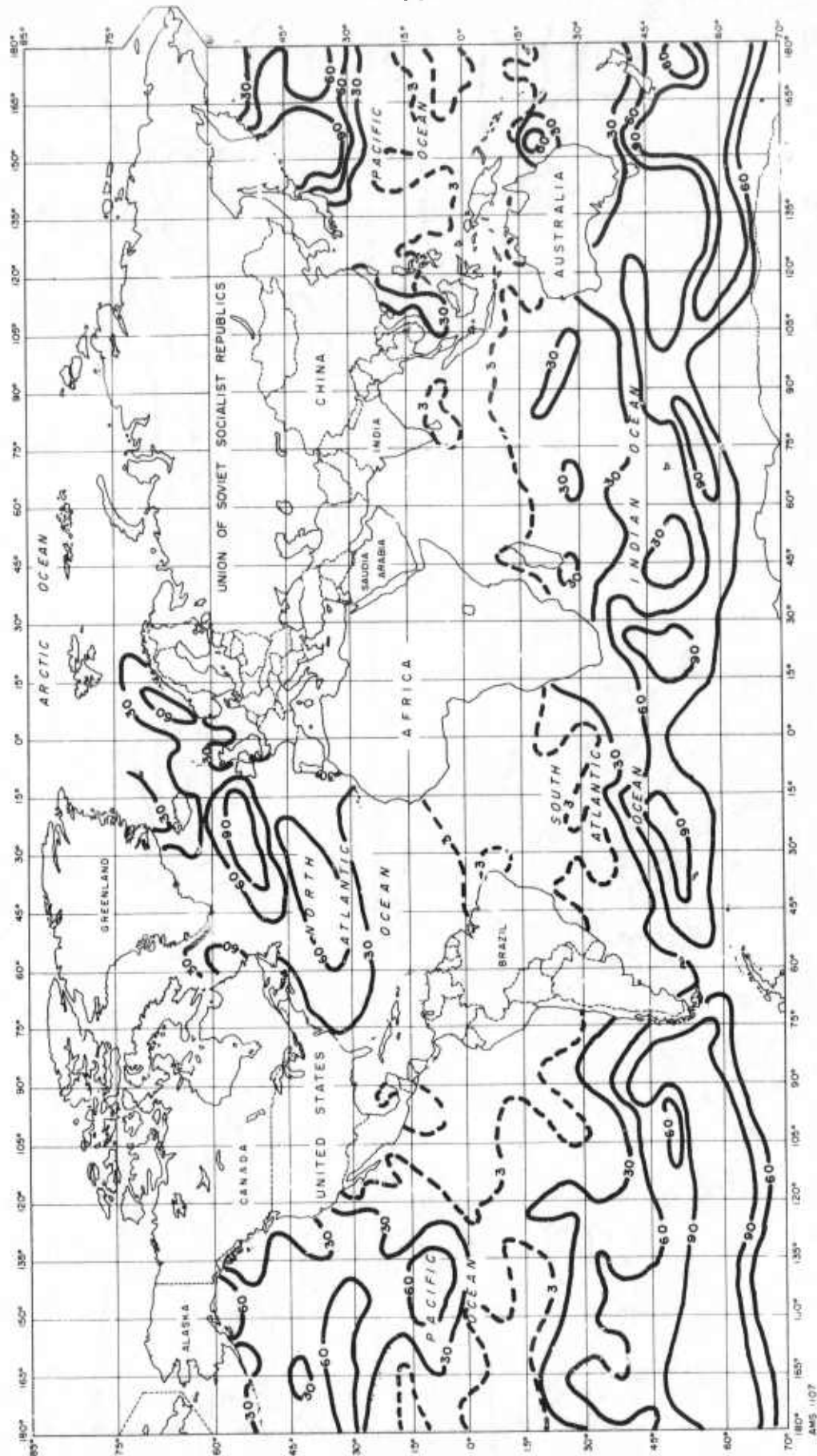Fig. A-16—Average potential wave power density: February (kW/m/WF)

Appendix B

CONVERSION OF WIND AND WAVE DATA TO POWER DENSITY UNITS

A technique was developed during the course of this study to translate wind and wave information, available in various climatic atlases in the form of isorithmic maps, into units of potential power density.[1] Isopleths indicating the probability of occurrence of winds of Beaufort force 5 were converted to power density probability of occurrence curves, as was the probability of occurrence of waves of 12 ft and above. Additional data in these atlases described the probability of wind velocity or wave height as a function of season and location. These distributions in wave height and wind velocity tended to change in a characteristic way as the average wind velocity or wave height changed with location and season. In each case (wind and wave) a family of these distributions was collected that spanned the practical intensity spectrum. Figure B-1 shows the set of wind velocity probability distributions that we developed for the North Atlantic from data in Office of Climatology, 1959 and 1961, which contains similar distributions for wave height.

These probability curves were integrated to obtain the average ideal power levels as a function of the probability at which the curve crosses the characteristic wind speed or wave height. In the case of wind, a characteristic velocity of 19 kn (Beaufort 5, a fresh breeze) was used. From the data in Naval Weather Service Command, 1969, we constructed worldwide isorithmic maps around the range of probabilities of wind velocities equal to or greater than 19 kn. Ideal power in kW/m^2 of perpendicular flow area is given by $(8.2356 \times 10^{-5} V_{kn}^3$. In the case of waves, the characteristic wave height equal to or greater than 12 ft was used in plotting the isopleths in Office of Climatology, 1959 and 1961. Ideal power in kW/m of wave width is given by

---

[1]Naval Weather Service Command, 1969; Office of Climatology, 1959 and 1961; U.S. Naval Oceanographic Office, 1966.
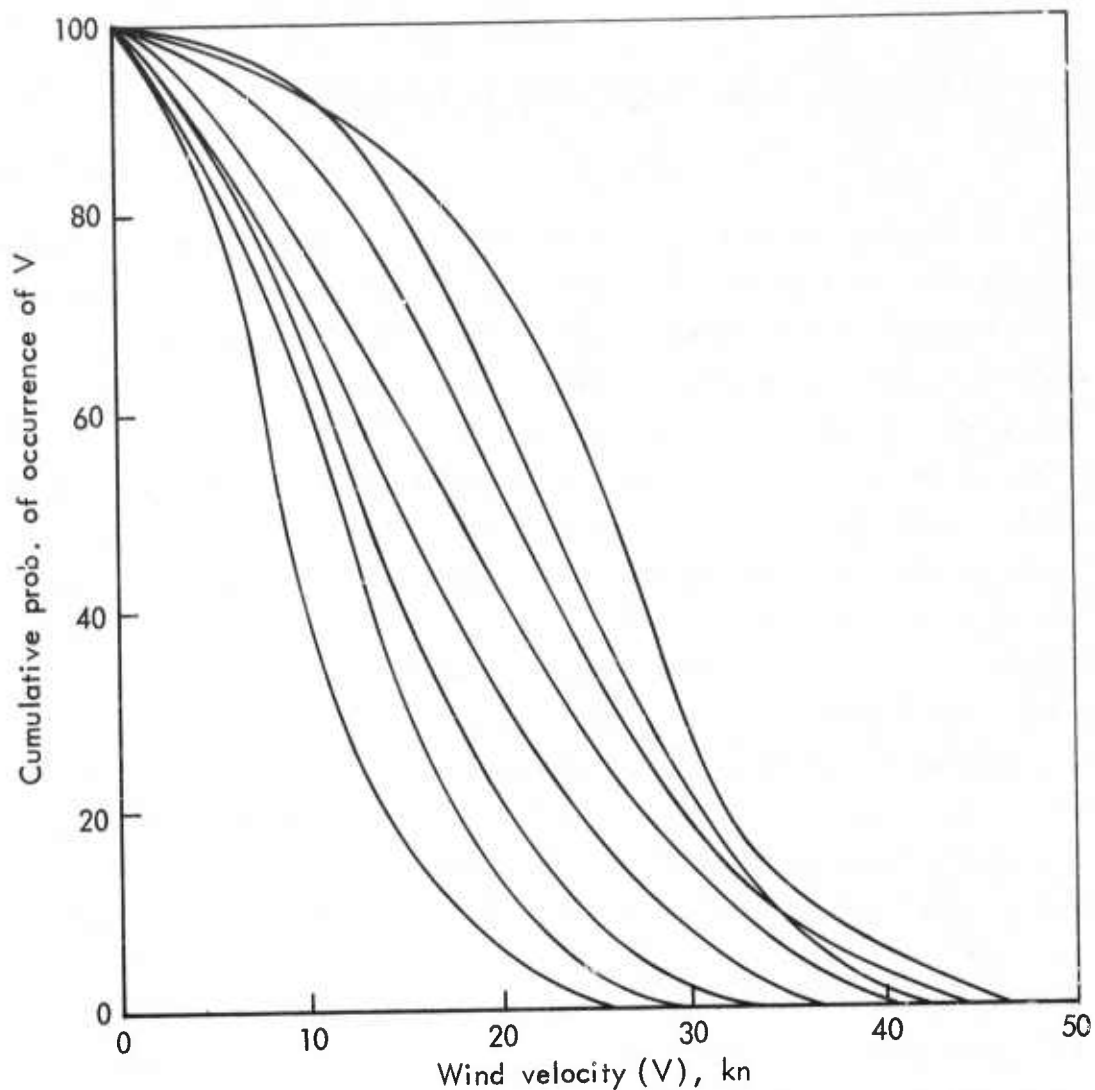
Fig. B-1 — Family of wind velocity probability distributions

(0.091) TH_{tc}^2 (where T is the crossing time peak to peak and H_{tc} is the wave height).

A check of our approximate technique was possible using data from India Station in the North Atlantic as analyzed more precisely by S. H. Salter (1974) of Edinburgh. Our results differed from Salter's by only 3 percent for annual average ideal power potential, which he quotes at 77 kW/m of wave front based on a detailed computer analysis of actual wave occurrence data over a one-year collection period.
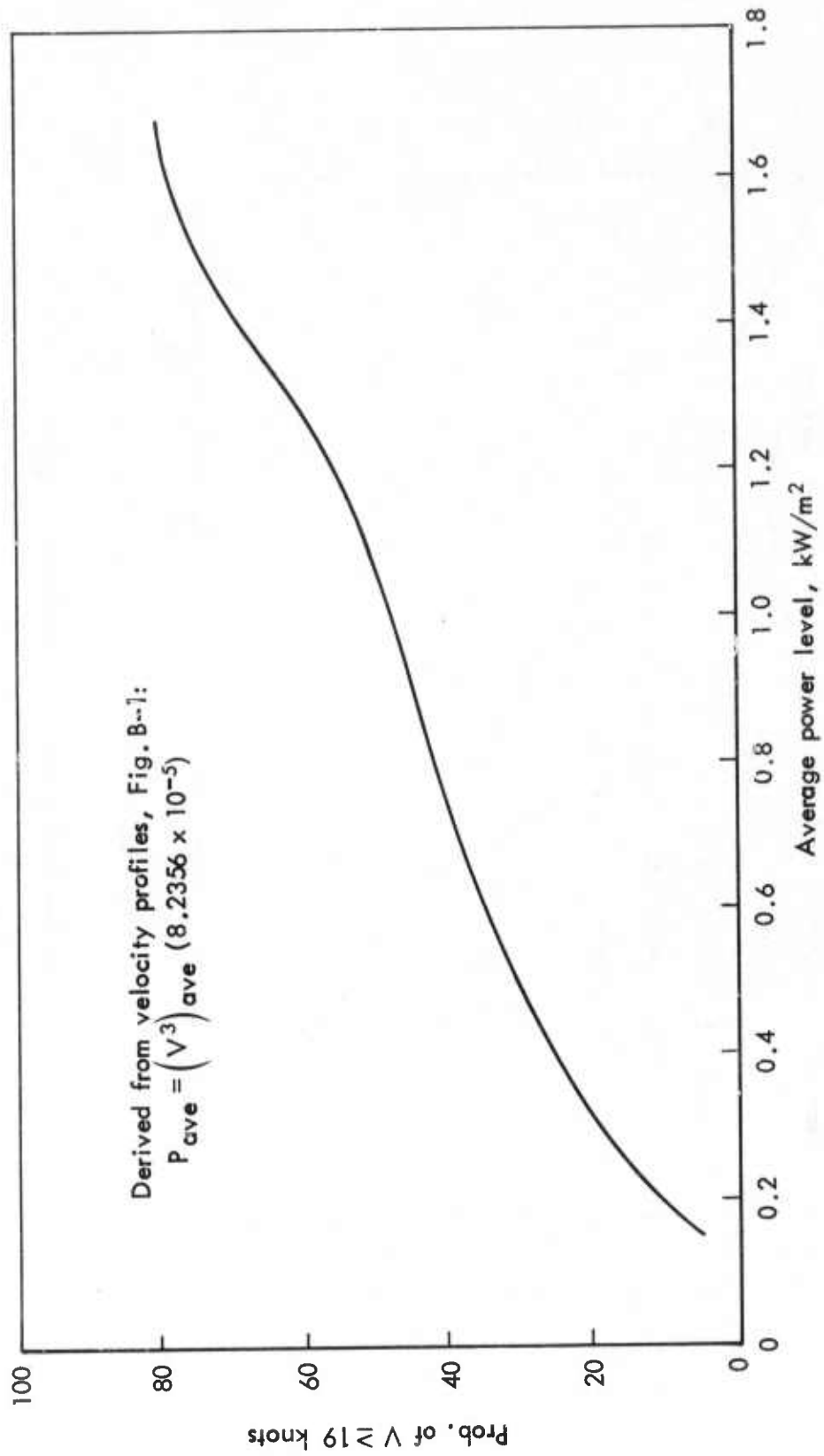
Conversion curves are shown in Figs. B-2 and B-3.

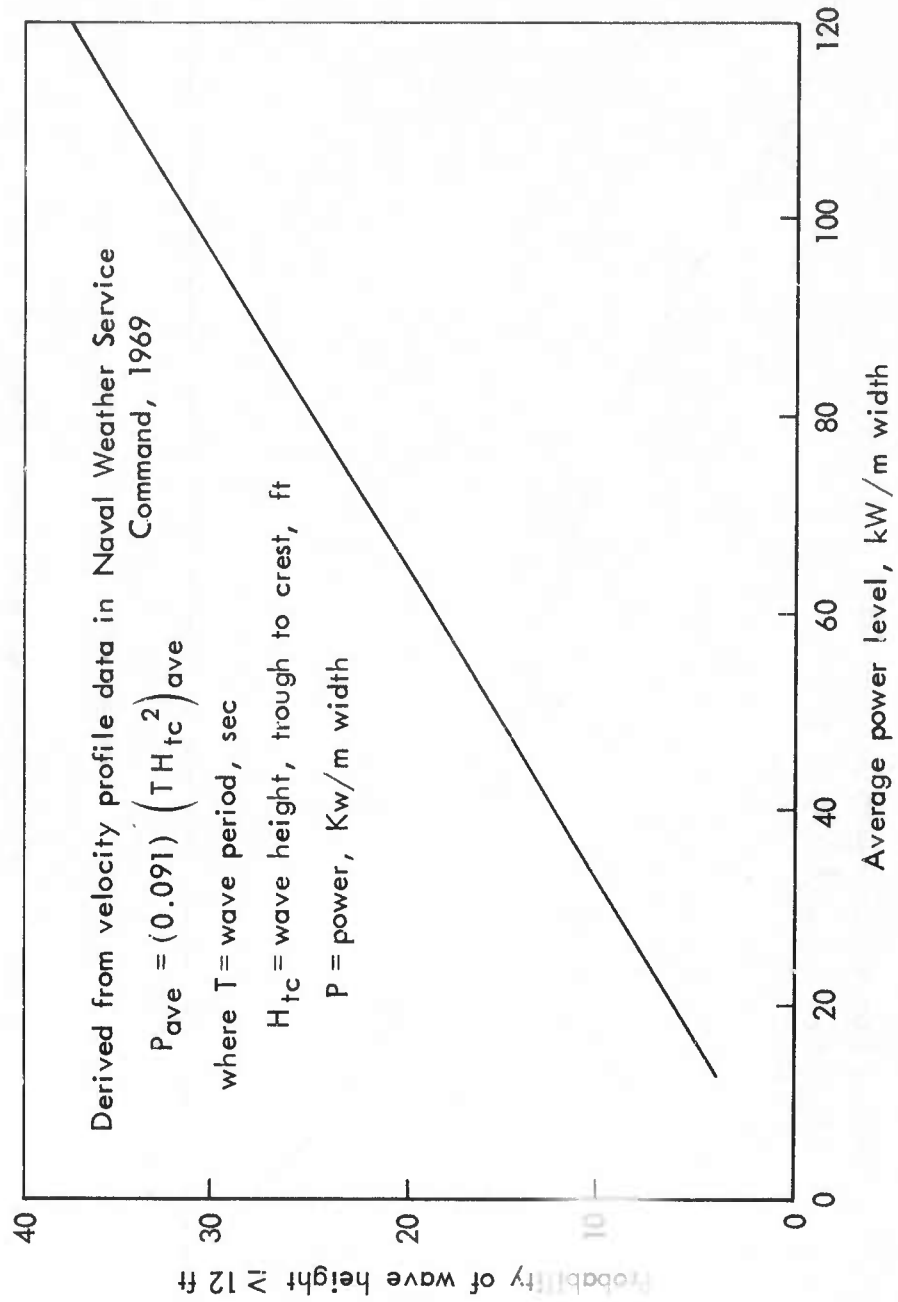Fig. B-2 — Ideal wind power potential

Fig. B-3— Ideal ocean wave train power potential

Appendix C

CONVERSION OF SOLAR RADIATION FROM HORIZONTAL
TO ZENITH-NORMAL INCIDENCE

In this appendix we present the formalism by which the Budyko-Schutz solar radiation data were converted from radiation incident on a surface tangent to the earth to radiation incident on a surface normal to the rays of the sun at noon.
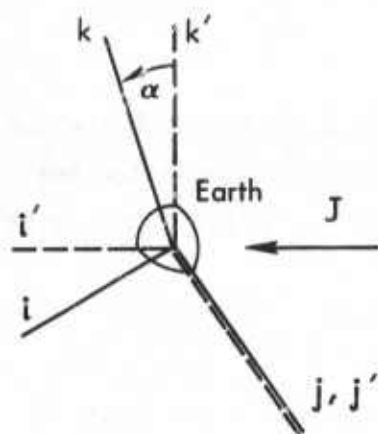
Several approximations have been made:

1. The orbit of the earth around the sun is circular with a radius equal to the orbit's annual average radius.

2. Except for the winter months in extreme northern latitudes, diffuse radiation does not have to be treated separately from direct radiation (the greatest errors due to this approximation occur for months that have high average cloudiness indices, and final radiation values for these cases may be too high by about 25 percent (see note at end of this appendix).

3. The January, April, July, and October average monthly fluxes of Budyko and Schutz represent total radiation at the corresponding equinoxes and solstices.

The following derivation applies to direct solar radiation. The coordinate system used is shown in Fig. C-1. The double primed system is centered at the sun, and the values of the azimuthal angle ϕ'' give the seasons of the year:

$$\phi'' \begin{cases} 0 = \text{January} \quad \frac{\pi}{2} = \text{April} \quad \pi = \text{July} \quad \frac{3\pi}{2} = \text{October} \end{cases}$$

The single primed axis is simply a translated solar axis centered at the earth. $\alpha = 23.5°$ (0.4102 radians) is the inclination of the earth's axis, which for January is a clockwise rotation of the primed system about j'.

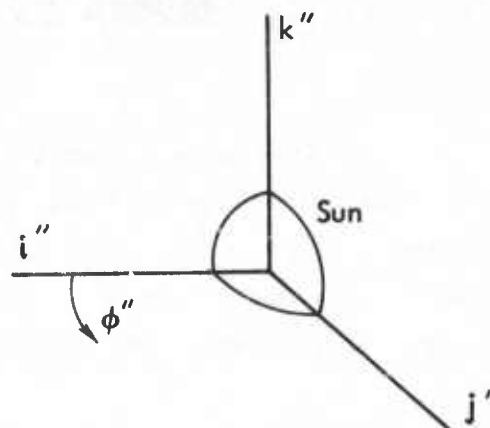Terrestrial coordinate system   Solar coordinate system

Fig. C-I—Coordinate systems for solar incidence transformation

(January $\phi'' = 0$)

Let $\underline{J}$ be the flux vector directed from the sun to the earth. In solar coordinates,

$$\underline{J} = J (\cos \phi'' \underline{i}'' + \sin \phi'' \underline{j}'') . \tag{C.1}$$

To express J in the (unprimed) earth's coordinate system, the coordinate axes must be rotated according to:

$$\underline{J} = \begin{bmatrix} J_x \\ J_y \\ J_z \end{bmatrix} = J \begin{bmatrix} \cos \alpha & 0 & -\sin \alpha \\ 0 & 1 & 0 \\ \sin \alpha & 0 & \cos \alpha \end{bmatrix} \begin{bmatrix} \cos \phi'' \\ \sin \phi'' \\ 0 \end{bmatrix} = J \begin{bmatrix} \cos \alpha \cos \phi'' \\ \sin \phi'' \\ \sin \alpha \cos \phi'' \end{bmatrix} . \tag{C.2}$$

Next the unit normal to the earth's surface at any point $(\underline{n}_\nabla)$ is given by the gradient of the scaler equation for a sphere (ϕ):

$$\phi = x^2 + y^2 + z^2 \qquad (= R^2 = \text{constant})$$

(C.3)

$$\underline{n}_\nabla = \frac{\nabla\phi}{|\nabla\phi|} = \sin\theta\,\cos\phi\,\underline{i} + \sin\theta\,\sin\phi\,\underline{j} + \cos\theta\,k ,$$

where θ is the polar angle of a location on the earth.

The daily average flux measured by Budyko corresponds to the radiation through the projection of a unit surface area in the direction of the incoming flux vector J. Hence the Budyko flux (J_B) is

$$J_B = \frac{-\displaystyle\int_{\phi_1}^{\phi_2} J \cdot (\underline{n}_j \cdot \underline{n}_\nabla)\,\Delta S\,d\phi}{\Delta S \displaystyle\int_0^{2\pi} d\phi} ,$$

(C.4a)

where ΔS is a unit surface area, $\underline{n}_j$ is the unit vector in the direction of $\underline{J}$, and $\underline{n}_j \cdot \underline{n}_\nabla\,\Delta S$ is the projected surface area. The integrations over ϕ are equivalent to a 24-hr time average; the upper integration is over the range of ϕ corresponding to that portion of the earth illuminated during the day (ϕ_1 and ϕ_2 are the tangent points of J to the earth's surface) and the lower integration simply represents the full 2π rotation of the earth.

The absolute value of J depends on θ and ϕ if one defines J as the solar flux at the earth's surface (as had Budyko) because of angular dependent absorption and scattering effects. However, from Eq. (C.4a) an average J may be defined for each latitude (θ) so that

$$J_B = -\frac{\overline{J}}{2\pi} \int_{\phi_1}^{\phi_2} \underline{n}_j \cdot \underline{n}_\nabla\,d\phi .$$

(C.4b)

Hence for each geographic point of Budyko's data, this equation can be used to obtain the average daily incoming flux on a perpendicular surface.

Expressions for ϕ_1 and ϕ_2 are available from the condition of perpendicularity of $\underline{J}$ and $\underline{n}_\nabla$; i.e.,

$$\underline{n}_j \cdot \underline{n}_\nabla = 0 = \cos \alpha \cos \phi'' \sin \theta \cos \phi$$

$$+ \sin \phi'' \sin \theta \sin \phi + \sin \alpha \cos \phi'' \cos \theta , \qquad (C.5)$$

where we have used

$$\underline{n}_j = \frac{\underline{J}}{|\underline{J}|} = \cos \alpha \cos \phi'' \underline{i} + \sin \phi'' \underline{j} + \sin \alpha \cos \phi'' \underline{k} . \qquad (C.6)$$

Substituting the values of ϕ'' for each of the four months given above, one obtains

$$\phi = \arccos (- \tan \alpha \cot \theta) \qquad (C.7)$$

for January and July (solstice conditions), the two solutions of which are ϕ_1 and ϕ_2. For April and August (equinox conditions), $\phi_1 = 0$, $\phi_2 = \pi$ for all values of θ. Equation (C.4b) may be simplified by integration using Eqs. (C.3) and (C.6) to give

$$\overline{J} = - 2\pi J_B / [\cos \alpha \cos \phi'' \sin \theta (\sin \phi_2 - \sin \phi_1)$$

$$- \sin \phi'' \sin \theta (\cos \phi_2 - \cos \phi_1)$$

$$+ \sin \alpha \cos \phi'' \cos \theta (\phi_2 - \phi_1)] . \qquad (C.8)$$

Equations (C.8) and (C.7) have been solved for $\overline{J}$ for each of our five remote base regions. The original Budyko-Schutz data and the calculated $\overline{J}$ values appear in Table C-1. Variations in values of $\overline{J}$ primarily reflect different degrees of cloudiness.

Table C-1

AVERAGE SOLAR FLUX ON PERPENDICULAR SURFACE (MW/km^2)

(Budyko-Schtz data in parentheses)

Location	θ	January	April	July	October
Diego Garcia	96.3°	822 (257)	689 (218)	632 (170)	704 (223)
Sebana Seca	72.0°	834 (182)	880 (266)	817 (279)	709 (215)
Adak	38.5°	452 (24)	550 (109)	265 (97)	367 (73)
Azores	51.7°	610 (73)	727 (182)	595 (218)	679 (170)
Keflavik	26.0°	575[a] (12)	868 (121)	601 (218)	264 (37)

[a]For this data point only, diffuse radiation (approximately 5.7 MW/km^2) was subtracted from the original horizontal Budyko data. This was necessary because at this proximity to the Arctic Circle, winter days have very large diffuse radiation contributions to their total daily radiation.

The $\bar{J}$ values have been used to determine the solar radiation on a fixed collector surface perpendicular to the sun's rays at noon. If $\underline{n}_p$ is the unit normal to such a surface, the daily average flux on the surface (J_o) is

$$J_o = - \bar{J} \int_{\phi_1'}^{\phi_2'} (\underline{n}_p \cdot \underline{n}_j) \, \Delta S \, d\phi / (2\pi \Delta S) \, , \qquad (C.9)$$

where $(\underline{n}_p \cdot \underline{n}_j) \Delta S$ is the projection of the unit collector area in the direction of $\underline{J}$. ϕ_1' and ϕ_2' are the values of ϕ when the surface is at right angles to the incoming flux vector $\underline{J}$, unless the collector passes into the shadow of the earth before this condition is reached.

Expressed vectorially, ϕ_1' and ϕ_2' are chosen to be whichever solutions of

$$\underline{n}_p \cdot \underline{n}_j = 0 \qquad (C.10)$$

or

$$\underline{n}_\nabla \cdot \underline{n}_j = 0 \qquad (C.5)$$

give the smallest azimuthal range on the illuminated side of the earth. For points (below the Arctic Circle) in the northern hemisphere in January, Eq. (C.5) generally gives the tangent values; in July, Eq. (C.10) generally gives the results. ϕ_1' and ϕ_2' are simply 0 and π during the months of April and October.

An expression for $\underline{n}_p$ is derived by noting that in January it is just the surface gradient vector with the polar angle θ increased by α; for July, θ is reduced by α. Hence,

$$\underline{n}_p = \underline{n}_V \left(\frac{\pi}{2} + \alpha, \phi \right) = \cos\alpha \cos\phi\underline{i} + \cos\alpha \sin\phi\underline{j} \pm \sin\alpha\underline{k} , \quad (C.11)$$

where the positive version gives the January result and the negative version gives the July result.

The ϕ_1' and ϕ_2' tangent values for January and July are summarized in Table C-2.

Table C-2

ϕ_1' AND ϕ_2' TANGENT VALUES

Location	January		July	
	ϕ_2'	ϕ_1'	ϕ_2'	ϕ_1'
Diego Garcia	272.8	87.2	87.2	-87.2
Sebana Seca	261.9	98.1	98.1	-98.1
Adak	236.9	123.1	100.9	-100.9
Keflavik	206.9	153.1	100.9	-100.9

Finally, expression (C.9) was integrated using Eqs. (C.6) and (C.11) and the ϕ' values in Table C-2 to give values for J_o for all five of our base locations. The results of this computation appear as the data in Table 8.

NOTE: Annette, Alaska is quite cloudy in November, the diffuse radiative component being about 0.6 of the total horizontal surface radiation (Liu and Jordan, 1960). If this same value is assumed to

hold at Adak in October and it is noted that the direct radiation
calculation performed in this appendix results in multiplying the
original horizontal surface value by $117/73 = 1.60$, the calculation
with an initial diffuse radiation subtraction included results in:

$$J_o = [73 - 0.6(73)] \times 1.60 + (0.6) \, 73 = 90.5 \, ,$$

or 77 percent of the value tabulated in Table 8. January errors at
Adak are somewhat worse, but all other values are considerably better.

Appendix D

ENERGY BALANCES AND OPERATIONS EQUATIONS FOR

THE MODEL POWER SYSTEM

In this appendix we present the energy balances and rules of operation of the power system appearing in Fig. 6. Solution of the algebraic and integral equations presented here lead to the time-dependent power and storage levels pertinent to that power system. Besides presenting mathematical expressions, this appendix also discusses why the particular modes and rules of operations were chosen.

Energy balances may be written for the power system in Fig. 6 as follows. Denoting the input power density by J and the collector size by A (units of area for solar and wind input, units of length for wave input), the input energy is

$$J \cdot A = Q4 + Q5 , \qquad (D.1)$$

where Q4 is the power being used for electricity generation and Q5 is the power being used for space heating; $Q5 \equiv 0$ for the nonsolar systems. When Q4 and Q5 are radiative powers, they must both undergo conversion to thermal energy. The thermal energy corresponding to Q5 is contained in the working fluid of the solar system and must pass through a heat exchanger to provide space heating energy. Satisfying the space heating demand by means of a solar driven steam heat system obviates any need for a new heat distribution system at existing remote bases. Because these remote bases are physically small in area, steam lines do not have to cover large distances and distribution losses are small. The combined efficiency of the thermal conversion and heat exchanger steps is E7, and the power delivered to the space heating demand (q5) is

$$q5 = E7 \cdot Q5 . \qquad (D.2)$$

The conversion of indigenous power Q4 to output electrical power is given by

$$q4 = E4 \cdot Q4 \ , \tag{D.3}$$

where, in the solar case, E4 is the combined radiative-to-thermal conversion and turbine-generator efficiencies, and in the nonsolar case is the mechanical-to-electrical conversion (mechanical generator) efficiency.

The waste heat from the turbine used in the solar system could be used to partially satisfy space heating demands. It has not been used for this purpose in the present model because the high thermodynamic efficiency used here implies a very low sink temperature where recovery would not be indicated. In an actual operating system, however, the thermodynamic efficiency would be lower and the waste heat should be used for space heating.

The turbine-generator output is generally used to satisfy electrical demand (Q3) directly as well as provide input for the storage system (Q1). The energy balance corresponding to this is, from Eq. (D.3):

$$E4 \cdot Q4 = Q1 + Q3 \ . \tag{D.4}$$

Two storage systems are indicated in Fig. 6, hydrogen storage with its attendant fuel cells, and battery storage. In the hydrogen system, fuel cells may operate in either an electrolysis mode or fuel cell generator mode, each mode having a different efficiency: E1 for the former, E21 for the latter. The electrolysis power output, q_{11}, is

$$q_{11} = E1 \cdot Q1 \ . \tag{D.5}$$

The energy balance for the storage is equal to the input less that amount of hydrogen withdrawn for immediate combustion for space heating (Q6) and that withdrawn for electricity generation (q_{21}); i.e.,

$$\dot{S} = q_{11} - q_{21} - Q6 = E1 \cdot Q1 - \frac{Q2}{E21} - Q6 . \tag{D.6}$$

Heat exchanger No. 2 merely allows the heat of combusted hydrogen to be transferred to steam with efficiency E6; i.e., $q_7 = E6 \cdot Q6$.

When the battery system is used, E1 and E21 refer to the efficiency of electrical storage and are equal in value. That portion of battery-stored energy drawn off to supply space heat may be used as electrical energy or may be used indirectly to heat a working fluid. The former case is more efficient but does imply that a mixed type of electrical and steam heating system would be required since we have previously assumed that some heat is being delivered thermally. Since heat exchangers are very efficient, little energy loss is involved if we do assume the use of an all steam heat system. Hence, under this assumption, E6 represents the combined heat exchanger and battery output efficiencies. Battery input and total storage are still given by Eqs. (D.5) and (D.6).

The electrical demand of the base (D) is satisfied by the turbine-generator output, the fuel cell or battery output, and, when these are insufficient, by the engine-generator system. Hence

$$D = Q2 + Q3 + EB \cdot B1 , \tag{D.7}$$

where EB is the efficiency of the engine generator system and B1 is the rate of fuel oil consumption required to drive the generator.

$$BR \equiv (1 - EB) B1 \tag{D.8}$$

is the waste heat of the engine and constitutes the input to heat exchanger No. 3. The heat recovered by this exchanger, BRP, is used to help satisfy space heating demand. The energy losses due to inefficiency of the heat exchanger and any recovered energy that is not immediately usable constitute BL. For heat exchanger No. 3,

$$BRP = BR - BL . \tag{D.9}$$

When direct solar space heating (q5), storage, and turbine waste heat are all insufficient to satisfy space heating demand, fuel oil may be burned to make up the deficit. This is the function of the furnace and heat exchanger No. 4 in Fig. 6. Evidently,

$$B2 = (B2P - BRP)/EBP ,$$

(D.10)

where B2 is the rate at which fuel oil is burned and EBP is the efficiency of the heat exchanger. Finally, the balance for space heating demand (DP) is

$$DP = E7 \cdot Q5 + E6 \cdot Q6 + B2P .$$

(D.11)

To complete the description of the power system, rules and equations of operation are required. Five such rules have been chosen. The first applies to the split of incoming energy into Q4 and Q5. Because the direct use of solar power for heating is more efficient than converting it to electrical energy, only the excess of this power over space heating demands goes into electricity production. Thus

$$Q5 = \begin{cases} J \cdot A \left[1 - H \left(J \cdot A - \frac{DP}{E7} \right) \right] + \frac{DP}{E7} H \left(J \cdot A - \frac{DP}{E7} \right) & \text{(solar)} \\ \\ 0 & \text{(nonsolar)} \end{cases}$$

(D.12)

where H( ) is the Heaviside function and is used here to keep Q5 from ever exceeding the heating demand. Wind and wave power give no thermal input and hence Q5 = 0 for these sources. The second operational rule states that electrical output from the turbine generator must preferentially be used to satisfy current electrical demand, with only the excess over demand going to storage. This, of course, minimizes the losses due to storage conversion inefficiencies. Algebraically,

$$Q1 = (E4 \cdot Q4 - D) H(E4 \cdot Q4 - D) .$$

(D.13)

Because the goal of the indigenous systems is to reduce the fuel oil dependence of remote bases, a third operational rule allows the engine generator and the furnace to be used only when the storage supply is fully depleted. Consequently, for the engine generator

$$B1 = EB^{-1} [1 - H(E4 \cdot Q4 - D)] [1 - H(S)] (D - E4 \cdot Q4) , \quad (D.14)$$

where

$$H(S) = \begin{cases} 1 & S > 0 \\ 0 & S = 0 \end{cases}$$

$S = S(t)$, the time dependent value of storage supply.

The first Heaviside function provides for the condition that when the turbine-generator output exceeds electrical demand, no additional power input from the engine generator is needed.

For the furnace,

$$B2P = [1 - H(S)] \Big\{ [1 - H(E4 \cdot Q4 - D)] (DP - E7 \cdot Q5) + H(E4 \cdot Q4 - D)$$

$$\times H[DP - E7 \cdot Q5 - E1 \cdot E6(E4 \cdot Q4 - D)] \cdot [DP - E7 \cdot Q5$$

$$- E1 \cdot E6(E4 \cdot Q4)] \Big\} + H(S) \cdot \min \Big\{ ER \cdot BR, DP - E7 \cdot Q5 \Big\} .$$

$$(D.15)$$

When the storage is fully depleted, the first term in the braces gives B2P. There are two subcases of operation when $S = 0$: The first corresponds to the turbine-generator output being less than electrical demand $(E4 \cdot Q4 - D) < 0$ and the second to the reverse condition. In the first subcase, the combined furnace and recovered waste heat must equal the space heating demand less (in the solar case) that amount of power shunted to this demand directly. No portion of the output of the turbine generator flows through storage since all power goes to satisfy electrical demand. In the second subcase, however, the portion of generated power in excess of electrical demand (but less than the net space heating demand $DP - E7 \cdot Q5$) passes directly through storage. The

second term in braces gives B2P when stored energy is present initially. Here recovered waste energy (ER · BR) is allowed to satisfy the net space heating demand provided it does not exceed the net demand DP − E7 · Q5.

The energy losses from heat exchanger No. 3 are composed of the heat exchanger efficiency loss plus the amount of waste engine heat that exceeds what is required to satisfy the B2P value in Eq. (D.15). Hence,

$$BL = (1 - ER) \, BR + (ER \cdot BR - B2P) \, H(ER \cdot BR - B2P) \,, \qquad (D.16)$$

where ER is the efficiency of recovery and the Heaviside function is introduced to suppress a nonzero second term (and an unphysical loss) when all waste heat may be utilized for space heating.

A total annual energy balance for the power system is given by

$$A \int J dt + \int (B1 + EBP \cdot B2) dt = \int \left[D + DP + (1 - E4)Q4 + (1 - E6)Q6 \right.$$

$$\left. + (1 - E7)Q5 + (1 - E1)Q1 + \frac{(1 - E21)}{E21} \, Q2 + BL \right] dt + \int \dot{S} \, dt \,,$$

$$(D.17a)$$

where the integrals cover a one-year time span. We assume that the average energy inputs and demands change insignificantly from year to year. Hence, the amount of energy in storage at the beginning of a year's period should equal that present at the end of the year in order to avoid long-term gains or losses of energy. Thus in a correctly operating system,

$$\int \dot{S} \, dt \equiv 0 \,. \qquad (D.17b)$$

Equations (D.1), (D.3), and (D.6) through (D.17) are the complete set of equations that describe the model power system. Given known

fluxes and demands, they were solved for B1, B2, S, and the various Q_i power levels.

The method of solution of the model equations is as follows. The equations are first solved for the totally indigenous case in order to determine the maximum value of A. Since the initial storage value was unknown, it was assumed to be zero initially and was allowed to go either negative or positive during the time course of the $\dot{S}$ integration. A was determined from Eq. (D.17) after algebraic solution of Eqs. (D.1), (D.4), and (D.7) through (D.16); and the initial storage value was determined from the minimum of the computed storage function.

The mixed indigenous and conventional engine generator cases were solved in a similar fashion except that collector sizes were chosen as successively decreasing fractions of the totally indigenous collector size and were used as input. Initial values of S(t) were then obtained iteratively from Eq. (D.17a) (with the storage integral set equal to zero) by comparing input and calculated values of A. The iterative solution was necessary because several terms in the integrand depended implicitly on S(t) through the H(S) Heaviside function. Output was computed on a grid as fine as 4 hr and variables have been expressed in units of MW, MWh, km^2, or km.

Examples of the time-dependent functions representing input flux (J), electrical energy demand (D), and space heating demand (DP) are presented in Fig. D-1 for the case of our standard base occupying a location in the Azores and using wave motion as its indigenous energy source. Solutions of the power model equations above for the amount of stored energy (S), the rate of fuel oil consumption of the engine generator (B1), and the rate of fuel oil consumption for space heating (B2) for three system configurations are presented in Figs. D-2, D-3, and D-4. The data at the top of Figs. D-2 through D-4 correspond to a system powered entirely by wave energy, while the next two data sets correspond to combined conventional and indigenous power systems whose wave machine frontages are 75 and 50 percent of that required for totally indigenous operation.

The data in Fig. D-2 show that there is a very rapid decline in the amount of energy stored as conventional engine generators are
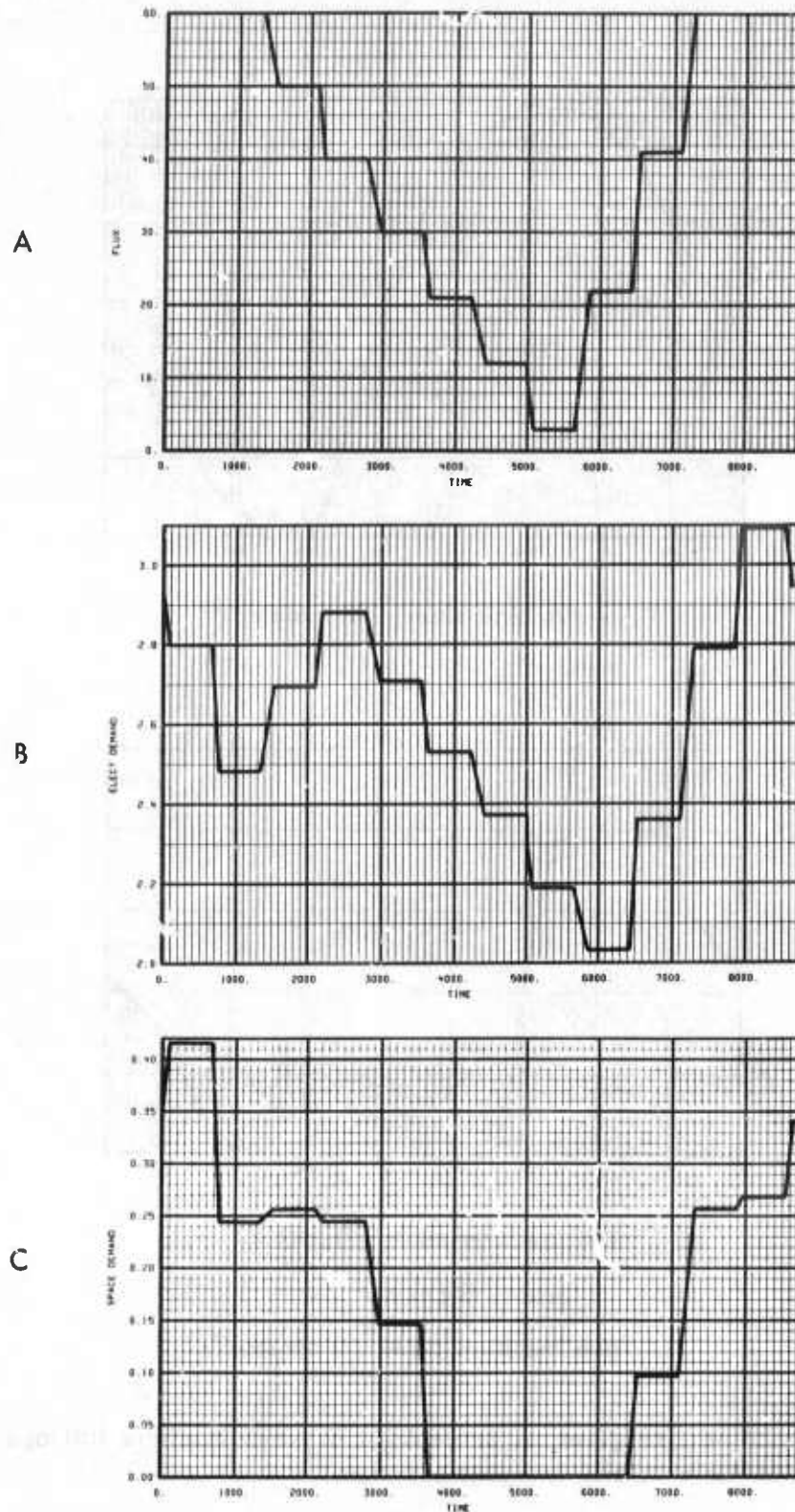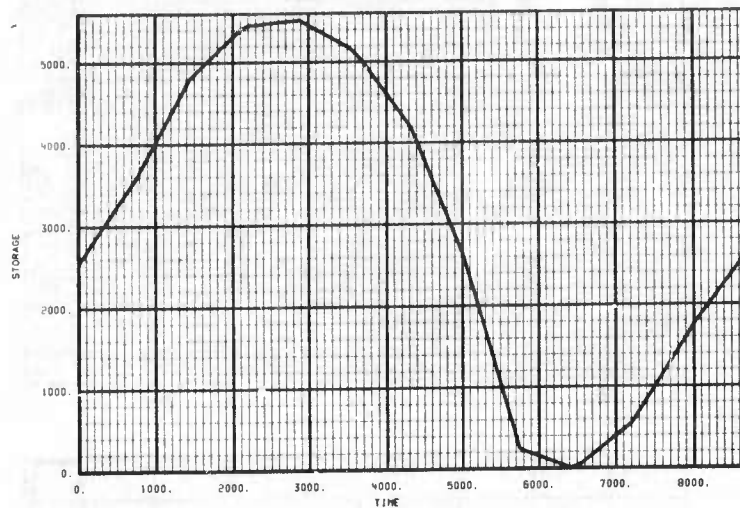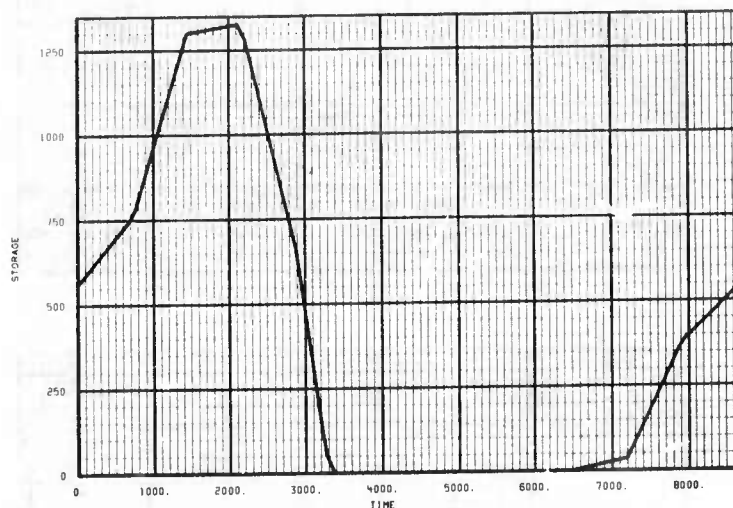
Fig. D-1 — (A) Annual wave power density in the Azores (MW/km), (B) Annual electricity, and (C) Annual space heating power demands for a standard base in the Azores (MW). (time in hours)

Wave machine size: 100 percent *
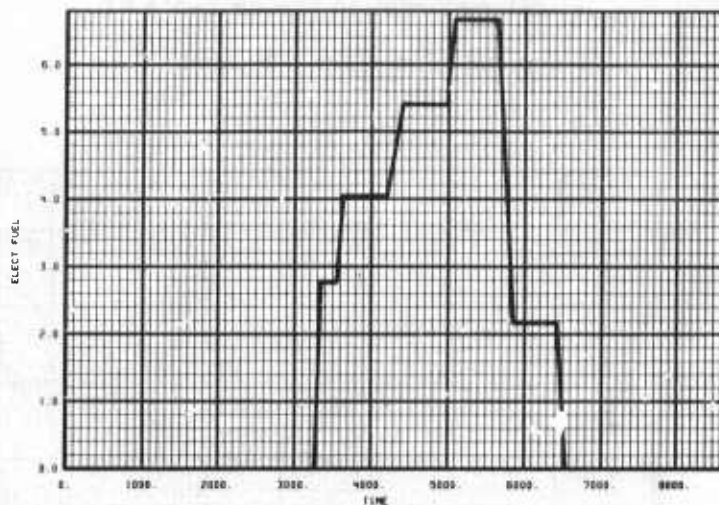

Wave machine size: 75 percent *

Storage: S (t) = 0

Wave machine size: 50 percent *

---

*Wave machine size given as percentage of wave machine frontage
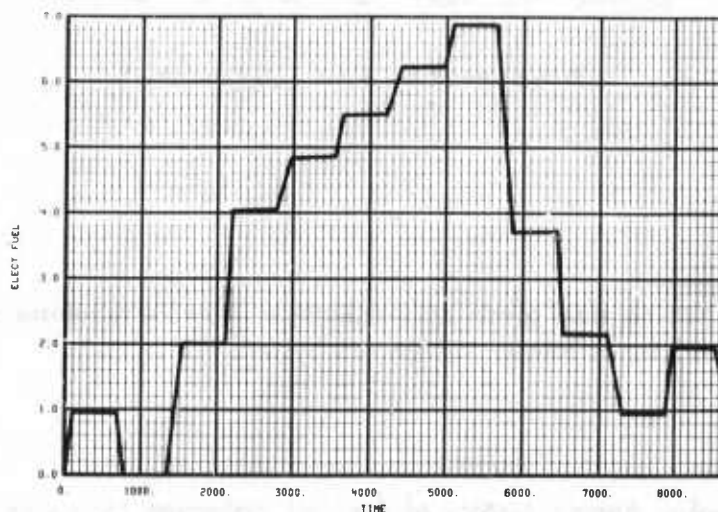required for a totally indigenous system.

Fig. D-2—Annual time course of stored energy (MWh) for combined
conventional/wave power system in Azores

Fuel oil consumption (elec) = 0

Wave machine size: 100 percent*

Wave machine size: 75 percent *

Wave machine size: 50 percent*

---

*Wave machine size given as percentage of wave machine frontage
required for a totally indigenous system.

Fig. D-3—Annual history of fuel oil consumed for electrical power
generation in the Azores (MW) (time in hours)

Fuel oil consumption (space heat) = 0

Wave machine size: 100 percent*

Fuel oil consumption (space heat) = 0

Wave machine size: 75 percent*

Wave machine size: 50 percent*

* Wave machine size given as percentage of wave machine frontage required for a totally indigenous system.
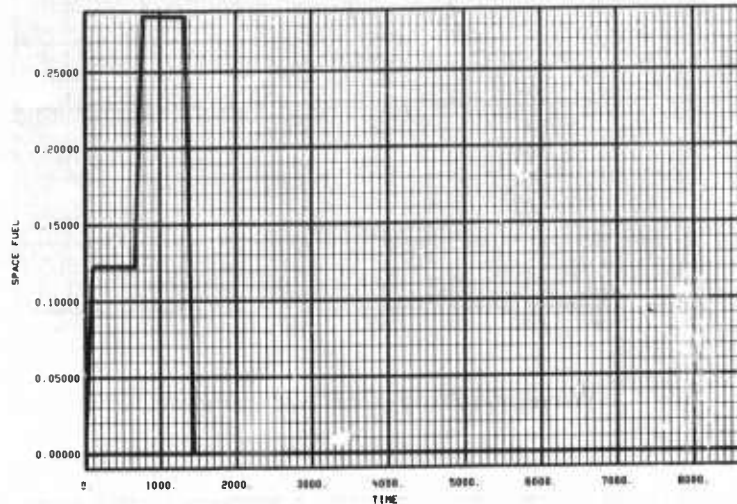
Fig. D-4—Annual history of fuel oil consumed for space heating in the Azores (MW) (time in hours)

phased into the power system. When wave machine frontage is only down to 75 percent of the totally indigenous value, required storage capacity (the maximum of the storage curve) has already dropped from 5500 MWh to 1325 MWh. By the time wave machine frontage has been reduced by 50 percent, required storage capacity has dropped to zero.

By definition there is no fuel oil consumption when a base operates only by using indigenous energy sources, hence the zero consumption figure at the top of Figs. D-3 and D-4. There is also zero fuel oil consumption by the space heating furnace (Fig. D-4) when machine frontage is down by 25 percent. This results from the ability of the engine generator waste heat to satisfy the small excess of space heating demand over that supplied by indigenously derived energy.

The dynamics of power supply are evidence in the data for the 50-percent frontage case. The fuel oil consumption in Fig. D-3 shows a peak at 5500 hr. This occurs because the wave energy available at this time is at its lowest (see Fig. D-1(A)) and no stored energy is available because required capacity is zero through the year (see Fig. D-2).[1]

In Fig. D-4, it is apparent that fuel oil is consumed for space heating only in the early part of the year. This consumption task corresponds to the peak in space heating demand at this time of year (see Fig. D-1(C)). Waste heat from the generator turbine is not available in sufficient quantity at this time of year to eliminate this fuel oil requirement because wave energy fluxes are at their maximum (see Fig. D-1(A)), and the turbines are not operating at high power levels.

---

[1]One might notice that electrical demand is also at its lowest at this time of year (see Fig. D-1(B)), but this low differs from mean demand only slightly compared with the amount that the wave energy flux differs from its mean. Thus the low flux condition dominates the dynamics.

Appendix E

PEAK POWER DEMAND EQUATIONS

In this appendix we develop the equations that give the peak power demands on the turbine-generators, fuel cells, and heat exchangers in Fig. 6. These peak power levels determine the cost of these pieces of equipment, and they have therefore been used in conjunction with the unit cost figures in Table 15 to give total system equipment cost. The parameters derived from these equations appear in Tables 16 through 18.

We first discuss the hydrogen-storage solar system and then turn to the wind and wave systems, saving our comments on battery storage systems to the end.

The peak power delivered by the turbine-generator system is the difference between the peak solar input and the minimum amount used for space heating multiplied by the efficiency of the turbine; i.e.,

$$\text{TUR1} = \left(1000\text{A} - \frac{\text{DP}_{min}}{k \cdot \text{E7}}\right)\text{E4} \cdot \text{H}\left[1000\text{A} - \frac{\text{DP}_{min}}{k \cdot \text{E7}}\right] \quad \text{(solar) . (E.1)}$$

DP_{min} is the lowest monthly average space heating demand, and k has been taken as 1.25 to give an instantaneous minimum demand that is 25 percent lower than DP_{min}. H[ ] is the Heaviside function. This states that no power flows through the turbine if the lowest possible space heating demand exceeds the peak power collected.

The fuel cell may operate in either the electrolysis or electrical generation mode. Hence the peak power input was determined for both modes and the higher value used for sizing and costing. The peak power delivered to the fuel cell for electrolysis (FCES) is the peak output of the turbine-generator reduced by the minimum electrical demand. From Eq. (E.1), this can be seen to be

$$\text{FCES} = \left[\left(1000\text{A} - \frac{\text{DP}_{min}}{k \cdot \text{E7}}\right)\text{E4} - \frac{\text{D}_{min}}{k}\right] \cdot \text{H}\left[\left(1000\text{A} - \frac{\text{DP}_{min}}{k \cdot \text{E7}}\right)\text{E4} - \frac{\text{D}_{min}}{k}\right]$$

$$\text{(solar)} , \quad \text{(E.2)}$$

where D_{min} is the lowest monthly average electrical demand and
k (= 1.25) has been used as above to reduce this to a 25 percent lower
instantaneous demand. This choice of 1.25 has been made so that kD_{max}
gives a peak instantaneous demand for our standard base that is 50 per-
cent greater than the annual average demand, a percentage increase over
average that equals that determined for Los Angeles by the Southern
California Edison Company (1971). (Greater peaking due to increased
space heating demand in colder areas is not relevant here since we
have used a separate demand to account for this.) The Heaviside func-
tion has again been included to account for the lack of fuel cell in-
put when the collector area is (1) so small that all collected energy
flows to satisfy the space heating demand, or (2) sufficiently large
to satisfy some electrical demand but small enough never to exceed
this demand and provide excess power for the fuel cells.

The peak power input for the electricity generation mode (FCEL) is

$$FCEL = \left(\frac{D_{max}}{E21}\right) k \cdot H(FCES) . \tag{E.3}$$

This expression states that the maximum output is that required to
satisfy the electrical demand when there is no indigenous power input,
such as at night in the case of solar. The Heaviside function accounts
for the two cases discussed above where there is no storage of energy
and hence no possibility of electricity generation.

The peak power requirement of the fuel cell (FC) is therefore

$$FC = \max (FCES, FCEL) . \tag{E.4}$$

Note that FCES and FCEL reach their maximum values at different times;
in the case of solar energy, the FCES peak occurs in daytime and FCEL
reaches its peak at night. As the size of the collector is reduced and
relative use of the engine generator system is expanded, the peak elec-
trolysis rate is eventually reduced enough so that the peak power demand
for electricity dominates the two modes of operation and thus determines
the size and cost of the fuel cell system.

The peak output of the engine-generator system (TUR2) is given simply by the peak electrical demand of the base, except when the power supply system is totally indigenous. Hence,

$$TUR2 = \begin{cases} kD_{max} & \text{(indigenous/engine generator)} \\ \\ 0 & \text{(totally indigenous)} \end{cases} \qquad (E.5)$$

where D_{max} is the highest monthly average electrical demand and k is the instantaneous peaking factor of 1.25 used above. The simple value for TUR2 results from the operating rule that the engine-generator is not turned on at all unless the storage is completely exhausted. Since the indigenous input flux may always become zero during this period, the engine-generator would have to satisfy the entire (possibly peak) electrical demand.

The peak power of the various heat exchangers must next be considered. Still confining our attention to solar energy, we note that the peak input for heat exchanger No. 1 (HE1) is given by

$$HE1 = min \left\{ \frac{k \cdot DP_{max}}{E6}, \ 1000 \ A \cdot \frac{E7}{E6} \right\} \qquad \text{(solar)} , \qquad (E.6)$$

where the variables have their usual meaning. This states that the peak power is determined by the maximum space heating requirement—i.e., by $k \cdot DP_{max}/E6$—unless the collector area is so small that even the peak solar input (1000A $\cdot$ E7/E6) is less than this heating demand. The peak input of heat exchanger No. 2 (HE2) is likewise determined by the space heating demand. Peak input occurs when the indigenous source is making no contribution to space heating demand, such as at night in the case of solar energy. Since operation of heat exchanger No. 2 requires that the storage not be exhausted, the engine-generator remains turned off and no waste heat is available to help reduce the space heating demand. Thus,

$$HE2 = \frac{k \cdot DP_{max}}{E6} \cdot H(FCES) , \qquad (E.7)$$

where H(FCES) has again been included to cover the special case of no power input to the heat exchanger when the collector area is so small that no energy is ever stored. Heat exchanger No. 3 is sized by noting that all waste heat from the engine-generator passes through it. From Eqs. (E.5) and (D.8), the peak power input (HE3) is thus

$$
HE3 = \begin{cases} kD_{max} \ (1 - EB)/EB & \text{(indigenous/engine-generator)} \\ \\ 0 & \text{(total indigenous)} \end{cases} \tag{E.8}
$$

The peak power input of heat exchanger No. 4 (HE4) depends on the difference between maximum space heating demand and the minimum energy available from the recovery of waste heat from the engine-generator. Thus,

$$
HE4 = \max \left\{ \frac{k \cdot DP_{max} - ER \cdot \dfrac{D_{min}}{k} \cdot (1 - EB)/EB}{EBP}, \ 0 \right\} . \tag{E.9}
$$

The max notation is used to account for those cases where more recovered heat is available than is required for space heating; i.e., a negative power input is not physically allowed. This condition may occur when the collector area is small and the engine-generator is operating, and when electrical demand is larger than or equal to space heating demand. No account is taken of direct solar space heating input in Eq. (E.9) since this is a zero contribution at night.

The equations presented above for peak power levels must be modified somewhat when one considers the wind and wave indigenous energy systems. This is necessary because these indigenous energy sources may not be used directly for space heating, and the generation of electricity from them does not require the thermal/electrical conversion capability of a turbine generator. Therefore, TUR1 must be interpreted as the mechanical to electrical output of either a windmill or wave machine.

$$
TUR1 = P_w \cdot A \cdot E4 \qquad \text{(nonsolar)} , \tag{E.10}
$$

where P_w is the peak wind or wave flux and A is either the windmill area or wave machine frontage. With no energy being used directly for space heating,

$$FCES = \left(P_w \cdot A \cdot E4 - \frac{D_{min}}{k} \right) H \left(P_w \cdot A \cdot E4 - \frac{D_{min}}{k} \right) \qquad \text{(nonsolar)}$$

(E.11)

$$HE1 = 0 .$$

(E.12)

FCEL and HE2 remain as in Eqs. (E.3) and (E.7) but with FCES now being given by Eq. (E.11). FC, TUR2, HE3, and HE4 remain as above.

A combined indigenous energy/engine generator system has also been considered using battery storage. Power inputs corresponding to FCES and FCEL are not necessary for this configuration, since costing of the type of battery systems required here is generally done on the basis of total energy storage rather than power.

REFERENCES

Adams, D. F., *Wind Turbine Rotor Blade Materials Design Technology*, University of Wyoming, UWME-DR-5011060, August 1974.

Cuomo, J. J., J. Ziegler, and J. Woodall, "A New Concept for Solar Energy Thermal Conversion," *Appl. Phys. Letters*, Vol. 26, p. 557, May 1975.

Defense Energy Information System, DEIS II, Dept. of Defense, Defense Supply Agency, 1974.

Encyclopedia Americana, Americana Corp. Publ., N.Y., 1967.

General Electric Space Division, *NSF/NASA Wind Generator System Program*, December 17, 1974.

Gillette, P. R. and W. Schubert, *Energy Requirements and Policy Alternatives Analysis for Remote Naval Bases*, Stanford Research Institute, Naval Warfare Research Center, NWRC-TN-45, August 1974.

Goen, R. L. et. al., *Assessment of Total Energy Systems for the Department of Defense*, Vol. II, Stanford Research Institute, November 1973.

Golding, E. W., *The Generation of Electricity by Wind Power*, Philosophical Library, N.Y., 1955.

Heronemus, William E., "Pollution-Free Energy From Offshore Winds," *Preprints, 8th Annual Conference and Exposition, Marine Technology Society*, September 1972.

Hottel, H. C and J. R. Howard, *New Energy Technology: Some Facts and Assessments*, The M.I.T. Press, Cambridge, 1971.

Interagency Task Force on Solar Energy, *Project Independence*, Federal Energy Administration Project Independence Blueprint, Final Task Force Report, November 1974.

Liu, H. and R. C. Jordan, "The Interrelationship and Characteristic Distribution of Direct, Diffuse, and Total Solar Radiation," *Solar Energy*, Vol. IV, July 1960, p. 1.

Naval Weather Service Command, *U.S. Navy Marine Climatic Atlas of the World, Vol. VIII, The World*, NAVAIR 50-1C-54, March 1969.

NSF/NASA Solar Energy Panel, *An Assessment of Solar Energy as a National Energy Resource*, University of Maryland, College Park, December 1972.

Office of Climatology and Oceanographic Analysis Division, *Climatological and Oceanographic Atlas for Mariners*, Vol. 1, *North Atlantic Ocean*, Department of Commerce, 1959; Vol. 2, *North Pacific Ocean*, 1961.

Putnam, Palmer C., *Power From the Wind*, D. Van Nostrand Co., Inc., 1948.

Reed, J. W., R. C. Mayden, and B. F. Blackwell, *Wind Energy Potential in New Mexico*, Sandia Laboratories, SAND74-0071, July 1974.

Salter, R. G., R. L. Petruschell, and K. Wolf, *Energy Conservation in Non-Residential Buildings*, The Rand Corporation, R-1623-NSF, March 1975.

Salter, Steven H., "Wave Power," *Nature*, Vol. 249, June 21, 1974, pp. 720-724.

Savino, J. (ed.), *Wind Energy Conversion Systems; Workshop Proceedings*, sponsored by NSF/RANN/NASA, Washington, D.C., June 1973.

Schutz, C., *Monsoonal Influences on Wind, Rain and Cloud Throughout Southeast Asia: A Study Covering the Peninsula and the Archipelago*, The Rand Corporation, RM-5418-PR, 1967.

Schutz, C. and W. L. Gates, *Global Climatic Data for Surface, 800 mb, 400 mb: January*, The Rand Corporation, R-915-ARPA, November 1971; *July*, R-1029-ARPA, November 1972; *April*, R-1317-ARPA, December 1973; *October*, R-1425-ARPA, March 1974.

South, Peter and Raj Rangi, "NRC's Vertical Wind Turbine," *Agri. Eng.*, February 1974, pp. 14-16.

Southern California Edison Company, *System Forecasts, 1971-1995*, February 1971.

Stahl, Albert W., "The Utilization of the Power of Ocean Waves," *ASME Trans.*, Vol. 13, presented May 1892, San Francisco, pp. 438-506.

Stein, Dimitry, *The Importance of and Progess in the Utilization of Wind Power in Denmark*, NASA Technical Translation, NASA-TT-F-15, February 1974, p. 333.

The Times Atlas of the World, Times Newspapers Ltd., London, 1967.

U.S. Naval Oceanographic Office, *Atlas of Pilot Charts, Central American Waters and South Atlantic Ocean*, 2nd ed., 1955; *South Pacific and Indian Oceans*, 3rd ed., 1966.